CHARACTERIZATION OF FAILURE MECHANISMS IN CROSS WEDGE ROLLING

by

Qiang Li

BS, Xi'an Jiaotong University, China, 1996

MS, Xi'an Jiaotong University, China, 1999

Submitted to the Graduate Faculty of

School of Engineering in partial fulfillment

of the requirements for the degree of

Doctor of Philosophy

University of Pittsburgh

2003

UNIVERSITY OF PITTSBURGH

SCHOOL OF ENGINEERING

This dissertation was presented

by

Qiang Li

It was defended on

March 11, 2003

and approved by

Bopaya Bidanda, Chairman and Professor, Industrial Engineering Department

Dipo Onipede, Assistant Professor, Mechanical Engineering Department

William Slaughter, Associate Professor, Mechanical Engineering Department

Patrick Smolinski, Associate Professor, Mechanical Engineering Department

Dissertation Director: Michael Lovell, Associate Professor, Mechanical Engineering Department

ABSTRACT

CHARACTERIZATION OF FAILURE MECHANISMS IN CROSS WEDGE ROLLING

Qiang Li, PhD

University of Pittsburgh, 2003

Cross wedge rolling (CWR) is a metal processing technology in which a heated cylindrical billet is plastically deformed into an axisymmetric part by the action of wedge shape dies moving tangentially relative to the workpiece. The CWR process offers several innovative and unique features over traditional machining operations. Despite these advantages, the CWR process has not been widely accepted throughout the manufacturing community, particularly in the U.S. This can mainly be attributed to complexities involved in CWR tool design. The design of CWR tooling is difficult because of the potential failure mechanisms that can be encountered during the CWR process. In this dissertation, extensive experimental investigation and numerical simulation have been performed to characterize the major failure mechanisms in cross wedge rolling. Based on the combined experimental and numerical analysis, criteria for predicting improperly formed workpiece cross section due to excess interfacial slip and internal defects due to the formation of internal voids have been determined. Based on these criteria, it is believed that the design of CWR tooling can be simplified, making CWR a more viable manufacturing process in the US.

DESCRIPTORS

Cross Wedge Rolling

Deformation Coefficient

Failure Mechanism

Finite Element Method

Interfacial Friction

Internal Defects

ACKNOWLEDGMENTS

This research is funded by Division of Design, Manufacture and Industrial Innovation, National Science Foundation (Grant number: DMII-9900060). I would like to express my sincerely gratitude to my advisor Dr. Michael Lovell for his invaluable contributions toward my professional growth and for his guidance and advices on my PhD study.

I express my truthful thanks to Dr. William Slaughter, Dr. Patrick Smolinski, Dr. Dipo Onipede, and Dr. Bopaya Bidanda for serving at my dissertation committee members and for their valuable comments and suggestion.

I would also like to thank my wife, Yong, for her gracious support and care. I am grateful to my parents for their constant encouragement throughout my academic career.

TABLE OF CONTENTS

LIST OF TABLES

LIST OF FIGURES

NOMENCLATURE

A_0	cross-sectional area before deformation, m^2
A_1	cross-sectional area after deformation, m^2
a	distance between the friction forces, m
b	distance between the normal forces, m
c	Cowper-Symonds strain rate parameters
D	fracture criterion in Johnson-cook model
D_1	radius of the roller, m
d_0	radius of the original workpiece, m
d_1	radius of the deformed workpiece, m
d_k	radius of rolling, mm
E	elastic modulus of the workpiece, N/m^2.
E_P	plastic hardening modulus, N/m^2
E_t	plastic modulus of the workpiece, N/m^2.
f	lubrication parameter in Oxley's friction model
J	J-integral value
J_k	critical J-integral value for the start of crack extension
k	relative amount of stretching deformation on the workpiece
L'	Length of the workpiece, m
L_1'	Length of the deformed part of workpiece, m
L_2'	Length of the undeformed part of workpiece, m

M_T	frictional moment by friction forces, N·m
M_P	normal moment by normal forces, N·m
P	normal force, N
p	Cowper-Symonds strain rate parameters
S	global slip
T	friction force, N
t_x	traction vector along x axis
t_y	traction vector along y axis
U_T	rotational distance of the forming dies, mm
U_W	rotational distance of the workpieces, mm
v	forming velocity, m/sec
W	strain energy density, J/m^3
Z	amount of compression
α	forming angle of the die, deg
β	stretching angle of the die, deg
ΔA	area reduction in the forming process
$\dot{\varepsilon}$	strain rate, 1/sec
ε_{def}	deformation coefficient
ε^f	effective strain to fracture
$\dot{\varepsilon}_{ij}$	total strain rate, 1/sec
ε_p^{eff}	effective plastic strain
$\dot{\varepsilon}_{ij}^{e}$	elastic strain rates, 1/sec

$\dot{\varepsilon}_{ij}^{\ p}$	plastic strain rate, 1/sec
$\dot{\varepsilon}^*$	dimensionless plastic strain rate
θ_T	rotational angle of the forming dies, deg
θ_W	rotational angle of the workpieces, deg
μ	friction coefficient
μ_s	static friction coefficient
μ_d	dynamic friction coefficient
σ	von Mise tensile flow stress, N/m^2
σ_0	initial yield stress, N/m^2
σ_1	first principal stress, N/m^2
σ_2	second principal stress, N/m^2
σ_3	third principal stress, N/m^2
σ_m	mean normal stress, N/m^2
$\bar{\sigma}$	effective stress, N/m^2
T^*	homologus temperature
Γ	path surrounding the crack tip, m

1.0 INTRODUCTION OF CROSS WEGE ROLLING

1.1 Background

In the metal processing industry, it is important to refine and improve manufacturing processes so that higher quality, lower cost products are generated. To this end, an innovative metal forming technique, cross wedge rolling (CWR), has obtained overwhelming popularity in several foreign countries for making stepped rotational products. In fact, in Eastern Europe and Asia, CWR has replaced many conventional machining, forging, and casting processes in the manufacturing of shafts and axles.

Cross wedge rolling (CWR) is a metal processing technology in which a heated cylindrical billet is plastically deformed into an axisymmetrical part by the action of wedge shape dies moving tangentially relative to the workpiece. Shafts with tapers, steps, and shoulders can be made by the CWR technique. Figure 1.1(a) illustrates the cross rolling of a stepped shaft using a pair of flat wedge tools. As shown in Figure 1.1 (a), two identical wedge-shaped forming dies move tangentially to one another and plastically deform a cylindrical workpiece in the CWR process. The cross wedge rolling mill is typically composed of one to three rollers on which wedge shaped toolings are mounted. As depicted in Figure 1.1, there are currently other two CWR machine configurations available. For each configuration, the workpiece is preheated to a prescribed temperature (which varies with workpiece material) and is fed into the roller gap in the axial direction of the rollers.

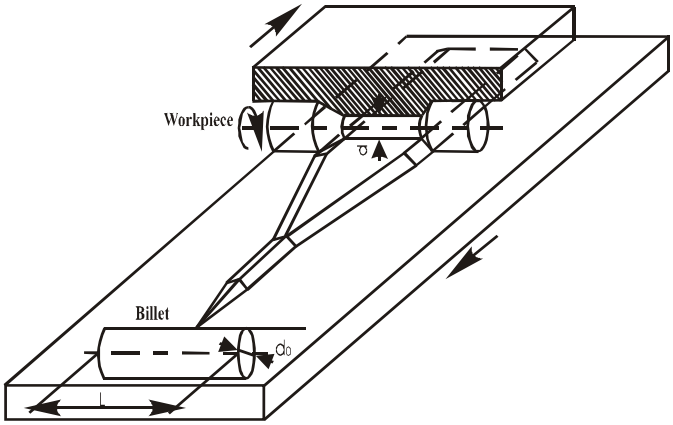

(a) Flat wedge CWR machine

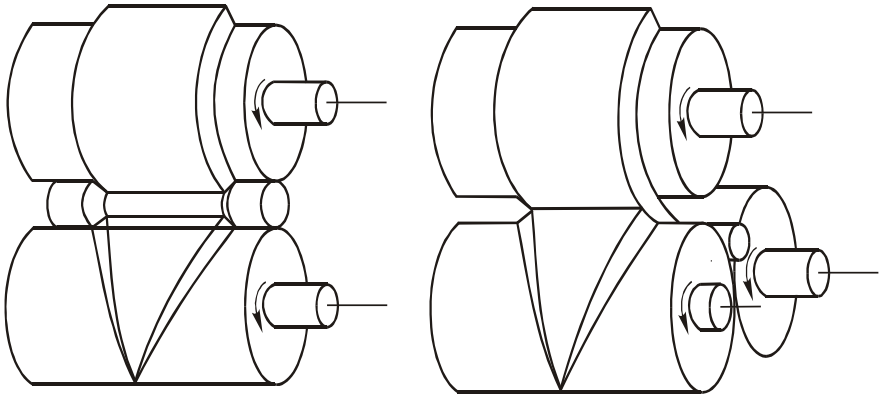

(b) Two-roll and three-roll CWR machine

Figure1.1 CWR machines

The CWR technique has significant potential in the material processing industry because it offers several well-documented benefits over other traditional manufacturing processes [1]. As shown in Figure 1.2, it is reported that hundreds of different kinds of products – ranging from crankshafts to drill bits – are currently being manufactured by CWR worldwide [2].

As a significant step towards making CWR a more viable manufacturing process in the US, a better understanding of the CWR deformation process needs to be established. Because cross wedge rolling combines the complex interaction of high strain rate plastic deformations with variable friction at elevated temperatures, the material flow behavior in CWR is not completely understood. In fact, there are currently no models of CWR that predict the three major failure mechanisms encountered during the deformation of the workpiece: (1) improperly formed workpiece cross section, (2) external defects on the surface of the workpiece (i.e. spiral grooves), and (3) internal defects within the workpiece (voids and cracks). Without an accurate prediction of workpiece failure mechanisms as a function of essential CWR process parameters (such as stretching angle, forming angle, rolling velocity, etc.), manufacturers are hesitant to choose CWR as the preferred manufacturing process. With typically as high as seven to eight prototypes currently being required for a single die design [3], fundamental research is required for this new and emerging technology to be fully accepted by the US manufacturing community.

With the advancement of computer hardware and numerical modeling techniques over the past decade, detailed simulations of complex physical phenomena are being performed in a matter of minutes of CPU. For investigating the complicated deformation process encountered in cross wedge rolling, the explicit finite element method is an excellent solution technique. For this reason, a parametric finite element model was developed to study the effects of varying CWR process parameters on product failure. All of the finite element analyses utilized an

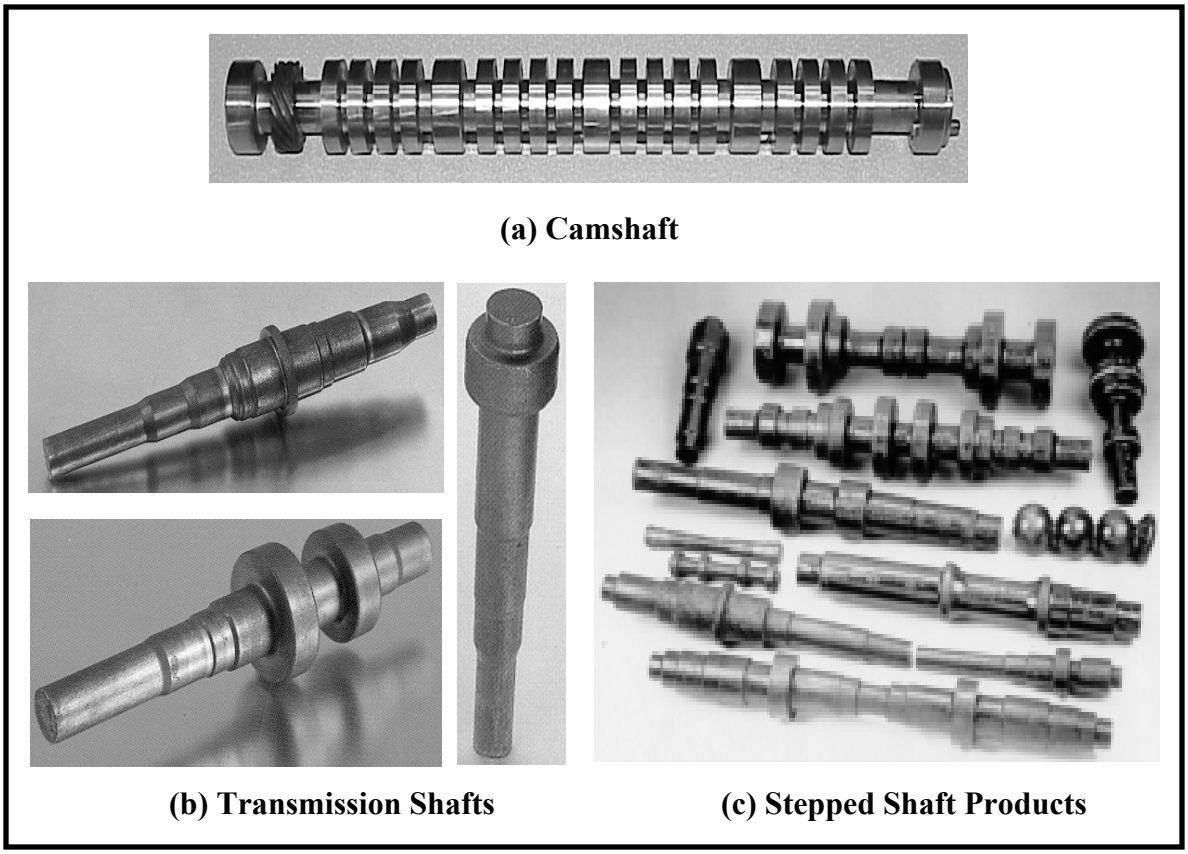

Figure 1.2 Products Produced by CWR

explicit dynamics finite element program initially developed by the author. Since there is no numerical analysis on two-roll CWR interfacial slip and internal defects currently available in the open literature, all of the FEM results generated are a significant contribution to the current state of understanding of the CWR process.

Together with the numerical simulations, extensive experiments were performed to quantify the conditions under which failure occurs during the CWR process. Along with gaining overall insight into the deformation behavior of the workpiece, the experiments were also used to validate the parametric finite element model of CWR. Experiments for the project were conducted using a CWR prototype testing apparatus developed at the University of Pittsburgh. By using a combination of experimental and numerical techniques, a physical model was developed for predicting the conditions under which CWR part failure occurs. The development of such a model will greatly simplify CWR tooling design, hence making CWR a more viable manufacturing process in the US.

1.2 Material Deformation Process

As shown in Figure 1.1, two identical forming dies move tangentially to one another and plastically deform a cylindrical workpiece in the CWR process. In cross wedge rolling there are four stages, or zones, in the workpiece deformation process corresponding to four zones of the wedged tool geometry (see Figure 1.3). These are the knifing, guiding, stretching, and sizing zones. Due to the changes in tool's geometry, the workpiece plastic deformation mechanisms are significantly different in each zone of the wedge shaped tool.

In the knifing zone, the tool is composed of a wedge whose height starts at zero and increases to the total reduction of height for the workpiece, Δr. The function of this zone is to drive the cylindrical billet and plastically deform a V-shaped slot into its circumference. The angle of this V-shaped slot is controlled by the forming angle of the tool, α.

In the guiding zone, the die's cross-section does not change as the tool enlarges the slot obtained in the knifing zone into a uniform V-shaped groove around the workpiece circumference.

The stretching zone is the most critical section of the tool because it is in this region that the most substantial workpiece plastic deformation takes place. Within the stretching zone, the workpiece material is stretched and forced to flow to the ends so that the shoulders of the shaft can be created. The amount of elongation and plastic deformation in the stretching zone is controlled by the stretching angle, β.

In the final region of the tool, the sizing zone, a small amount plastic deformation occurs as the dimensional tolerance and surface qualify of the product is finely tuned.

The CWR process is so highly automatic that the feeding, rolling and cutting end of the billet can be accomplished in a single pass.

1.3 Advantages of the CWR Process

Compared to traditional machining, forging and casting processes, CWR offers several innovative and unique features. These features include:

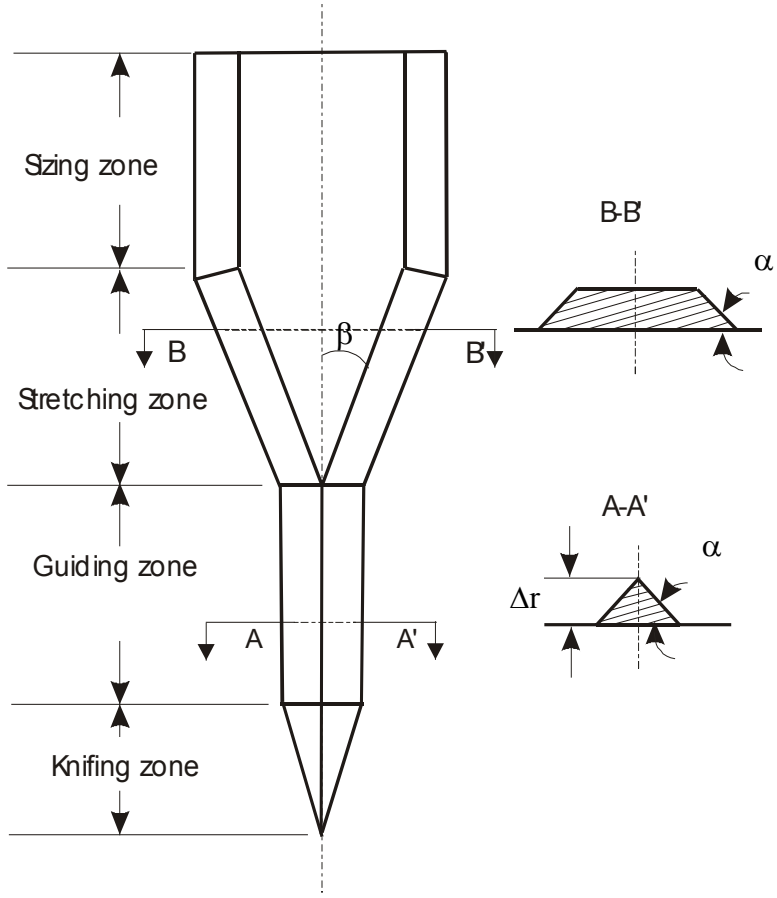

Figure 1.3 Structure of the forming tool in CWR

Higher productivity: One or more parts can be produced in each pass of the forming dies. If the product's geometry is not extremely complex, pairs can be made in one operation by a symmetrical tool layout. Normally, 10 to 30 parts are produced per minute making CWR's productivity 5 to 20 times higher than machining and forging.

Higher material utilization: In CWR, less than 10% of the raw material is wasted in end-cutting and grinding so that CWR greatly reduces the cost of raw materials. In contrast, 40% of the material is generally lost in machining processes in the form of chips. For hot rolling, dimensional accuracy of diameters is between ±0.1mm and ±0.5mm. Length accuracy is between ±0.5mm and ±1.5mm. Using cold CWR, greater accuracy can be obtained [6].

Better product quality: CWR is a metal forming process in which the desired product's shape is achieved by the plastic flow of metal material at an elevated temperature. In CWR the metal fabric is continuous due to the fine control of plastic deformations and forming temperature. Finer grains are obtained which makes the final products stronger. In machining, the metal is removed layer by layer in order to shape the shoulders and steps. Therefore, the metal fabric is broken along the axial direction which can reduce the strength of the product.

Less energy consumption: In CWR production, raw materials are normally in the form of long bar stocks that are continuously fed into the tool gap. Since only the length corresponding to one billet is heated at a time, little energy is wasted. Additionally, heat treatment of the workpiece is performed by utilizing the elevated temperature achieved after rolling.

Automation and lower costs: In CWR, shape forming, surface refining, and end cutting are automatically finished in a single pass of the forming tools. This greatly reduces the number of workers, auxiliary machines and work area.

Improved environment: Compared to forging and machining, CWR produces significantly less noise. Additionally, no waste materials such as cooling lubricants are created.

.

1.4 Research Objectives

The principle objectives of the current research are as follows:

- To create a better understanding of the CWR deformation process. The deformation and material plastic flow of the workpiece during CWR forming are extremely complicated, which is a combination of longitudinal elongation, radial compression and transverse rotation.
- To develop a physical model for predicting the three major failure mechanisms encountered in CWR and therefore to simplify CWR tooling design while maintaining the high quality so that parts can be produced in a single design cycle rather than by trial-and-error methods.
- The ultimate goal of this research is to establish CWR as a more viable manufacturing process in the US.

To achieve these objectives, the following approaches are employed:

- Generating a parametric explicit dynamic finite element model to realistically investigate the complex CWR deformation behavior over a wide range of operating conditions.
- Performing extensive experiments to quantify the conditions under which failure occurs during the CWR process. Experiments will also be used to validate the numerical results.

2.0 CWR FAILURE TYPES

The CWR technique has tremendous potentials in the material processing industry because it possesses several outstanding advantages over other traditional manufacturing processes [4], such as higher productivity, better material utilization, stronger product quality and improved environment. Despite these advantages, however, CWR has several failure mechanisms that restrict its more widespread application. This is partly due to the fact that the deformation and failure mechanisms of CWR are still largely unknown, which makes it very difficult to automate CWR tooling design.

As illustrated in Figure 2.1, Johnson and Mamalis [5] separated the defect mechanisms encountered during the CWR process into three categories: (1) improperly formed workpiece cross-section, (2) surface defects, and (3) internal defects. It is important to note that each of these failures is repeatable when encountered at a specific set of operating conditions [6]. Hence, the failure mechanisms encountered in CWR are direct functions of the process parameters such as the forming angle α, stretching angle β and the area reduction ΔA, as well as the initial micro-structural defects of the raw material.

2.1 Improperly Formed Cross-section

One of these failure mechanisms, improperly formed cross-section, is characterized by the compression of the workpiece without significant axial deformation. Improperly formed cross-sections develop in the CWR process due to excessive slip between the forming tools and the workpiece [7],[8]. In an excessive slip condition, the workpiece fails to rotate between the forming tools so that the workpiece cross-section is improperly formed (see Figure 2.1). This

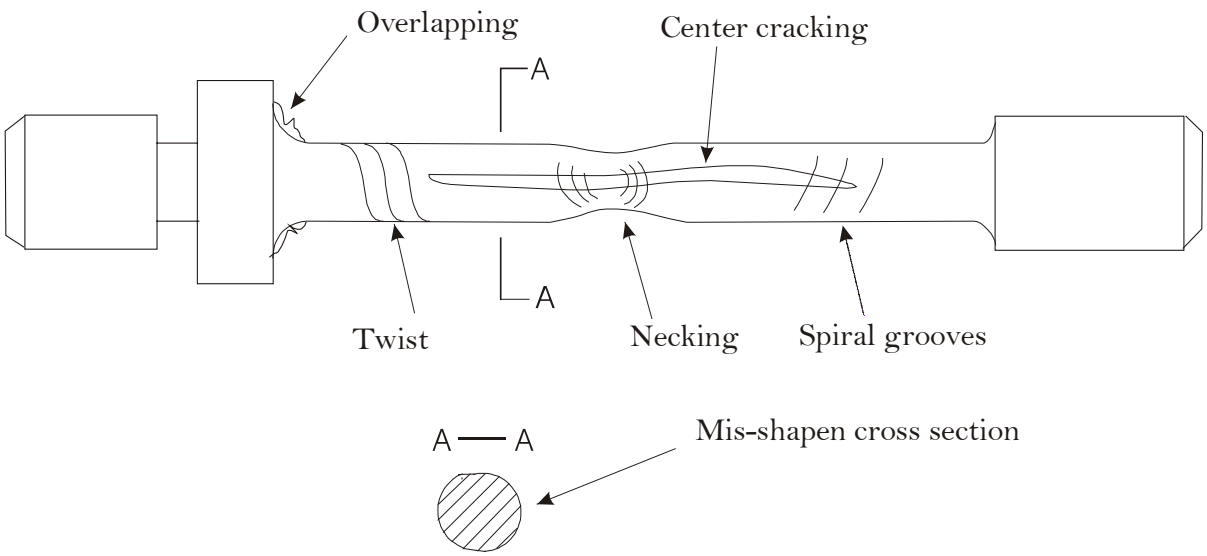

Figure 2.1 Common CWR failure mechanisms

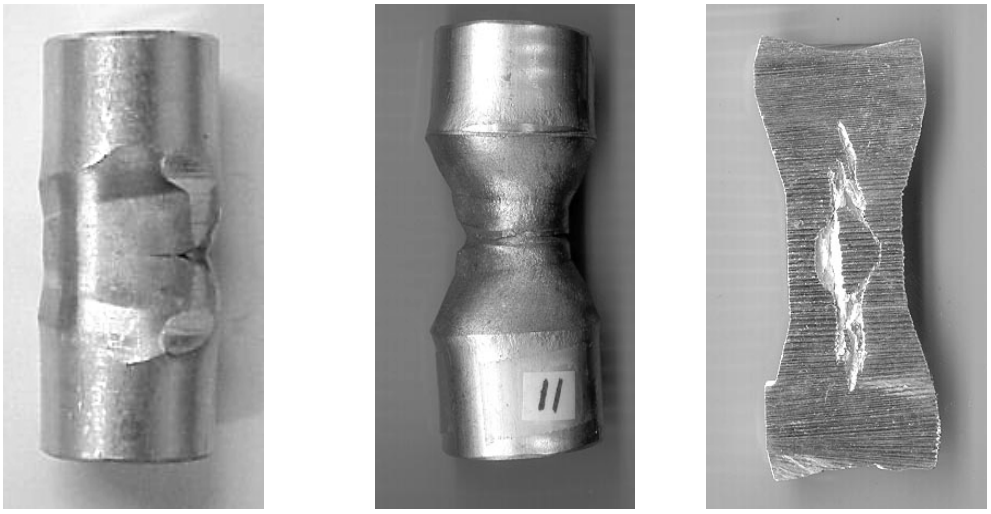

(a) Excess slip (b) Necking (c) Internal void

Figure 2.2 Failure Samples of three main defects

interfacial slip develops in CWR because the frictional forces between the workpiece and the forming tools are insufficient to initiate rotational motion. The normal and tangential forces at the two tooling/workpiece interfaces form couples in opposite directions. If the tangential force couple acting on the workpiece is larger than the normal force couple, rotation will not occur and the billet will slip between the surfaces of the forming tools. Such a slipping action compresses the workpiece without any axial deformation (see Figure 2.2a). Undesirable amounts of slip in the early stages of the CWR process can lead to workpiece misalignment and ultimately inconsistent or incorrect final cross-section formation. Excess interfacial slip is problematic to CWR tool designers because it is not currently possible to determine the minimum required tool-workpiece friction forces as a function tool geometry and operation conditions. As described in previous work by the investigators [1],[9], the amount of slip, particularly in the knifing and guiding zones, is a critical factor in determining the final shape of the workpiece and influences the required length of each section of the forming tool.

2.2 Surface Defect

The second common failure mechanism in CWR operations is the occurrence of surface defects. Surface defects include the formation of spiral grooves, excessive thinning or necking, and overlapping of the workpiece.

Spiral grooves: The appearance of 'twisting' spiral grooves in cross wedge rolling is due to the opening of cracks that exists near the outer surface of the billet. Spiral grooves or roll marks are screw-like features produced as result of an indentation of the roll edge on the rolled surface. Fu and Dean [6] found that spiral grooves are most common when the friction

coefficient between the tools and the workpiece is large. Bortunov [10] and Grechkin [11] attributed spiral grooves to the opening-up of flaws or cracks existing in the billet. Thompson and Hawkyard [12] noted that the requirement for high frictional contact between tool and workpiece leads to roll marks left on the surfaces rolled of a part due to the use of deep serrations on the wedge surfaces. Hu [2] found that spiral grooves always accompany necking in the rolling process.

Necking: Necking comprises thinning or breakage when rolling at a high reduction ratio and in the presence of an asymmetrical axial force. The axial force causes tension and if this tension exceeds the yield strength of the workpiece material, necking may occur. Necking failure consists of distortional thinning of the workpiece and is prevalent when the cross-section area ratio is larger than 70% [2],[5]. When the axial force is larger that the yield strength of the workpiece during the process, necking will occur first on the rolled portion with smallest diameter. Depending on the design of subsequent part of the rolling tools, necking and spiral grooves will either remain on the part or be eliminated by further reduction. Forging necking in the CWR process occurs if the tensile stresses (caused by the axial rolling forces) are greater than the material yield stress. The violent axial flow of material occurring in this case is accompanied by forging necking until the specimen is broken.

Lapping: When flat tools with sharp forming angles are used, overlapping failure occurs as the workpiece folds during radial reduction. Lapping has already been reported to occur when flat tools with sharp edges are used. The wedge has sharp edges and when the workpiece diameter is reduced, material tends to fold. Lapping is attributed to “tangent deformation”. Lapping areas are the most frequent surface defect of forgings produced in CWR processes.

Lappings resulting from defects of the charge material and those resulting from improperly designed CWR are distinguishable.

2.3 Internal Defect

The final failure mechanism found in CWR production, internal defects include the formation of internal cavities and cracks that develop during the CWR process. As shown in Figure 2.2, these defects significantly reduce the strength of the formed part and can ultimately lead to product failure. The formation of the internal defects in the CWR process can be attributed to several possible causes. Reviewing the literature, there is not complete agreement between researchers on the primary mechanism for the formation of internal voids and cracks. The main explanations include: 1) large tensile stresses in the central portion of the workpiece, 2) excessive shear stresses induced by the knifing action of the forming dies, and 3) low cycle fatigue that develops during the rolling process.

Smirnov [13] claimed that the combined interaction of shear stresses (major factor) and tensile stresses (minor factor) on the workpiece caused internal voids. By employing a plane deformation model, he found that internal defects developed rapidly under secondary tensile stresses that were generated by the cyclic compression of the workpiece. After performing a series of experiments on the CWR process, Danno and Tanaka [14] drew a similar conclusion that the central cracks were produced by a combination of the radial tensile stresses and the shear stresses that occurred within the central zone of the billet during rolling. This finding was supported by the experimental work of Tetern and Liuzin [15] who observed a region of large plastic deformation within the center of the billet directly before a void was formed. They

concluded that the large shear stresses drive the plastic strain beyond a certain limit and form microcracks. These microcracks then rupture during deformation and consequently generate internal voids. Tselikov [16] alternatively reported that accumulated plastic tensile stresses induced by several revolutions of the billet formed the central cavities in a low cycle fatigue mode of failure.

Though these researchers did extensive work on this topic, the influence of CWR tool parameters on the internal stress-strain characteristics of the workpiece is still not completely understood. This is primary due to the fact that it is very difficult to analyze the workpiece's deformation behavior during an actual CWR operation. Regardless of the exact physical phenomenon causing the internal defects, it clearly has been shown that specific sets of tooling parameters lead to internal defects within the workpiece. Determining these parameters, with respect to eliminating failure in CWR, is critical to allowing the manufacturing community better to utilize the technology involved in CWR. One of objectives of this dissertation is to develop a fundamental understanding of the reason and influential factors of internal voids and cracks that develop during the CWR process.

3.0 EXCESS INTERFACIAL SLIP IN CWR

In this chapter, analytical and numerical methods are introduced for characterizing the nature of interfacial slip in CWR operations. The analytical method determines the critical friction coefficient in a two-roll CWR operation based on a transverse section of the tool. After being validated by comparison to experiments performed with a CWR prototype machine, a three-dimensional finite element model (FEM) was parameterized to study the influence of CWR process parameters on the global slip at 32 different operating conditions. Based on the analytical and numerical results, the influences of process parameters in the cross wedge rolling process are ascertained and discussed.

3.1 Overview of Excess Interfacial Slip

3.1.1 Background

Excess tool-workpiece interfacial slip is controlled by the contact area and interfacial topography between the tool and workpiece surfaces. If a critical friction force is not achieved, the tools will compress the workpiece without significant axial deformation because the workpiece fails to rotate between the forming dies. If the machine power is sufficient to drive the tools through the workpiece, excessive slip in the CWR process will cause workpiece misalignment and improper cross section formation. Interfacial slip occurs in a CWR operation when the tool workpiece interfacial forces are insufficient to cause rotational motion of the workpiece. Excess interfacial slip is problematic to designers because it is very difficult to

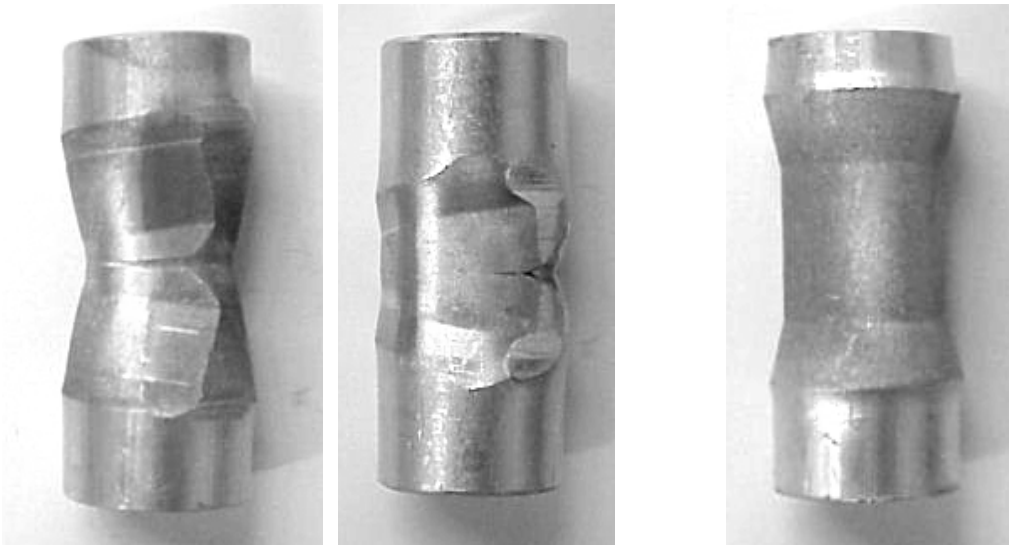

(a) Failure specimens (b) Rolled specimen

Figure 3.1 Comparison between the failure specimens with excess interfacial slip and rolled specimen

estimate the friction coefficient and the frictional forces between the tools and workpiece for a given set of operation conditions (see Figure 3.1). Therefore it is very hard to determine the required length of each section of the forming dies for a specific product. The problems associated with excess slip are compounded by the fact that recent research has shown that the critical friction coefficient required for causing rotation of the workpiece is different for each zone of the forming tool [17]. This is to be expected as the contact area between forming tools and workpiece changes in each zone of the tool.

In order to prevent excess interfacial slip failure and streamline CWR tooling design, it is necessary to establish the critical rolling condition for a CWR process. Reviewing the literature, several researchers have investigated interfacial slip in CWR. Lovell [4] introduced an explicit dynamic finite-element model to evaluate the interfacial slip in a flat wedge CWR process. An analytical method was presented for determining the critical friction condition in a cross wedge rolling process. Then a technique was introduced for determining the actual friction coefficient in a CWR operation with specialized pin-on-disk experiments. By comparing the critical and experimental friction coefficient values, a procedure for predicting the likelihood of excess interfacial slip failure in cross wedge rolling was established. The soundness of such a procedure was verified by the finite element method and CWR prototype experiments. Based on this innovative model, Deng et al [18] analyzed the interfacial slip behavior between the forming tools and the workpiece as a function of workpiece material, tool geometry, forming velocity and area reduction. Using a transverse section of the tool, this work introduces analytical and numerical methods for characterizing the critical rolling condition in two-roll CWR process.

3.1.2 Parameter Definitions

Before proceeding to the results of the analytical calculations, experimental investigations and numerical simulations, several parameters for the interfacial slip in the CWR process need to be defined. Due to the difference in radial distance from the billets axis of rotation and the deformations that occur during the rolling process, the interfacial slip in CWR varies from point to point along the contact area. In the deforming area of the workpiece, there exists a true neutral radius at which the tool and workpiece linear velocities coincide. Since the true neutral radius is a function of the radial displacements in the contact region, the magnitude and character of the interfacial slip in part depend upon the radial deformations of the workpiece. There also exists, however, a purely geometric neutral radius that develops in the absence of radial deformations and exists under a condition of pure adhesion between the forming tools and workpiece. The purely geometric neutral radius of workpiece, r_g, is defined as the average of the initial and minimum deformed radii of the workpiece. Similarly, the pure geometric neutral radius of the forming tool, r_g', is defined as the difference between the distance from the roll axis to workpiece axis and r_g. In this work, the purely geometric neutral radii are used as the reference points to calculate the interfacial slip that is referred to as global slip. The global slip is defined as the difference between the rotational distances that the forming dies and the workpiece respectively rotate during the specified forming period. The global slip, S, can be determined in the following equation [19]:

$$S = \frac{U_T - U_W}{\pi d_0} \tag{3.1}$$

and

$$U_T = r_g'\theta_T,\ U_W = r_g\theta_W \tag{3.2}$$

where U_T, θ_T and U_W, θ_W are the rotational distances and angles of the forming dies and the workpiece at the specified time step, respectively.

3.2 Analytical Study

3.2.1 Critical Friction Coefficient Calculation

As a first step towards understanding excess interfacial slip failure in a two-roll CWR process, it is important to analytical evaluate the conditions required to achieve rotation of the workpiece. A rotational condition in a CWR process is considered to develop when the frictional forces between the tools initiate rotational motion of the workpiece rather than plowing through it. The critical friction required to establish rotation of the billet can be estimated by examining a simple transverse section of a two-roll process, as shown in Figure 3.2 [2]. In order to cause the workpiece to rotate, the frictional moment M_T (generated by the friction force T between the roller and the workpiece) must be greater than the normal moment M_p (generated by the contact force P), which is:

$$T \cdot a \geq P \cdot b \tag{3.3}$$

From the standard friction theory,

$$T = \mu P \tag{3.4}$$

We find:

$$\mu \geq \frac{b}{a} \tag{3.5}$$

The geometric relationships depicted in Figures 3.2 show that:

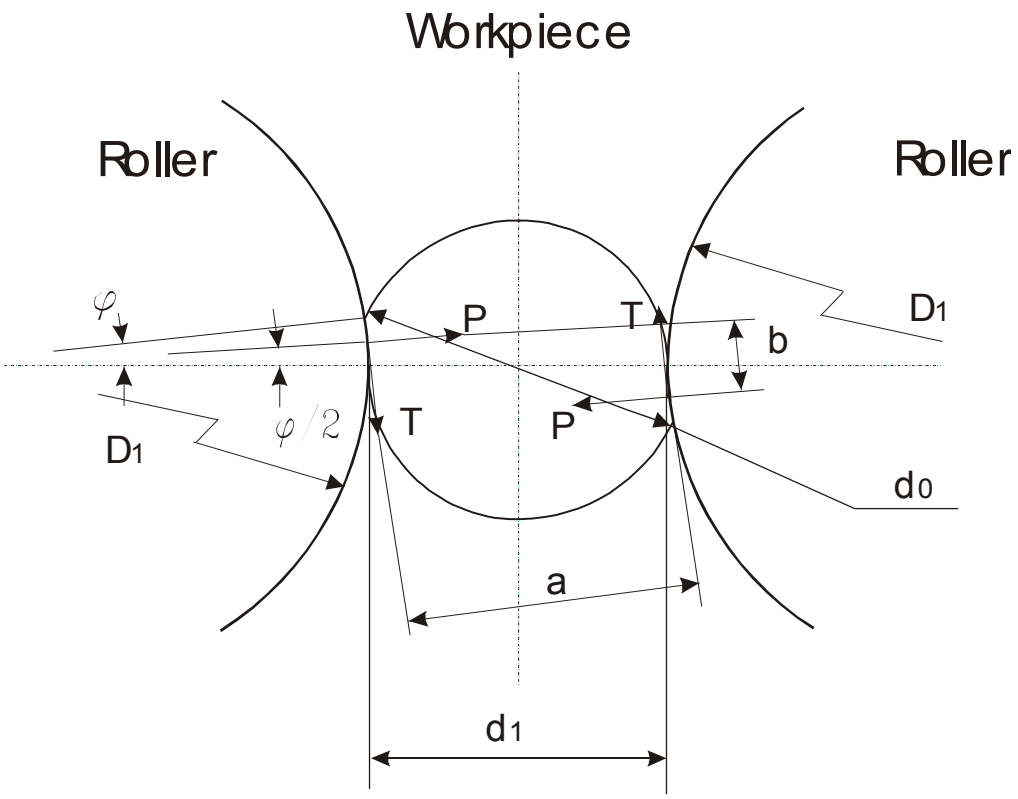

Figure 3.2 Rotational condition of the simple cross wedge rolling

$$b = (D_1 + d_1)\sin\frac{\varphi}{2} \tag{3.6}$$

$$a = \left(d_1 - D_1 \frac{1 - \cos\frac{\varphi}{2}}{\cos\frac{\varphi}{2}} \right) \cos\frac{\varphi}{2} \tag{3.7}$$

Since φ is relatively small, it is then assumed that $\tan\frac{\varphi}{2} = \sin\frac{\varphi}{2}$. From the geometric relationships, it is further formulated that:

$$\tan\frac{\varphi}{2} = \sqrt{\frac{d_1 Z + Z^2}{D_1(D_1 + d_1)}} \tag{3.8}$$

where Z is the amount of compression and defined as:

$$Z = \frac{d_0 - d_1}{2} \tag{3.9}$$

Substituting Eqs. (3.6)~(3.9) into Eq. (3.5), the critical friction condition for the simple transverse rolling is expressed as:

$$\mu^2 \geq \left(1 + \frac{d_1}{D_1}\right)\left[\frac{Z}{d_1} + \left(\frac{Z}{d_1}\right)^2\right] \tag{3.10}$$

In the above equations, d_0 and d_1 are the radii of the workpiece before and after deformation respectively, and D_1 is the radius of rollers.

Since the compression value Z varies in different sections of the forming tool, the compression value Z can be shown from Figure 3.2 to be:

$$Z = \frac{k}{2} \cdot \pi d_k \tan\alpha \tan\beta \tag{3.11}$$

where d_k is the radius of rolling, which can be calculated as $d_k = d_1 + 0.62(d_0 - d_1)$. k is a parameter that represents the relative amount of stretching deformation on the workpiece

($0 < k \leq 1$). k=1 means that the workpiece is stretched to its entire length in the stretching zone. Substituting (3.11) to (3.10), the critical friction condition for each stage of a two-roll wedge process is given by:

$$\mu \geq \frac{1}{2}\sqrt{\left(1+\frac{d_1}{D_1}\right)\left(C^2+2C\right)} \tag{3.12}$$

where $C = \frac{1}{d_1}\tan\alpha \cdot \tan\beta \cdot \pi d_k k$.

When $D_1 \to \infty$, the rotation condition of the flat wedge rolling is expressed as:

$$\mu \geq \frac{1}{2}\sqrt{\left(C^2+2C\right)} \tag{3.13}$$

Using the above expressions, the critical friction in a two-roll CWR process can be estimated as a function of tool geometry and area reduction.

3.2.2 Application of Bowden's friction model

In an effort to predict excess slip failure in an actual CWR process, Lovell [4] introduced a technique for determining the friction coefficient in a specific CWR operation using specialized pin-on-disk experiments. By comparing the experimentally determined friction coefficient to a critically calculated value [9], an indirect procedure for predicting the likelihood of excess interfacial slip failure in cross wedge rolling was established. Such a procedure, however, has been found to be difficult for CWR tool designers due to the nature of the experiments involved. Therefore, in this section, previous work by author will be extended through the incorporation of two well-known friction models [20],[21] that are applicable to metal working processes. Utilizing these friction models, a method for predicting excess slip failure directly from a machine configuration and CWR operating condition will be developed.

Using Equation (3.12), the critical friction coefficient in a two-roll CWR process can be determined as a function of tool geometry and workpiece radius reduction. In Equation (3.12), however, the friction coefficient is an undetermined parameter for a given set of operating conditions. In fact, without specialized experiments, it is not possible to estimate the friction coefficient in a specific CWR process. In this section, we will use Bowden and Oxley's models to express the friction coefficient as a function of CWR process parameters.

From the viewpoint of microscopic mechanics, the tool-workpiece interfacial friction in CWR can be modeled by the interaction of asperities. In such a model, friction results from the action of harder asperities on the tool sliding over and plastically deforming the asperities on the workpiece surface. Due to the high forming pressures encountered in CWR, the apparent and real contact areas between the tool and workpiece are nearly identical. As described in Lovell [4], the CWR forms tools essentially act as single conical asperity as they deform the workpiece. In such a condition, Bowden's asperity friction model can be applied to analyze the flow of the softer workpiece material. In Bowden's plowing theory, it is assumed that a hard (tool) conical asperity of semi-angle $\pi/2-\alpha$ penetrates and plastically deforms a soft metal surface (workpiece) [22]. In this case:

$$\mu = \frac{T}{P} = \frac{2}{\pi}\tan\alpha \tag{3.14}$$

where α is the wedge angle of the conical asperity. When applied to the CWR process, α can be considered the forming angle of the tool [4].

Substituting (3.14) into (3.12),

$$\frac{2}{\pi}\tan\alpha \geq \frac{1}{2}\sqrt{\left(1+\frac{d_1}{D_1}\right)\left(C^2+2C\right)} \tag{3.15}$$

Since $C = \frac{1}{d_1} \tan\alpha \tan\beta \cdot \pi d_k k$ and $d_k = d_1 + 0.62(d_0 - d_1)$,

$$C = k\pi \tan\alpha \tan\beta \left[1 + 0.62\left(\frac{d_0}{d_1} - 1 \right) \right] \tag{3.16}$$

In addition, the workpiece area reduction, ΔA, will be defined to represent the amount of plastic deformation that occurs in the workpiece. The cross-section area reduction of the workpiece, ΔA, is given by the relationship:

$$\Delta A = 1 - \left(\frac{d_1}{d_0} \right)^2 \tag{3.17}$$

where d_0 and d_1 are the diameters of the workpiece before and after deformation, respectively. Hence

$$C = k\pi \tan\alpha \tan\beta \left[0.38 + \frac{0.62}{\sqrt{1 - \Delta A}} \right] \tag{3.18}$$

Equation (3.18), when substituted into Equation (3.15), yields a direct expression for the critical rolling condition in terms of the CWR tool geometry and operating conditions.

3.2.3 Application of Oxley's friction model

In addition to Bowden's asperity model, Oxley's slip-line field model can similarly be applied to determine the critical rolling condition in CWR as a function of known process parameters. Based on the plane strain slip-line field theory, Oxley's *wave* model [21], determines the frictional force when a hard asperity slides over a softer surface. The frictional force is assumed to result from the pushing of a plastically deformed wave of the softer material ahead of

the hard asperity. In such a model, which has been shown to be valid for many forming processes, the resulting expression for the friction coefficient, μ, is given by:

$$\mu = \frac{A\sin\alpha + \cos(\arccos f - \alpha)}{A\cos\alpha + \sin(\arccos f - \alpha)} \tag{3.19}$$

where

$$A = 1 + \frac{\pi}{2} + \arccos f - 2\alpha - 2\arcsin\left[(1-f)^{-1/2}\sin\alpha\right], \tag{3.20}$$

α is asperity forming angle, and

f is a lubrication parameter.

Substituting (3.19) and (3.20) into (3.12), we obtain:

$$\frac{A\sin\alpha + \cos(\arccos f - \alpha)}{A\cos\alpha + \sin(\arccos f - \alpha)} \geq \frac{1}{2}\sqrt{\left(1 + \frac{d_1}{D_1}\right)\left(C^2 + 2C\right)} \tag{3.21}$$

where C is given in Equation (3.18). As with equation (3.15), Equation (3.21) expresses the critical rolling condition in CWR as a function of process parameters.

It is important to note that f in the above equations is defined as the ratio of the strength of the interfacial film to the shear flow stress of the soft workpiece material such that $0 \leq f \leq 1$ [21]. In the CWR process, the shear flow stress is much larger than the strength of the interfacial film, and therefore f should be close to 0.0. Since f is not sensitive to the value of μ as it approaches 0.0, a value of f=0.05 was chosen to demonstrate Oxley's friction model in the present investigation.

3.2.4 Discussion of the friction model results

In the CWR process, there are three primary parameters that determine the geometry of the final part – the forming angle α, the stretching angle β, and the area reduction ΔA. These parameters also play an important role in determining the critical rolling condition in a CWR operation. Previously, it has not been possible to predict the likelihood of interfacial slip failure in CWR solely on the values of α, β, and ΔA of a proposed CWR process. Using Equations (3.15) and (3.21), however, a procedure has been developed to evaluate the critical friction in a potential CWR process design. In order to assess the potential applicability of these equations, the critical rolling condition was evaluated for $d_1/D_1=0.2$, as shown in Figure 3.3(a) and 3.3(b). It is important to note that the curves in these figures represent the critical rolling condition for the CWR process. Therefore, points below the curves will not result in excess interfacial slip failure, while points above the curve are predicted to fail.

As illustrated in Figures 3.3(a) and 3.3(b), it is found that the critical friction results predicted from Oxley's and Bowden's models have very similar trends with respect to variations of α, β, and ΔA. In the figures, the first notable tendency is that to maintain a critical rolling condition, the stretching angle β must monotonically increases with increasing α. In fact, as shown in the curves, when α increases from 15° to 40°, β increases from approximately 3° to 9° for Bowden's model and from 6° to 20° for Oxley's model. Such a finding is to be expected, as both Eq. (3.14) and (3.19) predict that the critical friction coefficient will increase with the forming angle α. When the friction coefficient increases, the overall friction force between the tools and workpiece becomes greater. At greater frictional forces, a larger amount of plastic

material flow can be maintained within the workpiece, hence allowing β to increase while achieving a desired rolling condition.

A second tendency found in Figures 3.3(a) and 3.3(b) is that the area reduction ΔA has a moderate influence on the critical rolling condition. In both of the figures, the critical allowable stretching angle β decreases with increasing area reduction, especially at large forming angles. As the area reduction increases, the amount of plastic deformation in the workpiece increases because the amount of radial compression exerted by the tools on the workpiece is larger. Since fully plastic material offers less resistance to the motion of the tools, the stretching angle β must decrease to counteract the increase of plastic workpiece material flow at higher ΔA values when α remains constant. Likewise, when β is kept constant, the forming angle α (and corresponding friction coefficient) must increase with ΔA to maintain a critical rolling condition.

A final tendency to be noted in Figures 3.3(a) and 3.3(b) is that while exhibiting similar trends with respect to the CWR tooling parameters, the magnitude of the critical stretching angles β predicted by Bowden's and Oxley's models are substantially different. As noted previously, β increases from approximately 3° to 9° for Bowden's model and from 6° to 20° for Oxley's model over the same range of forming angles. Since both friction models can be applied for the forming contact conditions, it is important to establish which model best represents the physical behavior encountered in CWR.

For the purpose of assessing the applicability of both models, experiments (see Section 3.3 for further references) were conducted using a specially designed CWR prototype machine [9]. In the experiments, aluminum billets were rolled under an area reduction of 38%. Employing more than 6 pairs of forming tools with different combinations of forming angles and stretching angles, the critical rolling condition was discovered based on the experimental results.

For example, when forming angle $\alpha=15^o$ is fixed, several pairs of forming tools with different stretching angle β were applied. It was found the first critical rolling condition point is under the circumstance of $\alpha=15^o$ and $\beta=5^o$. Using the results of these experiments, the critical friction coefficient curve shown in Figure 3.4 was generated. In Figure 3.4, the predicted critical friction conditions from Equation (3.15) and (3.21) are also plotted. As illustrated in the figure, it is found that Bowden's model slightly under-predicts the critical rolling condition while Oxley's model substantially over-predicts it. The difference in accuracy between the two models is linked to the fact that Oxley's model is based on two-dimensional slip-line field theory while Bowden's model is developed for full three-dimensional contact. Under plane strain conditions, Oxley's model assumes that no material deformation occurs perpendicular to the direction of sliding, which is the not the case in CWR. Hence, Bowden's model more accurately describes the interfacial friction in CWR.

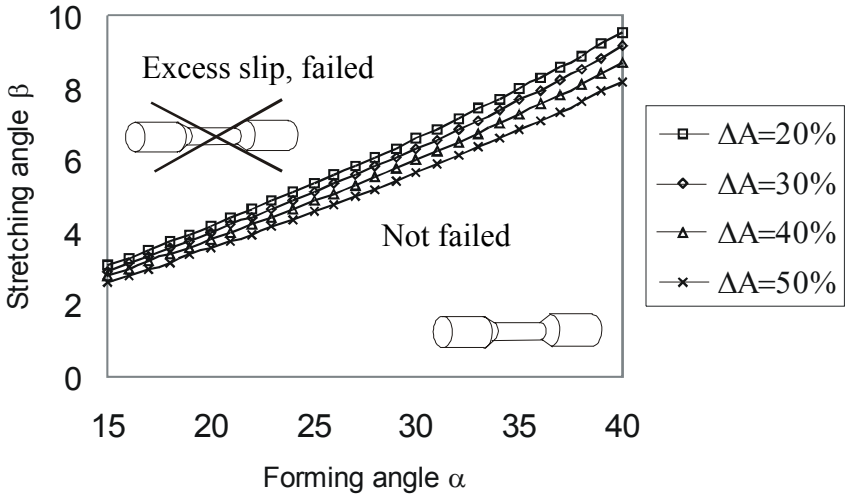

(a) Bowden's model

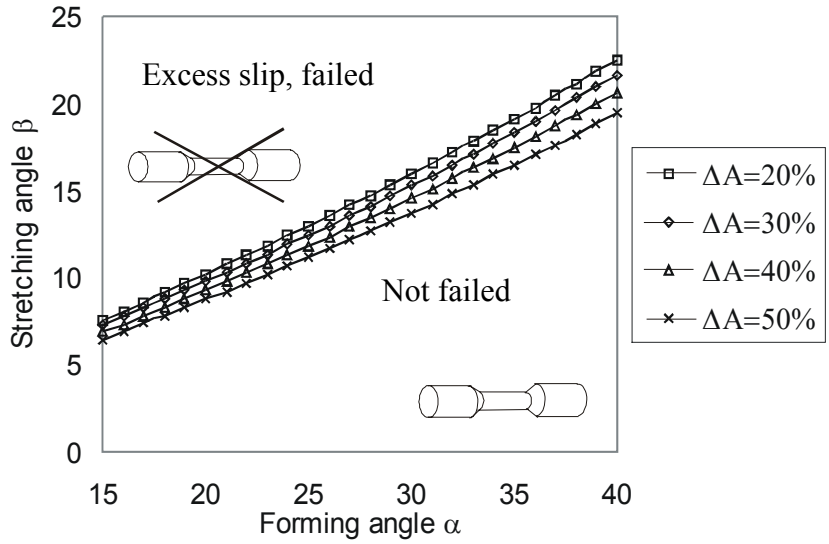

(b) Oxley's model ($f = 0.05$)

Figure 3.3 Critical geometric parameters (d_1/D_1=0.2)

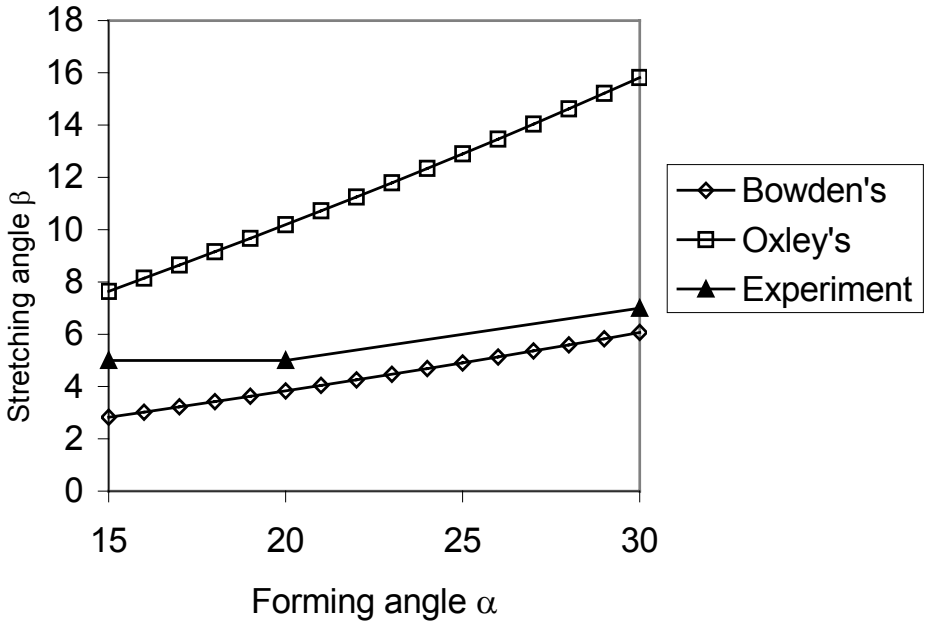

Figure 3.4 Comparison of Bowden's, Oxley's and experimental results (ΔA=38%)

3.3 Numerical Analysis

In this section, numerical and experimental methods are introduced for characterizing the nature of interfacial slip in a two-roll CWR operation. First a three-dimensional finite element model (FEM) model was generated for numerical investigation. After being validated by comparison to experiments performed with a CWR prototype machine, it was parameterized to study the influence of CWR process parameters on the global slip at 32 different operating conditions. Based on numerical results, the influences of process parameters in the cross wedge rolling are ascertained and discussed.

3.3.1 Overview of Finite Element Method (FEM)

In order to perform accurate numerical analyses for characterizing the interfacial slip behavior between the forming tools and workpiece in a two-roll CWR process, a three-dimensional finite element model was created using the ANSYS/LS-DYNA [23] program.

One of the primary advantages of the finite element method is its ability to parametrically analyze variables that are difficult to examine experimentally. This section reviews the basic concepts of the finite element method. The first step of any finite element simulation is to discretize the actual geometry of the structure using a collection of finite elements. Each finite element represents a discrete portion of the physical structure. The finite elements are joined by shared nodes. The collection of nodes and finite elements is called the mesh. The number of elements used in a particular mesh is referred to as the mesh density. In a stress analysis, the displacements of the nodes are the fundamental variables in FEM calculation. Once the nodal displacements are known, the stresses and strains in each finite element can be determined easily.

Numerous commercial packages are available for finite element analysis; the predominant three softwares are ANSYS, ABAQUS [24] and NASTRAN [25]. This study is based on ANSYS.

One component of ANSYS is ANSYS/LS-DYNA, which combines the LS-DYNA [26] explicit finite element program with the pre- and postprocessing capabilities of the ANSYS program. The explicit method of solution used by LS-DYNA provides fast solutions for short-time, large deformation dynamics, quasi-static problems with large deformations and multiple nonlinearites, and complex contact/impact problems. ANSYS/LS-DYNA supports both 2-D and 3-D explicit elements, and features an extensive set of single-surface, surface-to-surface and node-to-surface contact. Using this integrated product, we can model the structure in ANSYS, obtain the explicit dynamic solution via LS-DYNA, and review results using the standard ANSYS postprocessing tools. The procedure for an explicit dynamic analysis is in the three main steps are: 1) Build the model, 2) Apply loads & boundary conditions and obtain the solution, and 3) Review the results.

3.3.2 Geometric model of Two-roll CWR FEM

As shown in Figure 3.5, the model is composed of a cylindrical workpiece (25.4 mm diameter) and two wedge-shaped dies that are bounded by two rolls. Both the dies and rolls are considered rigid so that only the workpiece undergoes plastic deformation during the CWR process. In the model, all of the components are meshed using eight-noded, single point integration solid elements. For mimicking the operating conditions in the actual two-roll CWR process, the workpiece and both the dies and rolls are constrained to only allow the rotation about their central axes.

3.3.3 Material model of Two-roll CWR FEM

A strain-rate dependent constitutive plasticity model was defined for the workpiece in the FEM numerical analysis. Isotropic and kinematic contributions may be varied in the model by adjusting the hardening parameter β between 0 (kinemetic hardening only) and 1 (isotropic hardening only). Strain rate is accounted for using the Cowper-Symonds model [27] that scales the yield stress by the strain rate dependent fact as shown below:

$$\sigma_y = \left[1 + \left(\frac{\dot{\varepsilon}}{c}\right)^{\frac{1}{p}}\right]\left(\sigma + \beta E_p \varepsilon_p^{eff}\right) \tag{3.22}$$

where σ_0 is the initial yield stress, $\dot{\varepsilon}$ is the strain rate defined as $\dot{\varepsilon} = \sqrt{\dot{\varepsilon}_{ij}\dot{\varepsilon}_{ij}}$, c and p are the Cowper-Symonds strain rate parameters. ε_p^{eff} is the effective plastic strain.

$$\varepsilon_p^{eff} = \int_0^t \left(\frac{2}{3}\dot{\varepsilon}_{ij}^{\,p}\dot{\varepsilon}_{ij}^{\,p}\right)^{\frac{1}{2}} dt \tag{3.23}$$

The plastic strain rate is the difference between the total and elastic (right superscript e) strain rates:

$$\dot{\varepsilon}_{ij}^{\,p} = \dot{\varepsilon}_{ij} - \dot{\varepsilon}_{ij}^{\,e} \tag{3.24}$$

E_p is the plastic hardening modulus:

$$E_p = \frac{E_t E}{E - E_t} \tag{3.25}$$

where E_t and E are the plastic and elastic moduli of the workpiece.

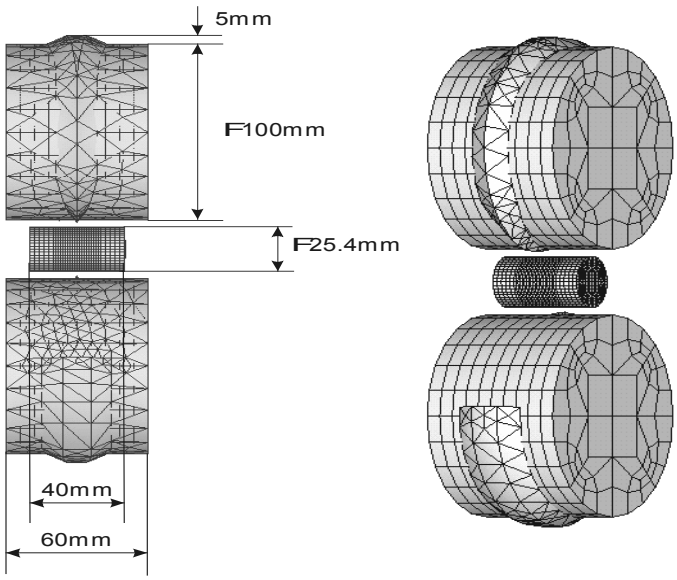

(a) Finite element model of two-roll CWR process

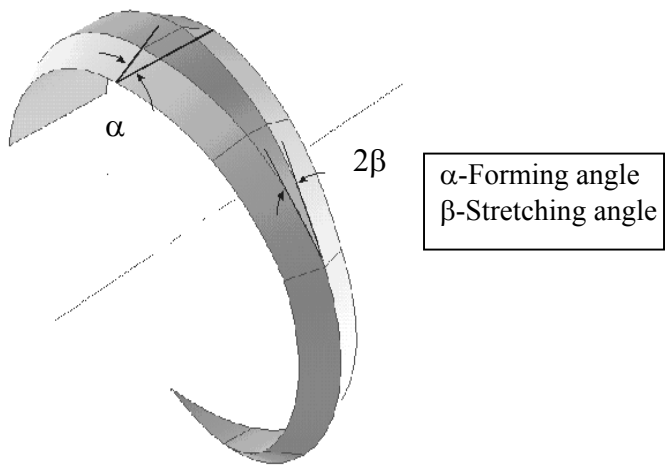

(b) Forming tool model in the two-roll CWR simulation

Figure 3.5 Two-roll FEM of CWR

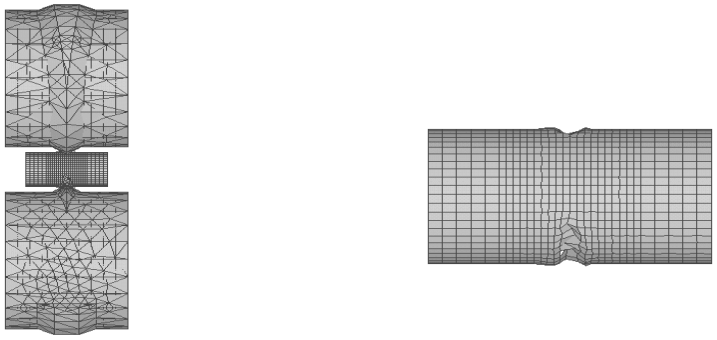

(a) The workpiece in the knifing zone

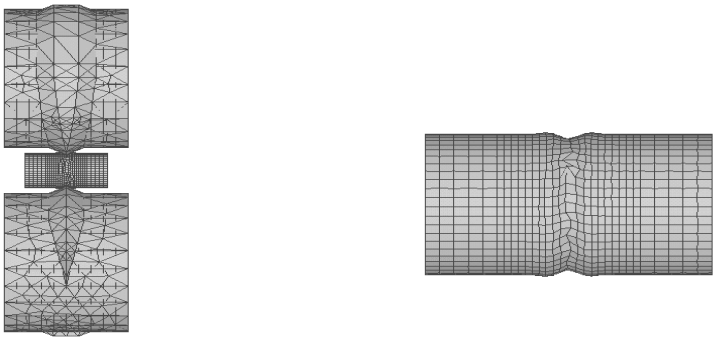

(b) The workpiece in the guiding zone

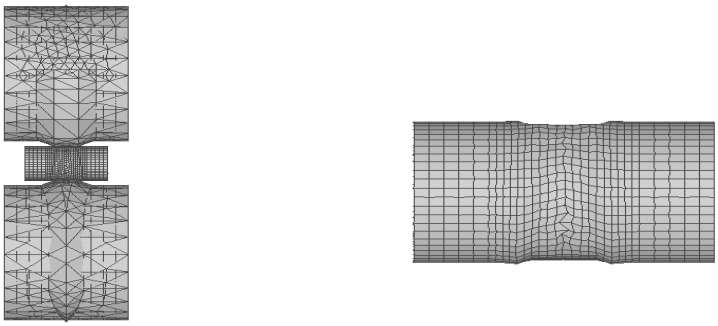

(c) The workpiece in the stretching zone

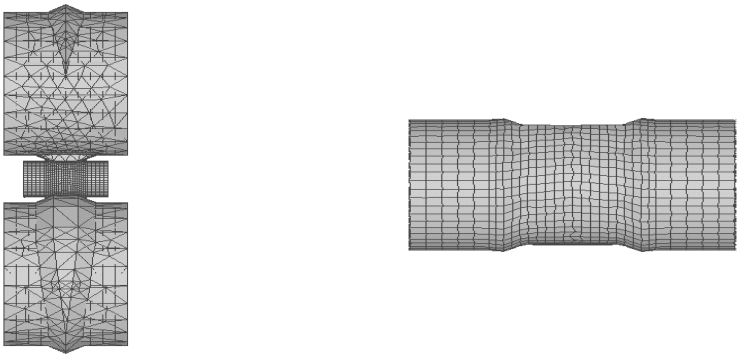

(d) The workpiece in the sizing zone

Figure 3.6 CWR process simulation by two-roll FEM

In the simulations, the strain rate parameters c and p were defined as 6500 and 4.0 respectively [28]. During the simulations, the workpiece and tools were respectively defined to be Aluminum 1100 H16 alloy and hardened carbon steel 1045. The material properties that are related to the numerical investigation are listed in the Table 3.1. For the purpose of capturing the actual slip characteristics of the two-roll CWR process, a surface-to-surface contact algorithm was employed to define the contact interaction between the workpiece and dies along with a classical coulomb friction model. Simulations of two-roll CWR process in four zones and corresponding deformations of workpiece are depicted in Figure 3.6.

Table 3.1Mechanical properties of the studied materials

Materials	Density (Mg/m^3)	Young's modulus (GPa)	Poisson's ratio	Yield strength (MPa)	Tangent Modulus (MPa)
Aluminum1100 H16	2.710	69.0	0.330	138.0	202.0
Tool steel 1045	7.801	207.0	0.292	NA	NA

3.3.4 Experimental validation of numerical model

For the purpose of validating numerical results, an experimental approach has been employed in this study to ascertain the dependence of CWR tool parameters on the interfacial slip. As a first step towards ascertaining the interfacial slip behavior of the workpiece, CWR experiments were carried out using the CWR prototype machine illustrated in Figure 3.7.

In the prototype machine, a cylindrical workpiece is bonded by two flat-wedge forming tools. The tools are parallel to one another and equidistant from the workpiece in both the horizontal and vertical directions. As decided by the construction of the prototype machine, the

fixture constrains the forming tools in both the vertical (z) and out-of-plane (y) directions. Hence motion of the tools was confined to motion in the horizontal (x) direction. As the apparatus construction was symmetric, it was not necessary to constrain the workpiece. With the prototype machine, cylindrical billets with diameters ranging from 15~60 mm can be deformed using a pair of the flat-wedge forming dies that are driven in the horizontal direction using hydraulic cylinders. The cylinders provide enough force to fully shape the billet material while maintaining a constant velocity. If there is enough frictional force to rotate the workpiece, the final deformed shape of the billet material will be controlled by the geometry of the forming dies.

In order to establish the merit of the two-roll FEM model, it is essential to first validate the FEM model with experimental results. By means of this machine, CWR experiments were performed on Aluminum 1100 H16 workpiece specimens with a diameter of 25.4 mm under the operating condition of $\alpha=30^0$, $\beta=5.25^0$ and $\Delta_A=22\%$. After testing, the deformed geometries of the workpiece specimens were measured using a coordinate measuring machine and averaged. As a first step in validating the FEM model, the experimentally measured workpiece profile from the CWR experiments were compared to that predicted from the FEM model. As shown in Table 3.2, the predicted workpiece profile from the two-roll CWR model coincides well with the experimental one where the average difference in geometry is less than 2%. This shows that the FEM model adequately captures the plastic deformation within the workpiece during the two-roll process examined.

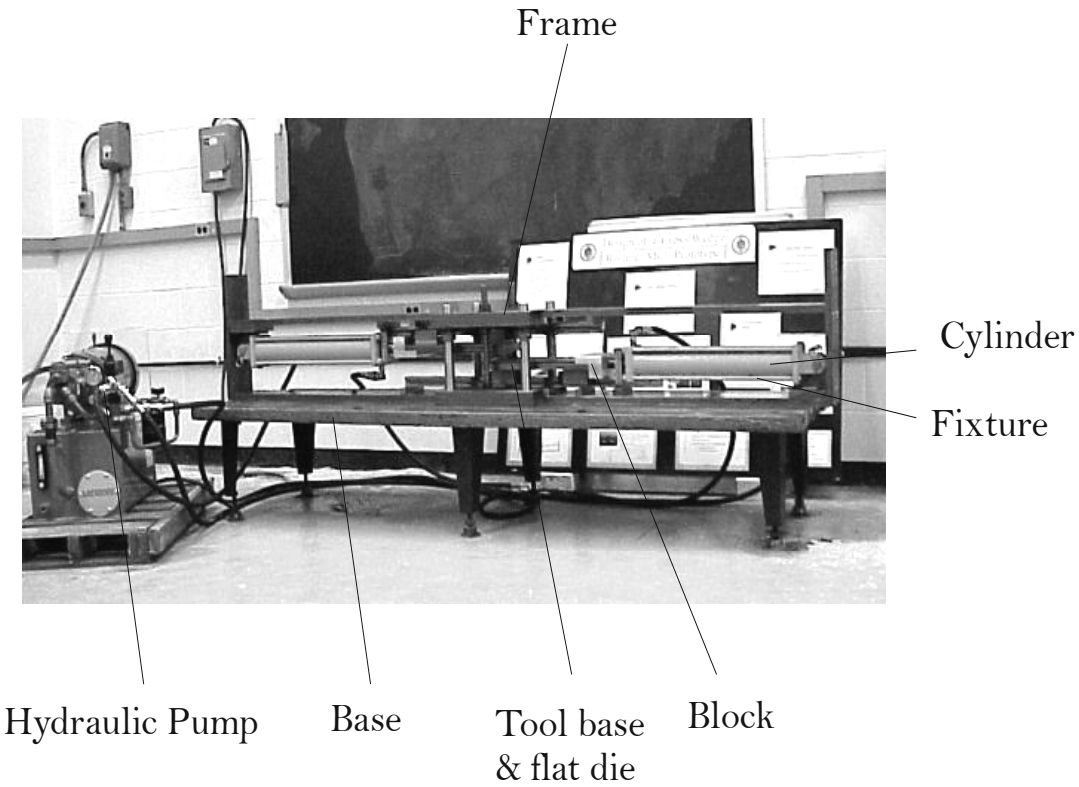

(a) Overall view of the CWR machine

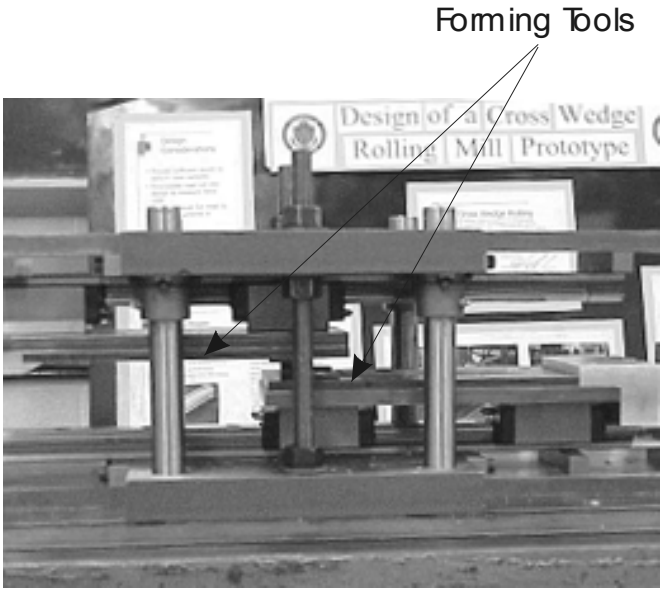

(b) Central portion of the CWR machine

Figure 3.7 CWR prototype machine

Since the billets deformation behavior is a secondary variable with respect to the critical rolling condition, further validation of the two-roll FEM model was required to study the critical friction. This step included performing CWR experiments with the prototype machine at friction coefficient levels above and below the critical values predicted in Section 3.2.1 (Eq. (3.12)). Then by implementing these same friction coefficient values in the finite element model, a second comparison could be made between the experimental and numerical results. Using the apparatus, two different friction experiments were conducted under the operating conditions (Δ_A=22%, $\alpha=30^0$ and $\beta=5.25^0$) specified in Section 3.2 for the proposed CWR process. In the first experiment, relatively smooth tools (R_a=1.42 μm) were utilized. For this tooling, specialized experiments were performed to measure the friction coefficient [4] between the tools and the workpiece (R_a=1.72 μm). These experiments found the tool-workpiece friction coefficient to be approximately 0.149 for the conditions examined. A total of ten CWR experiments were performed using the CWR prototype machine with the 1.72 μm surface roughness tooling. In each case, excess interfacial slip failure was found to occur at the transition between the knifing zone and guiding zone and the workpiece was ultimately malformed. Likewise, when the FEM model was run under the identical operating conditions and with a friction coefficient of 0.149, excess slip failure also occurred at the end of the knifing zone. Excess interfacial slip failure was expected for the smooth tools, as Equation (3.12) predicts a critical friction value of 0.201 for the conditions examined.

Table 3.2 Comparison of the experimental and FEM predicted workpiece profiles

Position (mm)	Radius (mm) (FEM)	Radius (mm) (Experiment)	Position (mm)	Radius (mm) (FEM)	Radius (mm) (Experiment)
-20.0	12.667	12.70	20.0	12.667	12.70
-18.0	12.661	12.70	18.0	12.661	12.70
-16.0	12.668	12.70	16.0	12.668	12.70
-14.0	12.661	12.835	14.0	12.661	12.835
-12.0	12.673	12.991	12.0	12.673	12.991
-10.0	12.894	13.313	10.0	12.894	13.313
-8.667	12.990	12.855	8.667	12.990	12.855
-7.333	12.420	12.287	7.333	12.420	12.287
-6.0	11.872	11.487	6.0	11.872	11.487
-4.667	11.506	11.487	4.667	11.506	11.487
-3.333	11.505	11.487	3.333	11.505	11.487
-2.0	11.505	11.487	2.0	11.505	11.487
-0.667	11.505	11.487	0.667	11.505	11.487

A second set of experiments were then conducted using the CWR prototype machine after the tooling used in original experiments were lightly sandblasted to increase the average surface roughness value to 3.76 μm. Increasing the surface roughness increases the real contact area and corresponding friction forces during motion between the tools and workpiece. In this regard, the experimentally measured friction coefficient value between the rough tools and the workpiece was found to be 0.210. Ten billets were again rolled with the CWR prototype machine with the rougher tools. In each of the ten cases, the billet cross section was properly formed. The finite element results at μ=0.21 identically were found to initially rotate, and the interfacial slip was negligible. The fact that excess interfacial slip failure was identically found in both the CWR experiments and FEM model for μ=0.149, but it did not occur at μ=0.210, demonstrates that the two-roll numerical model accurately captures the character of the critical interfacial friction during the CWR process.

3.4 Numerical Results of Excessive Slip

Using the two-roll FEM model, numerical simulations were performed by applying a constant rotational velocity to both cylindrical rollers. A total of 32 simulations were performed in order to ascertain the influence of friction coefficient, forming angle and stretching angle on the interfacial slip. These simulations corresponded to the following operating conditions:

Friction coefficient (μ): 0.2, 0.3, 0.35, 0.4, 0.5, 0.6

Forming angle (α):20^0,30^0,40^0

Stretching angle (β): 3.5^0,5.25^0,7.5^0

Area reduction (Δ_A): 22%, 27%, 32%, 38%, 45%, 53%

Forming velocity (v): 0.1m/s, 0.2m/s, 0.4m/s, 0.8m/s, 1.6m/s

Excess interfacial slip between the forming tools and the workpiece in CWR is the primary cause for improperly formed product cross sections. In addition to helping eliminate excess slip failure, determining the magnitude of interfacial slip between the forming tool and workpiece is essential for designing the length of each section of the forming tool.

3.4.1 Influence of friction coefficient

As discussed previously, the interfacial friction has been found to have a decisive role in controlling the amount of interfacial slip in the flat-wedge CWR process [29]. For the purpose of determining the influence of friction coefficient on the interfacial slip in the two-roll CWR process, Figure 3.8 was created to illustrate the variation of the accumulative global slip with the friction coefficient during the process for $\alpha=30^0$ and $\beta=5.25^0$. Examining Figure 3.8, several

trends can be observed for the relationship between the global slip and the interfacial friction coefficient. The first trend shows that the global slip continuously increases over the entire CWR process. This is to be expected, as the global slip will increase due to geometric effect and local friction variations even when a critical friction coefficient is achieved. This trend also implies that care should be taken to maintain a critical friction coefficient and adequate tool length in each zone of the tool to achieve the desired dimensional accuracy of the product. The second trend found in Figure 3.8 is that the global slip monotonically increases with decreasing interfacial friction coefficient. When the friction coefficient decreases from 0.3 to 0.2, however, the global slip is found to undergo a substantial jump in value in all of the forming zones. This jump is to be predicted by Eq.(3.12), which forwards a critical friction coefficient value of 0.201.

The separate influence of the friction coefficient on the global slip in the knifing, guiding, stretching and sizing zones is shown in Figure 3.9. In the figure, all the curves in each zone behave identically with the global slip monotonically increasing with the friction coefficient. The nature of the global slip in stretching zone, however, is significantly different than the other zones. In the other three zones (especially in the guiding and sizing zones), the amount of the slip substantially increases when the friction coefficient decreases from 0.3 to 0.2. This demonstrates that in these three zones, the critical friction coefficient was not attained for μ=0.2 and the interfacial slip was dramatically influenced. Examining Figure 3.9 (c) for the stretching zone, however, there is not a dramatic increase in the global slip between μ=0.2 and μ=0.3. In fact, all of the global slip curves gradually increase with decreasing friction coefficient. This phenomenon can best be explained by the fact that the large stretching deformations experienced by the billet in the stretching zone actually decrease the critical friction coefficient value. This is due to the fact that the contact area between the workpiece and forming tools increases in the

stretching zone, thus allowing a smaller critical friction coefficient to be required to maintain the minimum static friction force. The critical friction coefficient in the stretching zone is μ=0.181 from Eq.(3.12). Hence, as indicated in Figure 3.9 (c), a jump in the global slip does not develop. For the same reason, the global slip in the first zone increased less than that in the guiding and sizing zone since the workpiece in the knifing zone also experiences relatively large stretching deformations. These difference are predicted by Eq.(3.12) and were found by Xiong [17].

Examining the influence of friction coefficient from another point of view, the effective plastic strain can be monitored at internal points within the workpiece during the CWR process. As shown in Figure 3.10 (a), the two points located on the longitudinal axis were chosen for monitoring the strain. The effective strain .vs. time plots are shown for these two points in Figures 3.10 (b) & (c). Examining the plastic strain for the first point in Figure 3.10 (b), it is shown that all of the friction curves behave identically except for μ=0.2. For the μ=0.2 case, the plastic strain is identical to the other curves in the knifing zone but experiences a significant decrease in value in the guiding zone. Such a decrease in plastic strain indicates that the critical friction value was not attained and the tool intermittently plowed through the workpiece. It is important to note that such a tendency was also found in the experimental results where interfacial slip failure occurred at the knifing-guiding zone transition for μ=0.149.

Turning our attention to point 2, it is found that all of the friction coefficient curves behave identically in the first two zones of the tool. As shown in Figure 3.10 (c), the strain is significantly lower for μ=0.2 in the stretching and sizing zone. This again indicates that a critical friction coefficient was not achieved for the μ=0.2 case. Comparing Figure 3.10 (b) and 3.10 (c), the primary difference from the two plots is the point at which the excess slip failure becomes apparent. For point 2, the excess slip is not found until the sizing zone simply because of its

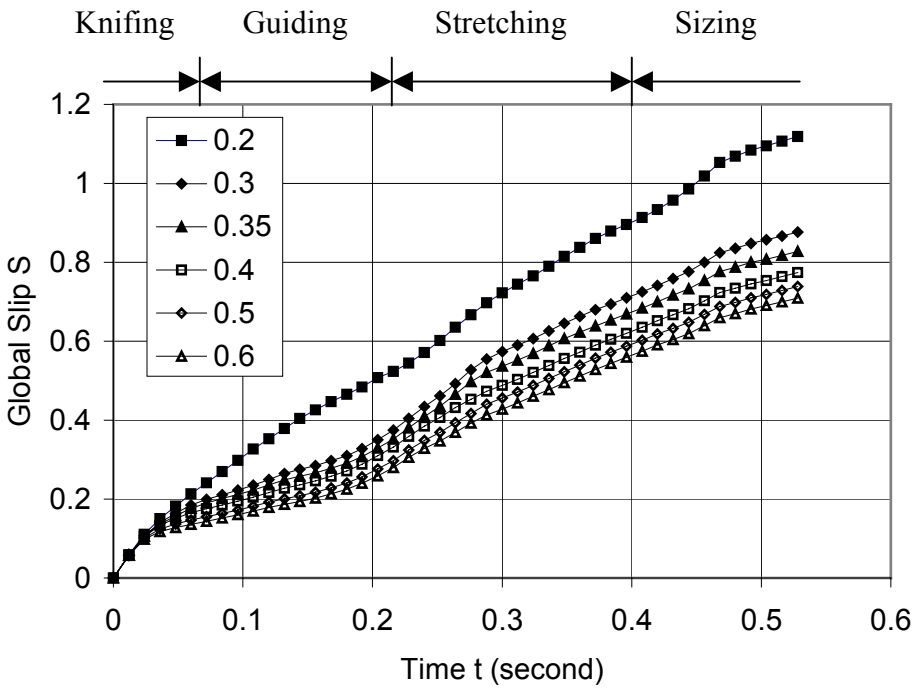

Figure 3.8 Variation of interfacial slip with friction coefficient (α=30°, β=5.25^o, ΔA=22%, and v=0.4m/s)

location. Since point 2 is located a short distance away from point 1 in the longitudinal direction, it doesn't experience significant plastic strain until the stretching zone, where the deviation in strain values occurs.

3.4.2 Influence of forming angle

The forming angle, α, is found to be a key tooling parameter for ensuring the product quality in the CWR process. In order to establish the effect of the forming angle on the global slip, Figure 3.11 was produced for $\beta=5.25^0$ and $\mu=0.5$. A friction coefficient of $\mu=0.5$ was chosen to isolate the influence of the forming angle on the global slip. In Figure 3.11, it is found that the global slip monotonically increases with increasing α. Examining the figure, a significant difference in slip variation with α is observed above $\alpha=30^0$. When the forming angle increases from 20^0 to 30^0, the interfacial slip is nearly identical over all four zones of the tool. In contrast to this, the global slip increases about 34% when the forming angle is increased from 30^0 to 40^0. Hence, the forming angle near 30^0 may be regarded as a threshold value for reducing the interfacial slip in the *specific* CWR tooling configuration examined in this section. The increase in slip between 30^0 and 40^0 is likely due to the fact that the contact area between the workpiece and forming tools decreases with increasing the forming angle. As discussed previously, the decrease in contact area will reduce the interfacial friction force that drives the workpiece to rotate. Hence, the minimum friction force (at $\mu=0.5$) required to rotate the workpiece is not maintained at $\alpha=40^0$, as indicated by the significant increase in the global slip.

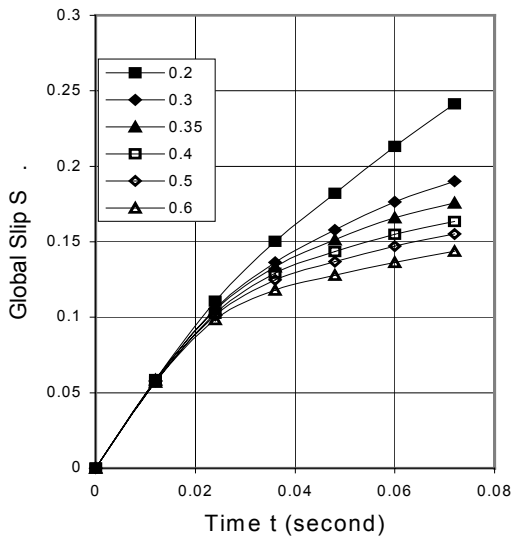

(a) Knifing zone

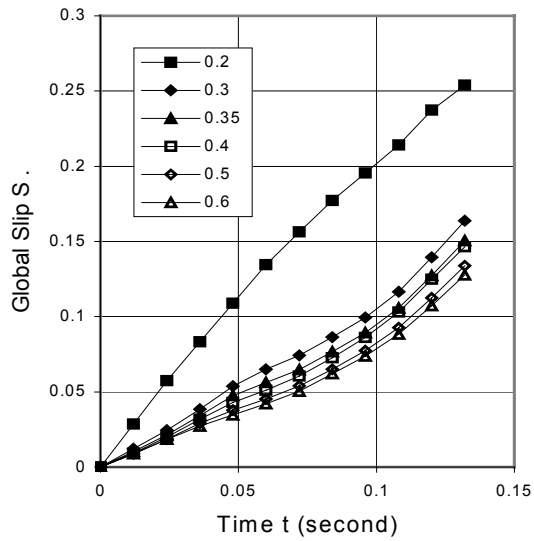

(b) Guiding zone

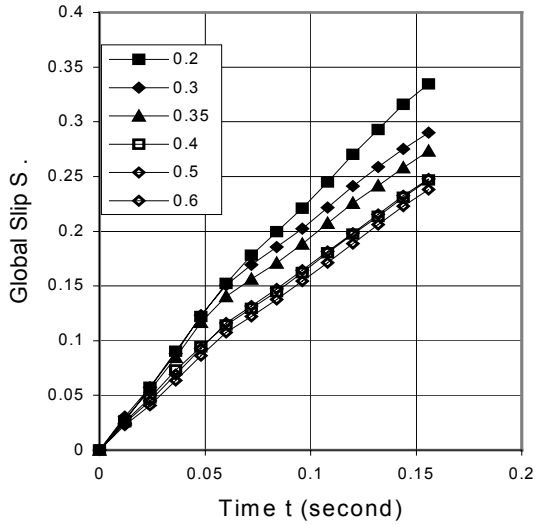

(c) Stretching zone

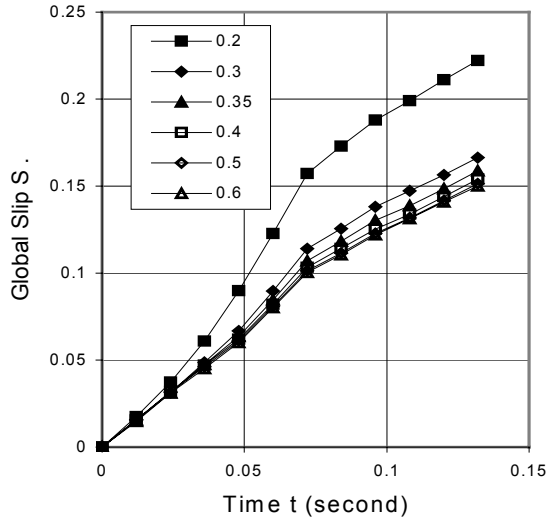

(d) Sizing zone

Figure 3.9 Variation of interfacial slip with friction coefficient in each zone (α=30°, β=5.25^o, ΔA=22%, and v=0.4m/s)

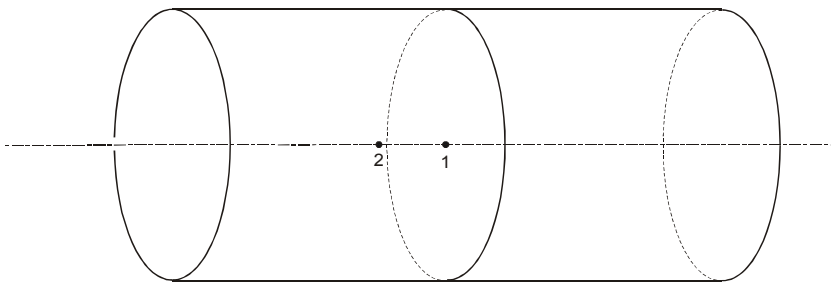

(a) Location of the investigated points

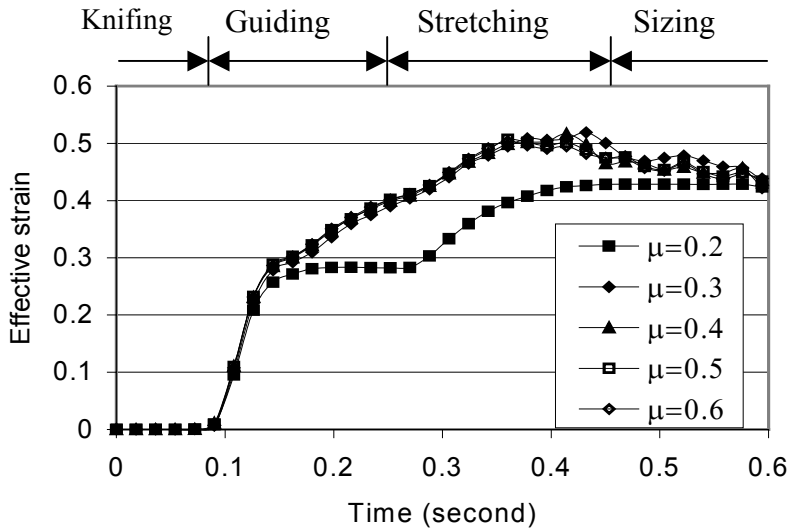

(b) At point 1 (central point)

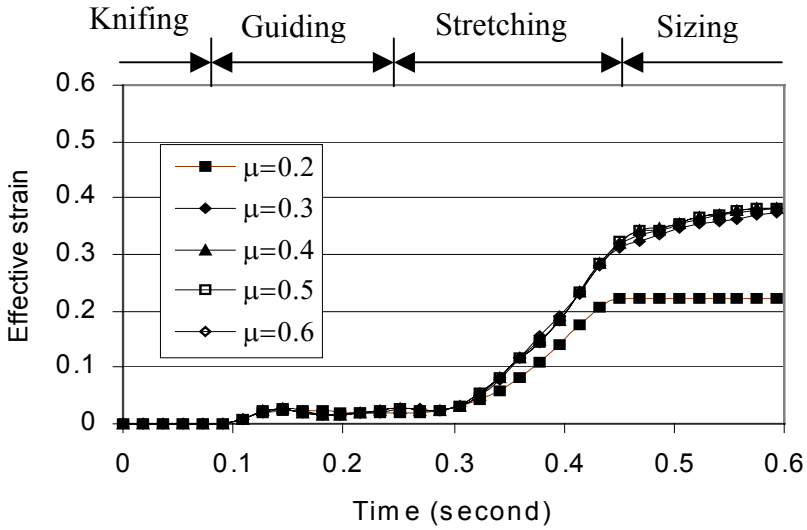

(c) At point 2

Figure 3.10 The effective strain distribution of the selected points with different friction coefficients (α=20°, β=5.25^o, ΔA=38%, and v=0.4m/s)

The separated influences of the forming angle on the slip behavior in the four tool zones are plotted in Figure 3.12. As shown in Figures 3.12 (a)~(d), it is found that the amount of the global slip in the knifing and stretching zones is significantly larger than that in the guiding and sizing zones. In the knifing zone, the material flow is controlled by the nature of the initial contact between the forming tools and the workpiece. Upon initial tool-workpiece contact, the contact area is small and therefore is strongly influenced by the forming angle as shown by the sharp increase in global slip for $\alpha=40^0$ in Figure 3.12 (a). In the stretching zone, the workpiece undergoes large amounts of plastic deformation and the contact area is largely dependent on the forming angle α. Corresponding to this, the influence of the forming angle on the interfacial slip is strong, which again leads to a dramatic increase in α for an angle of 40^0. Conversely, in the guiding and sizing zones, the tool is forming a uniform surface along the workpiece and only a small amount of plastic work is done. In both of these zones, the forming angle therefore has a less significant impact on the contact area, particularly in the sizing zone of Figure 3.12 (d).

3.4.3 Influence of stretching angle

The stretching angle β is another important tooling parameter in the CWR process. For ascertaining the influence of the stretching angle on the interfacial slip, Figure 3.13 was created under the conditions of $\alpha=30^0$and $\mu=0.5$. Since the stretching angle only changes the contact condition between the forming tools and the workpiece after the knifing and guiding zones, Figure 3.13 plots the global slip in the stretching and sizing zones for the three β values. As depicted in Figure 3.13, there is no clear variation of the global slip. This finding is coincident with industrial and experimental results found in the literature and is likely due to the contacting influences of decreased material flow resistance and increased contact area that occurs for larger

stretching angles [2],[30]-[32]. When the workpiece material is in a fully plastic state, it will offer less frictional resistance to the forming tool. A larger stretching angle will then require a higher friction coefficient to maintain a steady rolling condition if analysis is based solely on flow resistance. If one considers that the contact area and corresponding friction force increase with β, however, it would be expected that the slip would decrease with β. Hence, the influence of β on the global slip should be considered a complex function of material flow and contact area, as indicated by Figure 3.13.

3.4.4 Influence of area reduction

As defined in Equation (3.17), the area reduction, ΔA, is a measure of the amount of workpiece deformation. In this section, we investigate the relationship between the area reduction and the global slip. For the purpose of highlighting the influence of ΔA, the global slip was plotted as a function of area reduction under the conditions of $\alpha=20^0$, $\beta=5.25^0$, v=0.4m/s and $\mu=0.5$. In Figure 3.14, it is found that the amount of the global slip increases with area reduction. Closely examining the figure, we find that the global slip at a 27% area reduction is 40% lower than the 53% area reduction at the end of the sizing zone. This tendency is to be expected considering Equation (3.12). In Equation (3.12), it is shown that the critical friction coefficient increase with ΔA. Therefore, for a constant friction coefficient, the global slip should increases with ΔA. From a physical point of view, the excess slip is more likely to occur at higher area reductions due to the decrease in flow resistance of the workpiece material. Such a finding is important to the design of a two-roll CWR machine where a greater friction coefficient is required at larger area reductions.

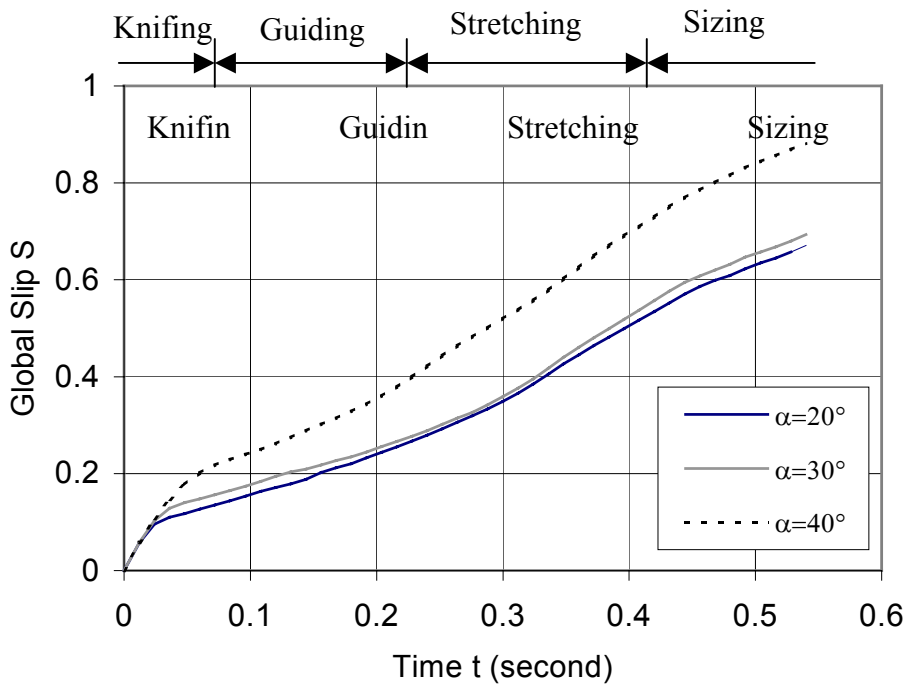

Figure 3.11 Variation of interfacial slip with forming angle (μ=0.5, β=5.25^o, ΔA=22%, and v=0.4m/s)

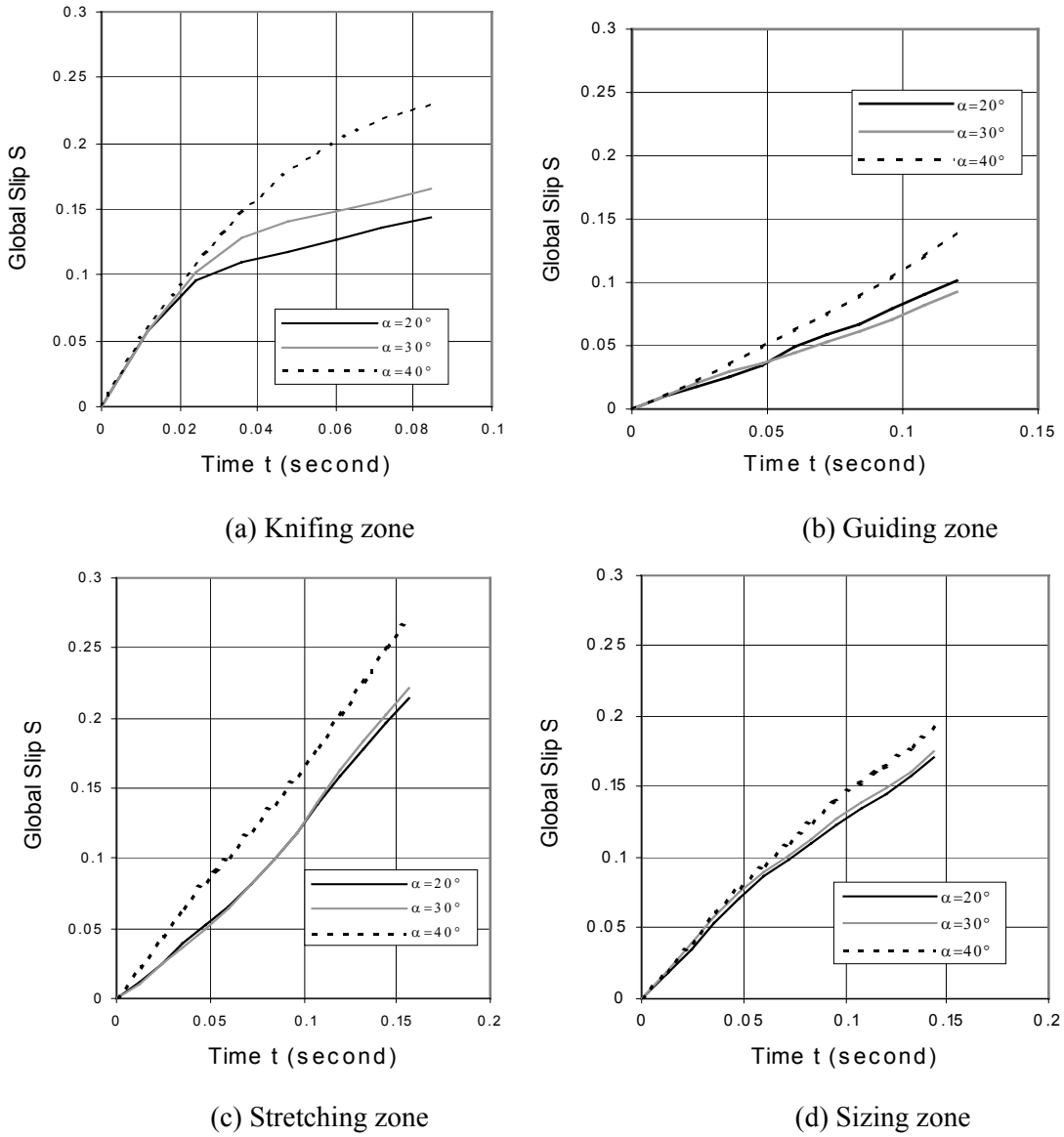

(a) Knifing zone

(b) Guiding zone

(c) Stretching zone

(d) Sizing zone

Figure 3.12 Variation of interfacial slip with forming angle in each zone (μ=0.5, β=5.25^o, ΔA=22%, and v=0.4m/s)

3.4.5 Influence of forming velocity

To investigate the influence of forming velocity on the global slip, Figure 3.15 was created to show the instantaneous variation of the global slip during the CWR process. In this figure, the range of velocity is valued from 0.1m/s to 1.6 m/s under the working condition of $\alpha=20^0$, $\beta=5.25^0$, $\Delta A=38\%$ and $\mu=0.5$. From Figure 3.15, it is obvious that the global slip significantly increases with forming velocity. At higher operating velocities, the workpiece experiences larger strain rate deformations. From the constitutive Equation (3.22) in the FEM, the strain hardening of the workpiece material increases at increased strain rates. Therefore, at higher forming velocities, more energy is required to deform the workpiece to its desired shape because of the increased hardening of the workpiece material. Such an increase in resistance of the workpiece material to plastic deformation at higher velocities clearly has a strong influence on the interfacial slip. In fact, careful observation of Figure 3.15 indicates that the forming velocity has a significant effect on the variation of the interfacial slip over the range of forming velocities investigated. In these working conditions, the minimum and maximum values of the global slip are 0.295 and 0.687 corresponding to the lowest and highest forming velocities. However, over the same range of velocities, the plastic flow stress of the workpiece material only increases by 12% as calculated by Eq. (3.22). For this reason, the high forming velocity is rarely applied in industry. In general, the forming velocity is less than 0.6m/s. Hence, it can be deduced that forming velocity, and its sequential influence on the material plastic flow resistance has a substantial effect on the global slip.

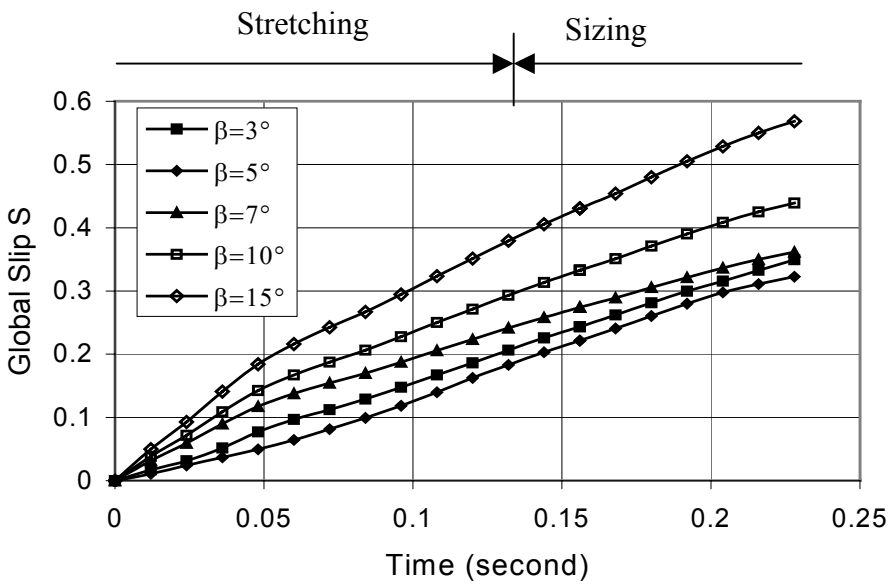

Figure 3.13 Variation of Interfacial Slip with Stretching Angle (μ=0.5, α=30°, ΔA=22%, and v=0.4m/s)

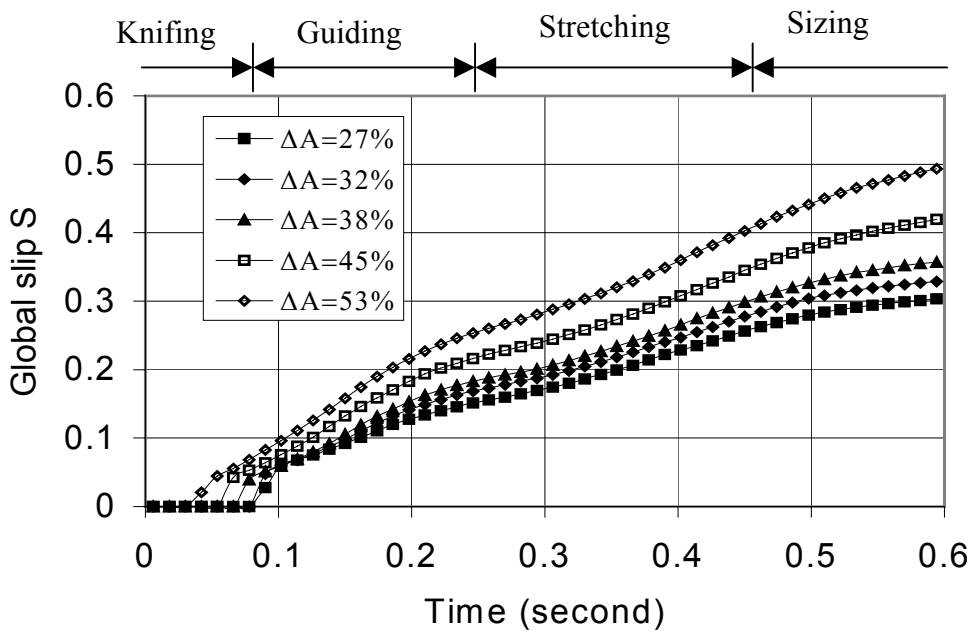

Figure 3.14 Variation of interfacial slip with area reduction (α=20°, β=5.25^o, μ=0.5, and v=0.4m/s)

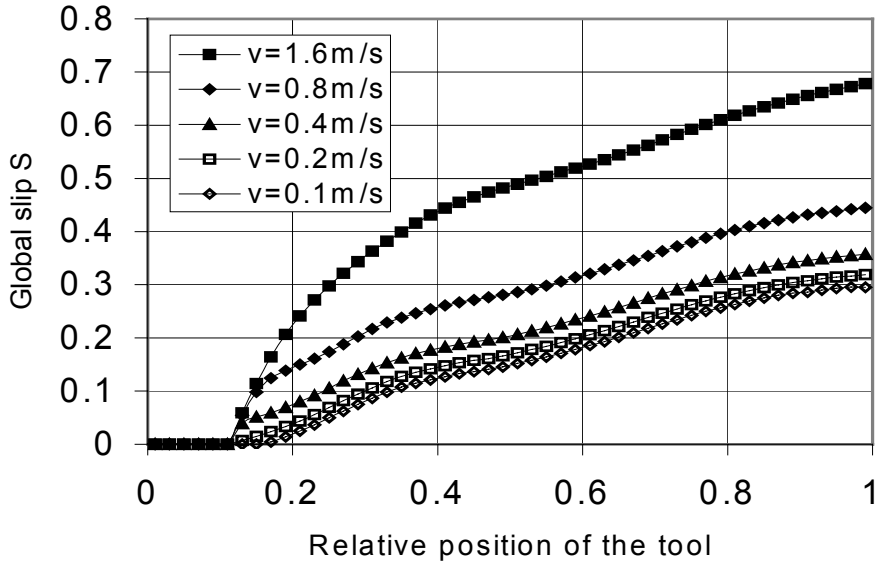

Figure 3.15 Variation of interfacial slip with forming velocity (α=20°, β=5.25^o, μ=0.5, and ΔA=38%)

3.5 Summary of Interfacial Slip Analysis

Analytical and explicit dynamic numerical models of a two-roll CWR process were introduced for the purpose of analyzing the critical interfacial friction in a two-roll CWR process. Using Bowden and Oxley's classical friction models, expressions for the critical rolling condition in the CWR process were generated as a function of tool geometry (α and β) and area reduction (ΔA). As specialized experiments are currently required to predict the critical friction in CWR, the derived expressions represent an important step towards automating CWR tooling design. Based on comparisons to actual CWR experiments, the critical friction condition predicted by Bowden's friction model was found to be more accurate than that predicted by Oxley's model. Furthermore, since Bowden's model under-predicts the required tooling and process parameters, it can be considered a safe criterion for designing CWR tooling with respect to eliminating excess slip failure.

The numerical model was validated by comparison to experiments, and several process parameters were analyzed by the FEM to establish their influence on the global slip. The conclusions of the numerical results are given below:

1. The friction coefficient between the forming tools and the workpiece was found to be the key parameter in controlling the interfacial slip in the two-roll CWR process. The global slip was found to increase with decreasing friction coefficient and a critical friction coefficient was found between μ=0.2 and μ=0.3.
2. The critical friction coefficient was found to be the same in all of the tool zones except the stretching zone. In the stretching zone the critical friction coefficient was found to decrease due to the larger contact area and frictional forces.

3. Increased forming angles resulted in larger global slip values due to the corresponding decrease in contact area with α. A substantial increase in the global slip was found between $\alpha=30^0$ and $\alpha=40^0$. The forming angle was found to have the least influence on the global slip in the guiding and sizing zones where less significant plastic deformations occur.
4. The global slip was found to be a complicated function with the stretching angle due to the combined influence of a decreased frictional resistance and an increased contact area that occur at larger β values.
5. With the increase of area reduction and forming velocity, the global slip increases due to the decreased flow resistance of the workpiece material.

4.0 INTERNAL DEFECT IN CWR

Although internal defects in CWR have been investigated for decades, the influence of CWR tool parameters on the deformation and internal stress-strain characteristics of the workpiece is still not completely understood. This is primary due to the fact that it is very difficult to analyze the workpiece's deformation behavior during an actual CWR operation. For this purpose, an experimental and numerical approach has been employed to ascertain the dependence of CWR tool parameters on the deformation behavior, the formation of internal defects, and productivity in a CWR process.

4.1 Experimental Investigation of Internal Defects in CWR

4.1.1 Experiment Working Conditions

Using the flat-wedge CWR experimental apparatus described in Section 3.3.4, experiments were performed to quantify several tool designs that lead to the formation of internal failures. Specifically, the forming (α), stretching (β) angles and area reduction (ΔA) of tool were varied in a specific CWR process. After a specimen was rolled in the apparatus, the formed part was examined to determine whether internal voids had formed. This was done by cutting the final parts in the longitudinal direction. If a defect was found, its size was measured using a coordinate measuring machine. In the experiments conducted for this work, 1100 H16 alloy aluminum and C11000 copper billets, with a diameter of 25.4 mm and a length of 50 mm, were deformed in the CWR experimental apparatus. The deformation of the billets was performed at room temperature under unlubricant conditions for different area reductions.

Using this experimental apparatus, experiments were performed at more than 50 distinct operating conditions to quantify several tool designs that lead to the formation of internal failures. Specifically, the forming (α), stretching angles (β), and area reduction (ΔA) of tool were varied in the CWR process as shown below (see Appendix):

Forming angle: 15°, 20°, 30°

Stretching angle: 3°, 5°, 7°

Area reduction: 28%-55%

Workpiece material: aluminum 1100 and copper C11000

After a specimen was rolled in the apparatus, the formed part was examined to determine whether internal voids had formed. This was done by cutting the final parts in the longitudinal direction. If a defect was found, its size was measured using a coordinate measuring machine. For each pair of forming angle and stretching angle, there are 3-5 different area reduction conditions examined to study the formation of internal defects. It should be noted that a minimum of three billets were rolled at each operating condition.

4.1.2 Internal Defect Generation Analysis

After performing the CWR experiments, the author believe that the initiations of central cavities or voids within the workpiece are an example of Mannesmann effects [2]. Pater et al [33] likewise acknowledged that the Mannesmann effect is the most common defect that limits the usage of the CWR technique. In the Mannesmann effect, the central portion of a billet becomes significantly weakened when it is rotated and compressed in the diameter direction. This weakness ultimately leads to the formation of axial voids. In the two-roll and flat-roll CWR

processes, axial voids are the most common because the central portion of the workpiece is subject to compression in the direction normal to the tool surface and to tension in the lateral direction. As the workpiece rotates, the compression and the tension regions alternate every 90°. This cyclic loading may cause fatigue cracks in the material after several rotations of the workpiece, as has been pointed out in the literature [13]. In the following paragraphs, mechanisms that lead to Mannesmann defect generation in CWR will be discussed.

From the viewpoint of plastic deformation, the metal flow of the workpiece is an unrecoverable deformation process. Investigated with the scanning electron microscope, a deformed CWR workpiece that will develop a large axial void has been found to have small inclusions (voids) by the start of the stretching zone. The opening of tiny flaws around these inclusions during the stretching zone generates cracks, which are formed when the workpiece deforms in the axial direction. Depending on the operating conditions, several cracks can merge to create macroscopic breakage [34]. With respect to the metallography that leads to macroscopic failure, the inclusions are nucleated by three probable mechanisms [35]: 1) fracture of the particle-matrix interface, 2) failure of the particle, and 3) micro-cracking of the matrix surrounding the inclusion. As stated earlier, large tensile stresses are the primary factor in initiating internal defects. If the tensile stresses are large enough in magnitude, they can also accelerate void growth by opening matrix material in the direction of the highest principal stress. Once the distance between two cracks is comparable to their lengths, micro-scale necking can merge two cracks as shown in Figure 4.1 (a).

When examined at a microscopic level, both shear and tensile stresses promote internal void formation. Shear stresses are the driving force for the movement aggregation and deformation of voids. In CWR, it is most likely that large tensile stresses initiate the opening of

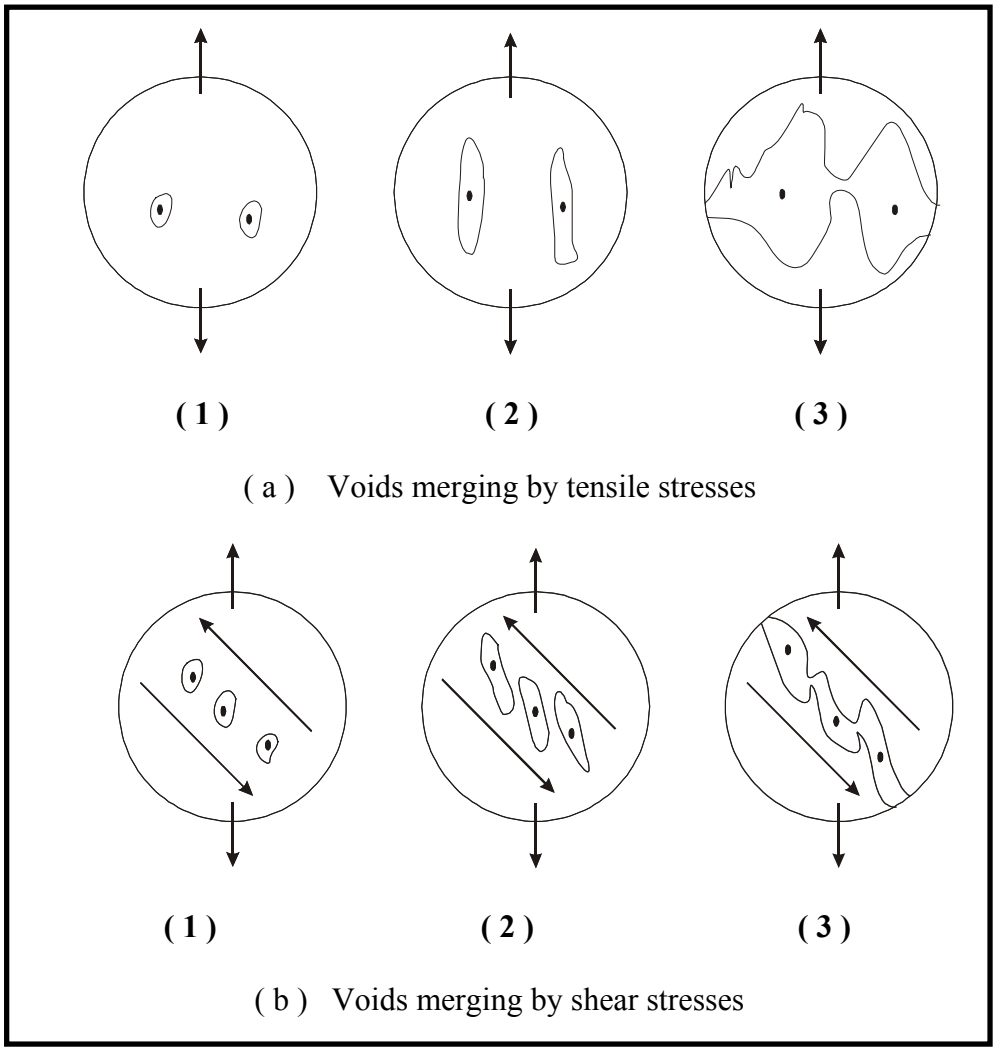

Figure 4.1 Illustration of the microscopic void development

voids and local shear determines the level of aggregation and the size of voids within the workpiece. The process of shear failure is shown in the region 2 on Figure 4.1(b). Under tensile stresses, the slip deformation occurs between the metal crystals. The preferential slips initiates at a 45^0 angle to the tensile stress direction. Hence the voids with inclusions are turned to this direction and elongated by the shear stresses. With the development of the slippage, voids merge into macroscopic fractures.

4.1.3 Morphology of Internal Defects

In order to study the morphology of the internal defects, several different material specimens generated under conditions known to produce internal defects were examined. For both aluminum and copper, there were internal cracks generated under some working conditions while defect did not exist under some other working conditions (see Figure 4.2). Therefore, changing only forming angle or area reduction can cause an internal defect. In order to characterize the evolution of internal defects, a series of experiments were performed. Figure 4.3 shows the longitudinal cross section of cylindrical billets that was produced for the conditions $\alpha=15^o$, $\beta=7^o$ and $\Delta A=38\%$. The specimen in this figure was obtained during a test interrupted at the end of the knifing zone. As shown in Figure 4.3, there is visible evidence of the initiation of the internal defect at the end of the knifing zone. In fact, a large elongated void is found with a series of smaller voids near the vicinity of the large void's "crack" tips. The presence of such a void pattern indicates that the internal defects in CWR are the result of void initiation that results from hydrostatic tension within the central regions of the workpiece. Once a series of small voids are formed, they expand and coalesce under the triaxial hydrostatic forces experienced by the

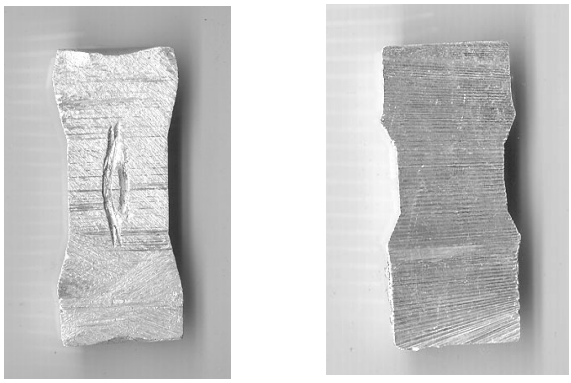

Internal void (α=15°,β=7° & ΔA=38%)

Defect-free (α=30°,β=7° & ΔA=38%)

(a) Aluminum samples

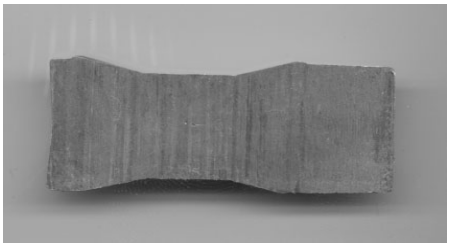

(α=15°,β=5° & ΔA=25%)

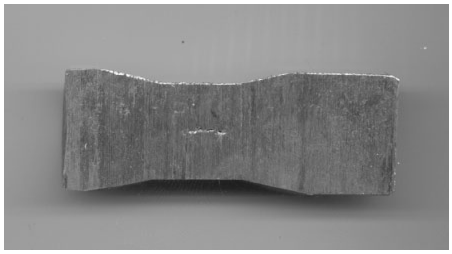

(α=15°,β=5° & ΔA=35%)

(b) Copper samples

Figure 4.2 Internal defects with different materials

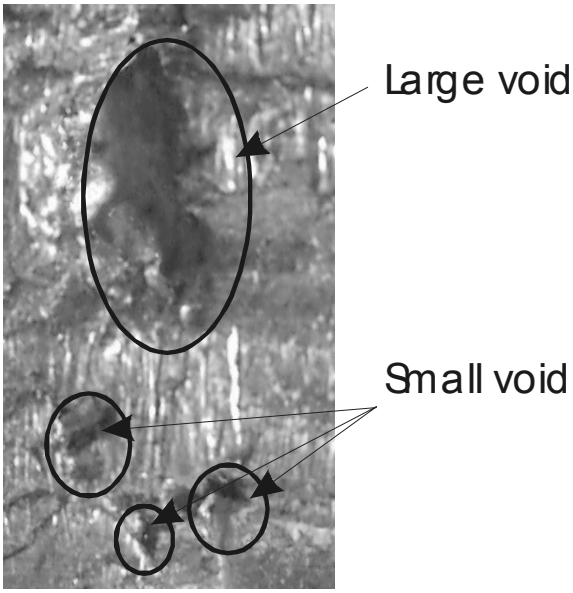

Figure 4.3 Profile view at the end of knifing zone. (α=15°, β=7° and ΔA=38.2%)

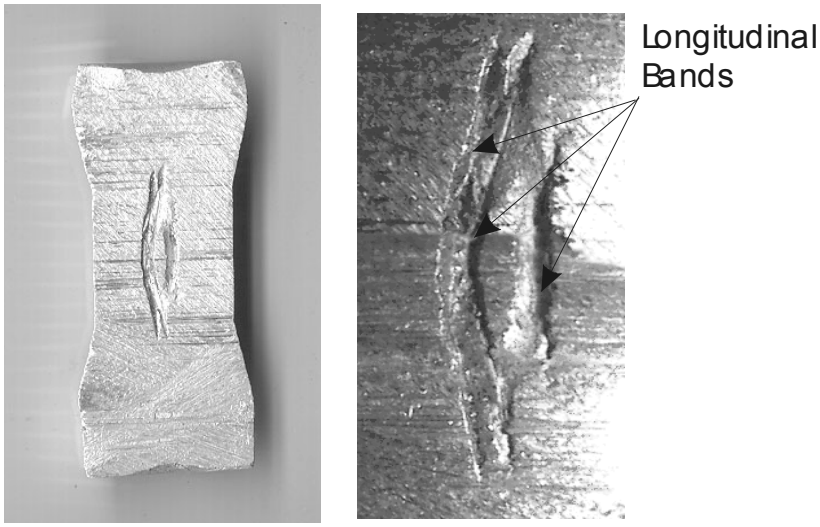

(5x)

Figure 4.4 Profile view at the end of last zone. (α=15°, β=7° and ΔA=38.2%)

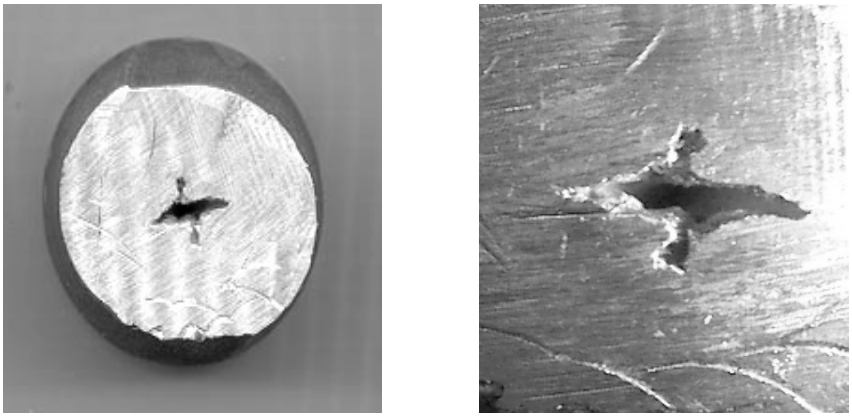

(a) Overall view. (b) Central part (5x).

Figure 4.5 Profile views from horizontal cross-section (α=15°, β=7° and ΔA=38.2%)

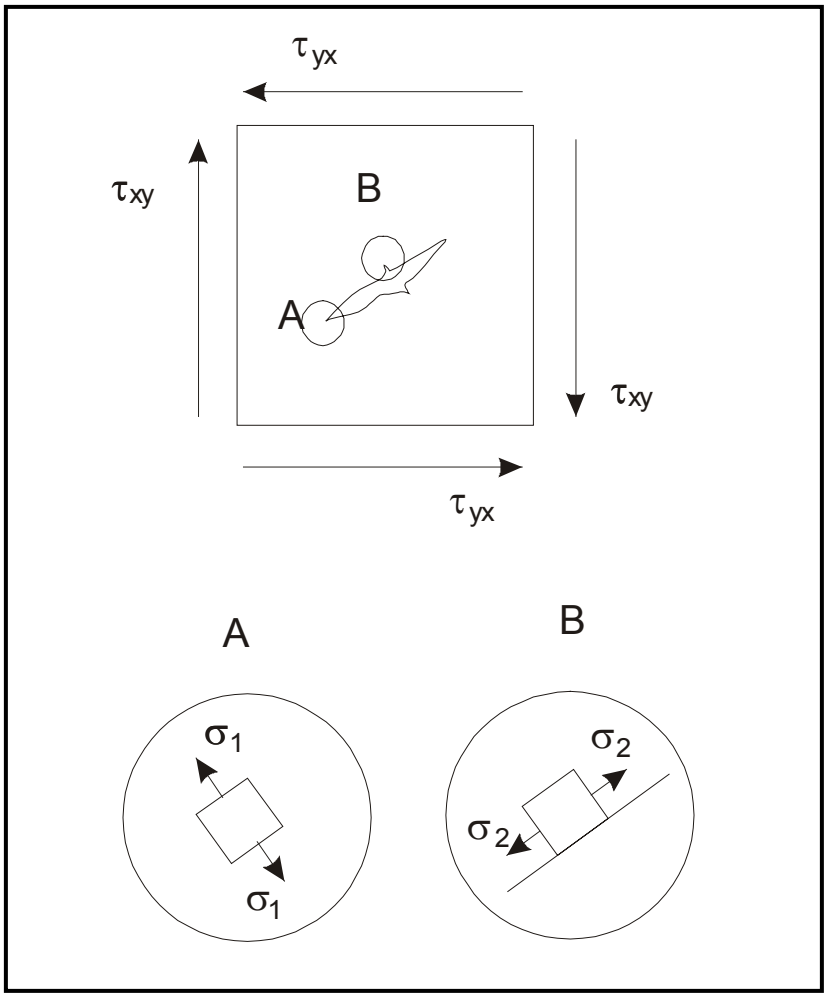

Figure 4.6 Illustration of the crack generation

billet in the stretching zone of the CWR process. Such a point is supported in Figure 4.4, which shows the presence of a large internal void at the end of a complete CWR process. The fact that the central region of the workpiece is characterized by several different voids in the early stages and a substantial large void after the billet has undergone significant axial stretching in the stretching zone would indicate that void growth and bridging have taken place.

Another interesting aspect to examine in Figure 4.4 is the presence of what appear to be parallel longitudinal bands in the central section of the workpeice. In order to gain a better understanding of the longitudinal bands, a fully rolled workpiece was cut through the horizontal cross section. As shown in Figure 4.5, the horizontal cross-section shows that the large internal void has a distinct cruciform shape. This shape likely develops during the CWR process because the workpiece orientation plastic flow direction changes as the workpiece rolls between the forming tools. The cruciform shape found in the horizontal cross-section explains the longitudinal bands since the shape of the large void will depend on where the billet is axially cut.

The cruciform phenomenon can be explained by examining the combined influence of shear and tensile stresses during the rolling process. The morphology of the cruciform crack is shown in Figure 4.6 where a major crack is generated in the direction of maximum principle stress (σ_1). The crack elongates in a direction normal to the maximum principle stress due to tensile force in the principal direction. Examining section B along the free surface of the crack, the stress state is characterized by the second principal stress (σ_2). It is the second principal stress that leads to the generation of a minor crack within the workpiece. As shown in Figure 4.5, this crack is normal to the principal direction, and will be expanded during rotation of the workpiece.

4.1.4 Effect of Forming Angle

The forming angle controls the size of the contact area between the tools and the workpiece in the knifing and guiding zone. In these zones, a smaller forming angle signifies a sharper tool, which reduces the contact area and produces a more localized plastic deformation. In the stretching and sizing zones, the forming angle establishes the geometry of the shafts shoulder such that a large value of α leads to a small draft angle. In order to establish the effect of the forming angle on the formation of internal defects, Figure 4.7(a) was created for $\beta=5^o$. In Figure 4.7(a), it is found that the void size monotonically increases with decreasing the forming angle. When the forming angle is $\alpha=30^o$, no internal voids are found until $\Delta A=55\%$. For $\alpha=20^o$, however, internal void formation begins at ΔA values near 30%. This phenomenon is more obvious at $\alpha=15^o$, where the size of void increases rapidly from 31 mm^2 under the second area reduction to 119mm^2 at the largest area reduction. Therefore, smaller forming angles can accelerate the formation and enlarge the size of internal voids. Such a finding was similarly found in Mise et al [36]. In his work, Mise explained that a smaller forming angle increased the piercing action of the tool in the knifing zone, which ultimately leads to stress concentrations that produce small internal voids in the early stages of CWR. Figure 4.7(b) shows that when the stretching angle is increased to 7°, the variation of void size and forming angle maintains the same trend but the size of the void enlarges substantially. This can be explained by the fact that when the stretching angle is increased, the workpiece is subjected to more axial plastic deformation. As discussed previously, larger amount of deformation in the axial direction will accelerate void growth by opening the matrix material in the principal stress direction.

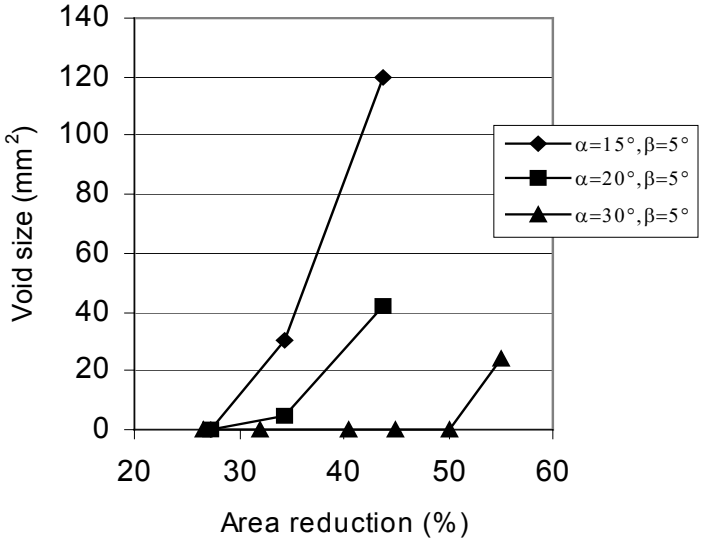

(a) β=5°

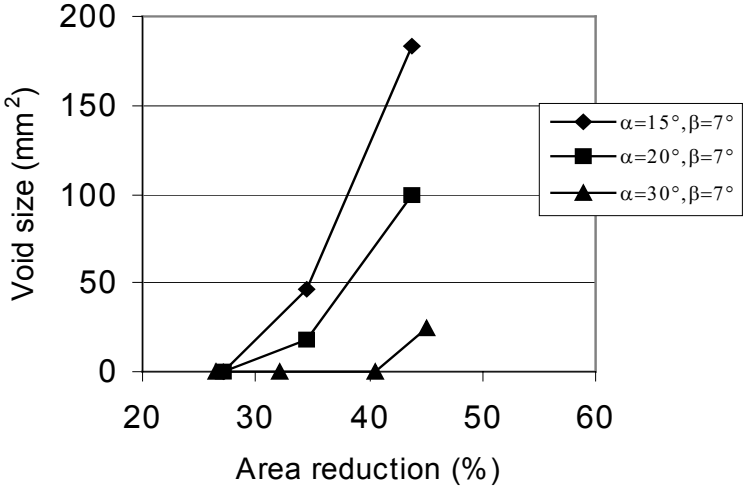

(b) β=7°

Figure 4.7 Relationships between the forming angle and void dimensions.

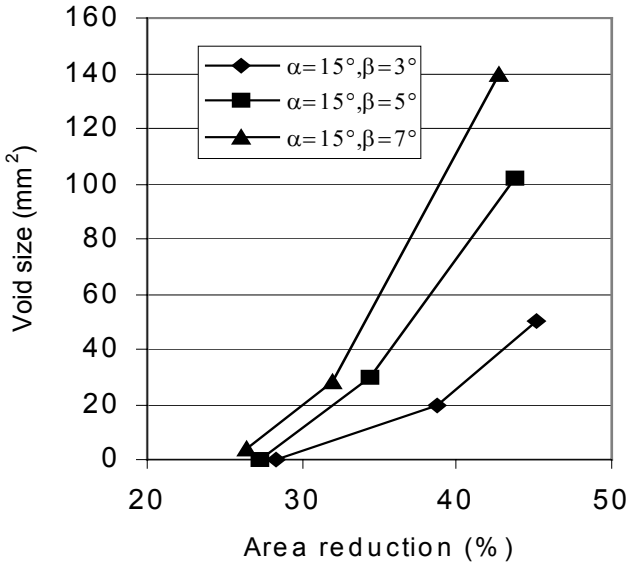

(a) α=15°

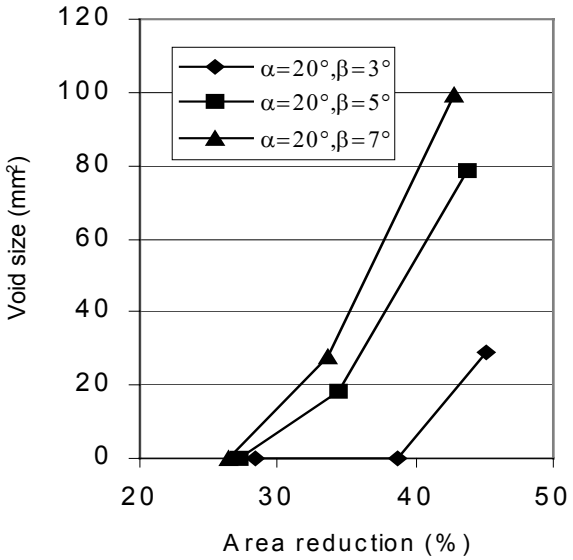

(b) α=20°

Figure 4.8 Relationships between the stretching angle and void dimensions

4.1.5 Effect of Stretching Angle

The stretching angle β is another important tooling parameter in the CWR process. It determines the amount of axial deformation experienced by the workpiece. Larger stretching angles within the tool lead to more elongation of the workpiece. For ascertaining the influence of the stretching angle on the formation of an internal void, Figure 4.8(a) was created under the condition of $\alpha=15^{o}$. In this figure, the internal void increases when the stretching angle increases. This finding is coincident with the results by Fu and Dean [36]. For large β, the billet enlarges rapidly in the axial direction, which accelerates the growth of small internal voids created in the knifing and guiding zones. Examining the figure, a significant difference in the void size variation with β is observed at $\beta=5^{o}$. When the stretching angle increases from 3° to 5°, the internal void increases about 110%. Hence, for the conditions examined, the larger stretching angles ($\beta=5^{o}$) made a substantial difference in the size of the internal void. When the forming angle is increased to 20° (Figure 4.8(b)), the size of void declines. This can be attributed to the fact that the shear stress within the central portion of the workpiece decreases with increasing forming angle.

4.1.6 Effect of Area Reduction

The final parameter, ΔA, is simply a measure of the amount of radial reduction of the workpiece. The larger the value of ΔA, the larger the radial compression experienced. Since CWR is a volume conservative process, larger area reduction values will increase the overall length of the workpiece. Figures 4.7 and 4.8 both show that the size of internal void increased

with an increase in area reduction. Considering the area reduction of the workpiece, it is indicated that there is a critical value of area reduction for which internal defects will develop. This is expected as the effective stress and strain within the central portions of the workpiece increase and become more non-uniform with an increase in area reduction. Hence, if any portion of the workpiece is in tension during the rolling process, the tensile forces will be larger as ΔA increases. Large tensile forces are known to open internal voids. In addition, from the viewpoint of low cycle fatigue theory, the larger the area reduction the more severe the stress cycles that will be experienced by the central position of the workpiece, thus increasing the possibility of void formation.

4.1.7 Effect of workpiece material

As shown in Figure 4.2, the workpiece material property has a significant influence on the generation of internal defect. During the CWR experiments, it was observed that the dimension of the cracks is substantially different between Aluminum 1100 and Copper C11000 billets. In each experiment, a crack was found. The size of the void was always greater in the aluminum material. It is important to note, however, the location of the void was identical for both workpiece materials and that voids were always found in both materials under a condition that produced a defect. One explanation for the difference in the size of the workpiece voids can be found by examining energy. In the CWR process, the volume of the workpiece was held constant regardless of the material being analyzed. Copper C11000, with the higher density, has a larger mass than Aluminum 1100. Since the energy required to deform the workpiece is proportional to its mass, the Copper C11000 clearly requires the more energy to be demanded

from a given tool geometry and operation condition in a CWR process. Considering the actual working conditions, however, the forming tools were specified to maintain a constant velocity and identical interfacial friction. Therefore, since the amount of deformation and energy within the process was held constant, the Aluminum 1100 is more prone to having larger internal defect. With a lower density, the aluminum will have less material during the volume persevering deformation process.

4.1.8 Deformation Coefficient

When considering the likelihood of an internal void forming during the CWR process, it is clear that the nature and magnitude of the workpiece deformation plays a critical role. The deformation of the workpiece is complex, as it is includes axial stretching, radial height reduction, and circumferential flow that varies with each zone of the forming tool. In last section, how the generation of voids varied with tool geometry and area reduction was described. In this section, we will attempt to predict the likelihood of an internal void forming in the workpiece based on its overall deformation. For this purpose, the non-dimensional deformation coefficient ε_{def} is defined as:

$$\varepsilon_{def} = \frac{2L_2'}{d_0 - d_1} \cdot \frac{L_1'}{L' - L_1'} \cdot \frac{A_0 - A_1}{A_0} \tag{4.1}$$

In Equation (4.1), d_0 and A_0 are the diameter and cross-sectional area before deformation; A_1 is the length and cross-sectional area after deformation; d_1, L_1', L_2' and L' are shown in Figure 4.9.

Note: $\Delta A = \frac{A_0 - A_1}{A_0} = 1 - \left(\frac{d_1}{d_0}\right)^2$.

In the expression for the deformation coefficient, the first term demonstrates the influence of the forming angle α on the deformation, the second term shows the affect of the stretching angle β on the deformation, and the last term reflects the influence of the area reduction on the deformation. In addition, the last two terms in the expression for ε can be regarded as the ratio of deformed volume $L' \cdot (A_0 - A_1)$ to the un-deformed volume $(L' - L_1') \cdot A_0$ of the final product.

The relationship between the deformation coefficient and the forming and stretching angles of the tool are shown in Figures 4.10(a) and (b). Examining Figure 4.10(a), it is shown that when the forming angle α increases the deformation coefficient decreases. For example, at an area reduction of 35%, the deformation coefficient is 0.78 for a forming angle of 15° and only 0.28 for a forming angle of 30°. This is to be expected, as the contact area and amount of plastic deformation within the workpiece decreases at higher forming angles. From Figure 4.10(b), the deformation coefficient is shown to increase with the stretching angle β. This trend also is expected, as larger stretching angles increase the amount of plastic deformation in the axial direction. It is important to note that these trends were similarly found in Figure 4.7 and Figure 4.8.

In addition to defining the amount of workpiece deformation that occurs for a specific CWR operation, the deformation coefficient can also be used to predict the likelihood of void generation. Based on the experiments conducted at more than 50 different operating conditions, it was found that rolling conditions with a deformation coefficient ***greater than 0.6 yielded an internal void*** while rolling conditions with a deformation coefficient lower than 0.6 did not. Such

a finding is fundamental to CWR tooling design, as it demonstrates that for a desired geometry of the final product, the likelihood of void formation can be predicted a priori. Hence, tooling design can be streamlined to eliminate conditions that lead to internal failures. It is important to note at this point, however, that the deformation coefficient value of 0.6 should only be considered valid for the billet material and geometry studied in this work. Further work is planned to establish whether the critical deformation coefficient varies with billet material and initial geometry or if $\varepsilon=0.6$ can be applied globally.

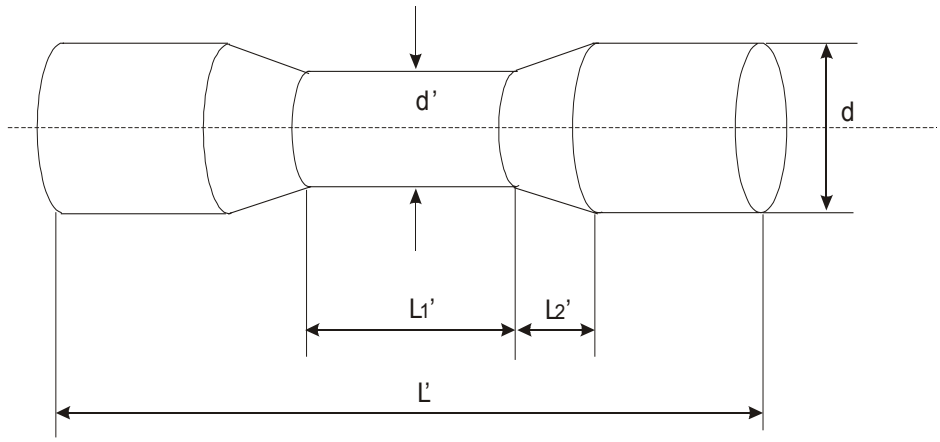

Figure 4.9 Definition of the parameters of deformation coefficient

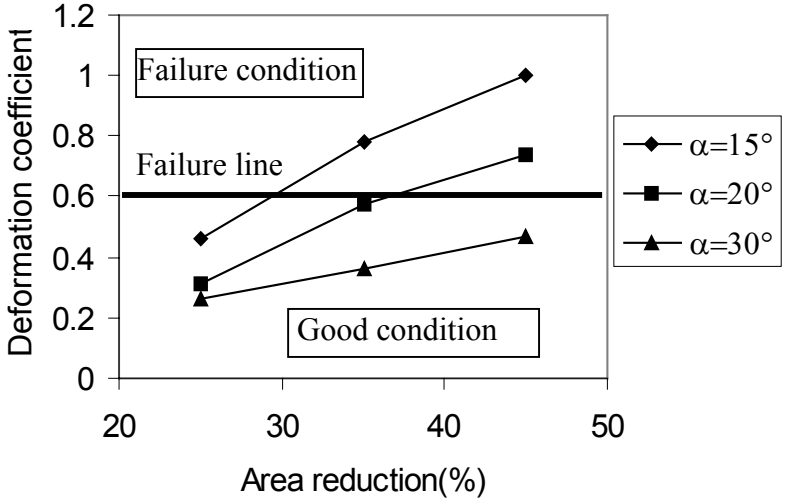

(a) relationship between deformation coefficient and forming angle

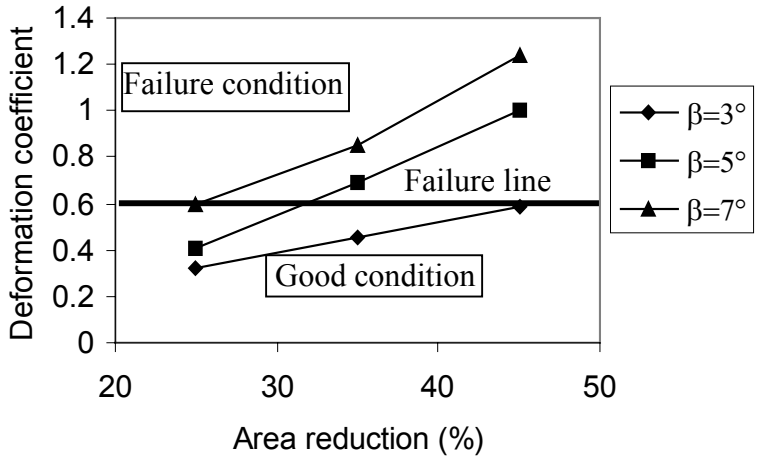

(b) relationship between deformation coefficient and stretching angle

Figure 4.10 Relationship between deformation coefficient and tool geometry

4.2 Numerical Study of Internal Defects in CWR

As description previously, the author believe that the initiations of central cavities or voids within the workpiece are a special case of Mannesmann effects [38], which are the most common defect that limits the usage of the CWR technique. In the Mannesmann effect, the central portion of a billet becomes significantly weakened when it is rotated and compressed in the diametric direction. This weakness ultimately leads to the formation of axial voids. Several other researchers have proposed alternative failure criterion in other metal forming processes. Huang et al [39] discussed the cavitation instabilities in elastic-plastic solids and considered the problem of cavitation states. They obtained a criterion for cavitation under multiaxial axisymmetric stressing that is related to a critical value of the mean stress. Using finite element analysis, Li et al [40] claimed that triaxial tension and large plastic strain surrounding the void are the key factors to drive void growth. Khraishi et al [41] investigated the void growth mechanisms during plastic deformation and found that strain rate sensitivity has an influence on the void size and the number of existing voids.

Despite these meaningful investigations, the influence of CWR tool parameters on the internal stress-strain characteristics of the workpiece is still not completely understood. Explicitly analyzing the workpiece's deformation behavior during an actual CWR operation is extremely difficult. For this purpose, a combined experimental and numerical approach is utilized in this work to ascertain the dependence of CWR tool parameters and operating conditions on the formation of internal defects. After being validated by comparison to the experimental results, an explicit dynamic finite element model of CWR was parameterized to determine the influence of tooling parameters on void formation within the workpiece. By

examining the effective stress and strain within the workpiece over a wide range of operating conditions, the mechanisms for void formation and growth are ascertained and discussed.

4.2.1 Flat wedge CWR Finite Element Model

One of the primary advantages of the finite element method is its ability to parametrically analyze a range of variables that are difficult to examine experimentally. In order to perform accurate numerical analyses for characterizing the formation of internal defects in the CWR process, a three-dimensional finite element model was created using the ANSYS/LS-DYNA program. As shown in Figure 4.11, a cylindrical workpiece and two forming tools were meshed using eight-noded structural solid element with six degrees of freedom ($u_x, u_y, u_z, \omega_{xy}, \omega_{yz}$ and ω_{zx}) per node. One-point integration and viscous hourglass control were employed for all the elements in the model to reduce computation time and to ensure robustness during large deformations. Simulations were performed by applying equal and opposite velocities to the forming tools in the horizontal (x) direction. In the numerical analyses, the workpiece was left unconstrained and the forming tools were held in the vertical (y) and out-of-plane (z) directions. Figure 4.11 shows the deformation process of the workpiece and translation of the tools in a typical numerical analysis of CWR.

For the purpose of capturing the interfacial conditions during the CWR process, a surface-to-surface contact algorithm was employed to define the contact interaction between the workpiece and dies. A friction model of the form:

$$\mu = \mu_d + (\mu_s - \mu_d)e^{-(c)|v|} \tag{4.2}$$

was used to define the interfacial boundary condition. In Eq.(4.2)

μ_s is the static friction coefficient,

μ_d is the dynamic friction coefficient,

c is an exponential decay constant.

v is the relative velocity of the contacting surfaces.

Based on previous experiments by the authors [9], μ_s, μ_d and c were respectively set to 0.30, 0.25 and 1 in the numerical analyses.

4.2.2 Possible Numerical Failure Criterion

In the cross wedge rolling process, the workpiece experiences alternative shear and normal stresses. Such an action deforms the metal crystal lattices and increases the likelihood of internal void development. The concurrent action of shear and tensile stresses is reflected by the values of the effective and mean stresses, and the plastic strains. Thus, using the finite element method, the formation of voids on cracks in the central portions of the workpiece can by analyzed by examining the internal stress and strain distributions.

The first criterion that will be evaluated by the finite element method will be the mean stress. The mean stress, also referred as the hydrostatic stress, is defined as the mean normal stress:

$$\sigma_m = \frac{1}{3}(\sigma_1 + \sigma_2 + \sigma_3) \tag{4.3}$$

where σ_1, σ_2 and σ_3 are the three principal stresses respectively. In most metal forming operations, it is advantageous to have the central portions of a workpiece subjected to a negative mean stress. This is because a negative mean stress reflects a three-dimensional compressive stress state that can close or even eliminate preexisting internal voids or cracks within the

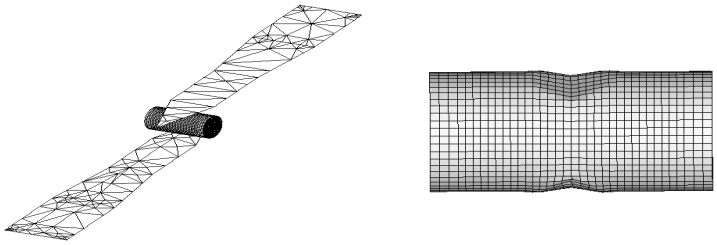

(a) The workpiece in the knifing zone

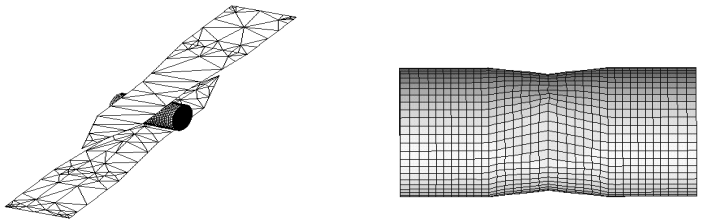

(b) The workpiece in the guiding zone

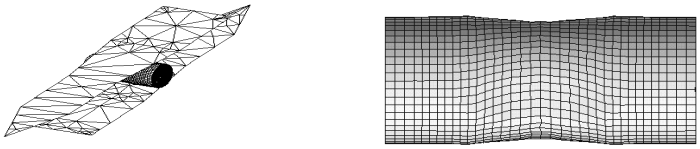

(c) The workpiece in the stretching zone

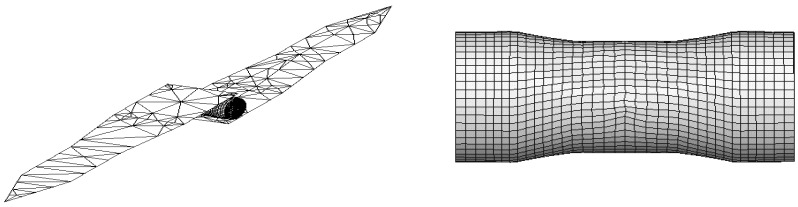

(d) The workpiece in the sizing zone

Figure 4.11 Flat wedges CWR process simulation

workpiece. Large positive mean stress values, on the other hand, facilitate the likelihood of internal void or crack formation.

A second criterion that will be evaluated by the finite element method will be the effective stress. For isotropic materials that fail by yielding, the distortion energy theory agrees well with published experimental data, and is therefore widely used in predicting failure of ductile metals [42]. In this theory, failure by yielding occurs at any point in a body when the distortion energy per unit volume equals the yield value in a simple tension test. The effective stress is defined as:

$$\bar{\sigma} = \sqrt{\frac{1}{2}\left[(\sigma_1 - \sigma_2)^2 + (\sigma_2 - \sigma_3)^2 + (\sigma_3 - \sigma_1)^2\right]} \tag{4.4}$$

where σ_1, σ_2 and σ_3 are the three principal stresses. The effective stress can measure the dislocation movement and material plastic flow generated by shear stresses. It should be noted that a non-dimensional parameter $\sigma_m / \bar{\sigma}$ can reflect the stress state and can be regarded as the measure of "tri-axiality" [35].

The final failure criterion that will be evaluated for CWR by the finite element model is the effective plastic strain. Due to the action of the high stresses, the billet material flows plastically toward the both ends and consequently increases the total effective plastic strain. To some extent, the tool geometry and working condition have substantial influences on the strain concentration and will ultimately influence the level of plastic strain experienced. The effective plastic strain is defined in Eq. (3.23).

4.2.3 Finite Element Failure Stress Analysis

Since the finite element model has been validated by the experiment results, it can be used to investigate the possible CWR failure criterion discussed in the last section. To evaluate each criterion, the stress and strain will be monitored at the centroid of the workpeice during the deformation process in the knifing and guiding zones. This point was specifically chosen because it is known to be the location for void and crack initiation. It should also be mentioned that only the stress and strain in the knifing and guiding zones are being considered because the void initiation is known to occur by the end of the guiding zone.

In the finite element analysis, the effective stress was first monitored at the centroid for aluminum, copper and steel workpiece materials. As depicted in Figure 4.12, several important trends are found for variation of the effective stress. The first notable tendency is that the effective stress curves behave similarly for all three workpiece materials and both forming angles. Specifically, the effective stress sharply increases in the knifing zone and then maintains a constant maximum value in the guiding zone. This can be explained by the fact that the tool initially knifes into the billet before forming a uniform V–shaped groove around its circumference where the stress maintains a constant maximum value. The second trend found in Figure 4.12 is that the magnitude of the maximum stress substantially changes with workpiece material. In the figure the effective stress values in the guiding zone are approximately 100% and 50% greater for steel and copper than aluminum. This is due to the fact that the Young's modulus and the yield stress of both steel and copper are significantly greater than aluminum. This makes them significantly less compliant, causing them to experience higher stresses in order to attain the same final shape and deformation level. The final and most important tendency in Figure 4.12 related to failure prediction is that there is little variation in the maximum effective

stress for α=15° and α=30°. This is especially true for the aluminum and copper cases, where a maximum difference of approximate 15% is found. As expected, the effective stress for α=15° is slightly greater than α=30° due to the larger plastic deformations that occur at smaller forming angles. For all three materials, the lack of a substantial difference in stress between the two angles, however, indicates that effective stress is not an adequate parameter to predict whether a void has formed.

Turing our attention to the mean stress, Figure 4.13 shows that the mean stress of the centroid demonstrates identical trends to the effective stress with respect to its shape, variation with material, and variation with forming angle. In fact, when comparing Figure 4.12 and 4.13, it is found that there is even less variation between the α=15° and α=30° cases in the mean stress plots. This shows that the mean stress predicts nearly identical values for a condition known to produce voids and well-formed parts. Hence, the mean stress criterion also appears to be inadequate for predict void initiation in CWR.

The final failure criterion to be evaluated by the finite element method is the effective plastic strain. The distributions of effective plastic strain during the first two zones of the tool are plotted for the three workpiece materials in Figure 4.14. Unlike the stress plots of Figure 4.12 and Figure 4.13, Figure 4.14 shows that the distribution of the effective plastic strain is substantially different for the α=15° and α=30°. In fact, in the first two zones of the tool, the effective strain at α=15° is dramatically larger than that of α=30°. Aluminum, for example, has an effective plastic strain of 0.249 with α=15°, whereas the effective strain with α=30° is only 0.049. Since an internal void is known to occur at α=15°, it appears that there is a direct correlation between the effective plastic strain and the formation of internal voids. Such a finding can be attributed to several factors. Since CWR is a volume-preserving process, there is a

deformation limit of the material for which a void will develop. Since strain is a measure of the intensity of deformation, it is logical that it will be a more accurate predictor of void initiation than stress.

4.2.4 Finite Element Strain Analysis

In the author's prior experimental work (Section 4.1), it was found that when the deformation coefficient exceeded 0.6 in aluminum 1100 samples, a void would form. Closely examining Eq. (4.1), it is found that the deformation coefficient is simply a measure of the produced by the forming angle, stretching angle, and area reduction within a CWR process. Hence, the maximum effective plastic strain can be considered the limiting criterion with respect to maximum deformation during the CWR process.

4.3 Temperature, Strain Rate and Material Property Effects on The Internal Failure

As mentioned in Chapter 1, the cross wedge rolling process offers numerous advantages over traditional manufacturing processes. Despite these benefits, there still exists the need to directly determine productivity: forming velocity and billet temperature. By increasing the forming velocity of the tools, more parts can be rolled in a shorten period of time. Due to an increased level of strain rate hardening in the workpiece and a greater likelihood of interfacial slip failure, however, there is a limit on the maximum forming velocity that can be attended in the CWR process. Considering billet temperature, the formability of the workpiece increases at

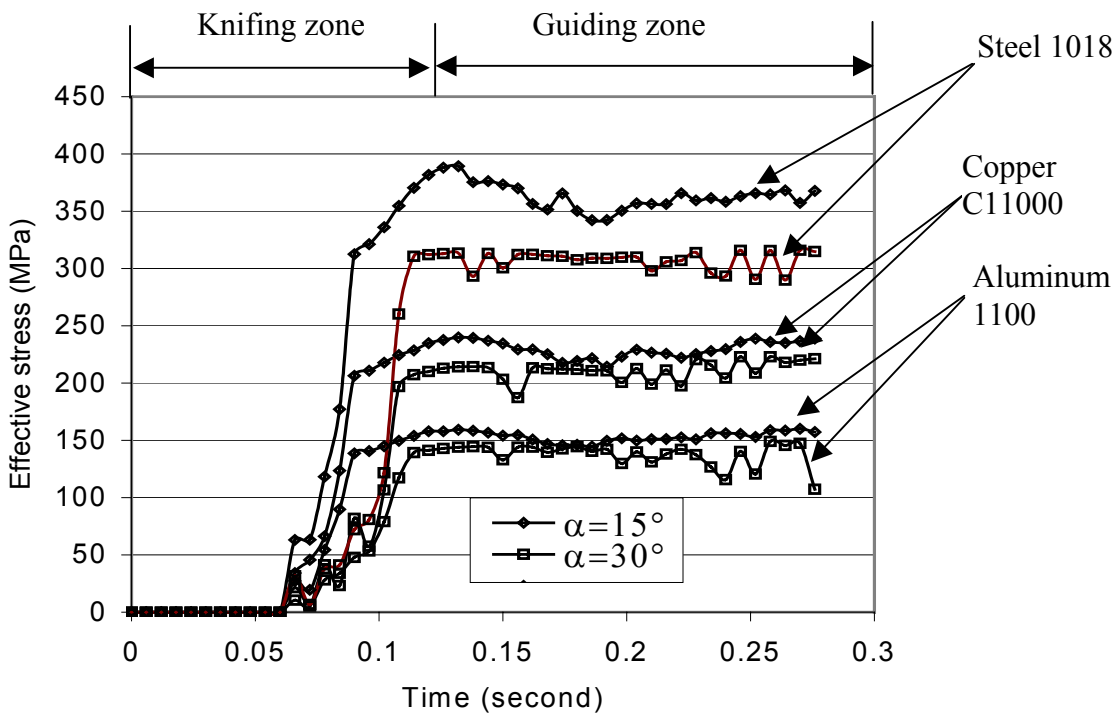

Figure 4.12 Effective stress distribution of the center point

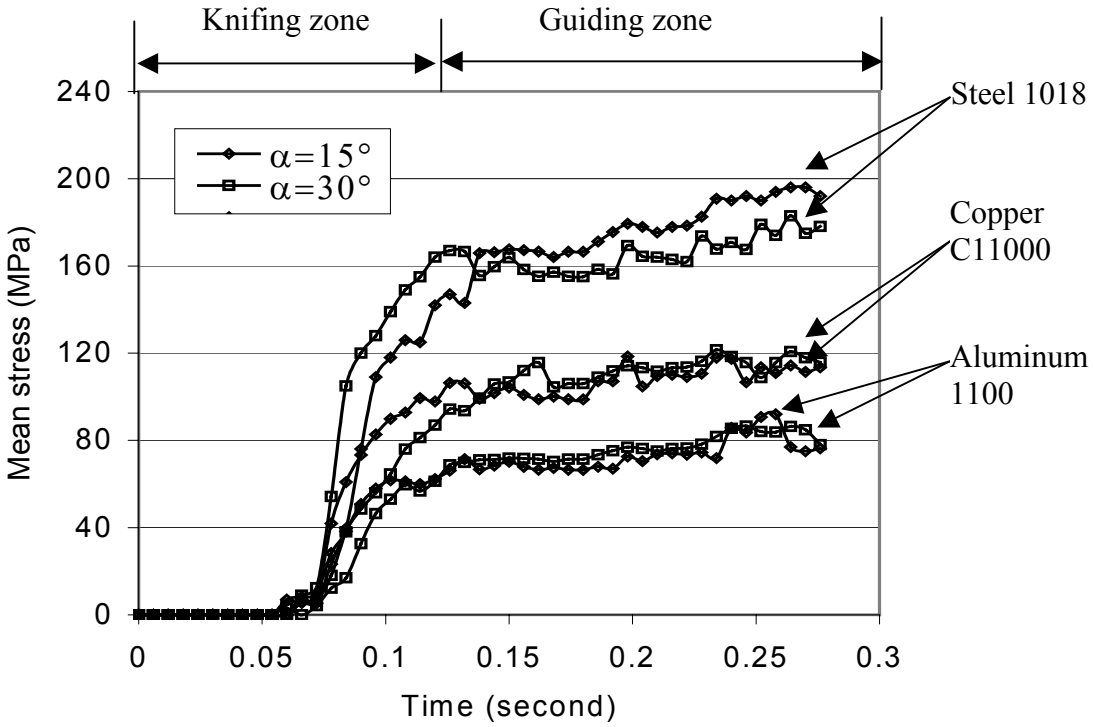

Figure 4.13 Mean stress distribution of the center point

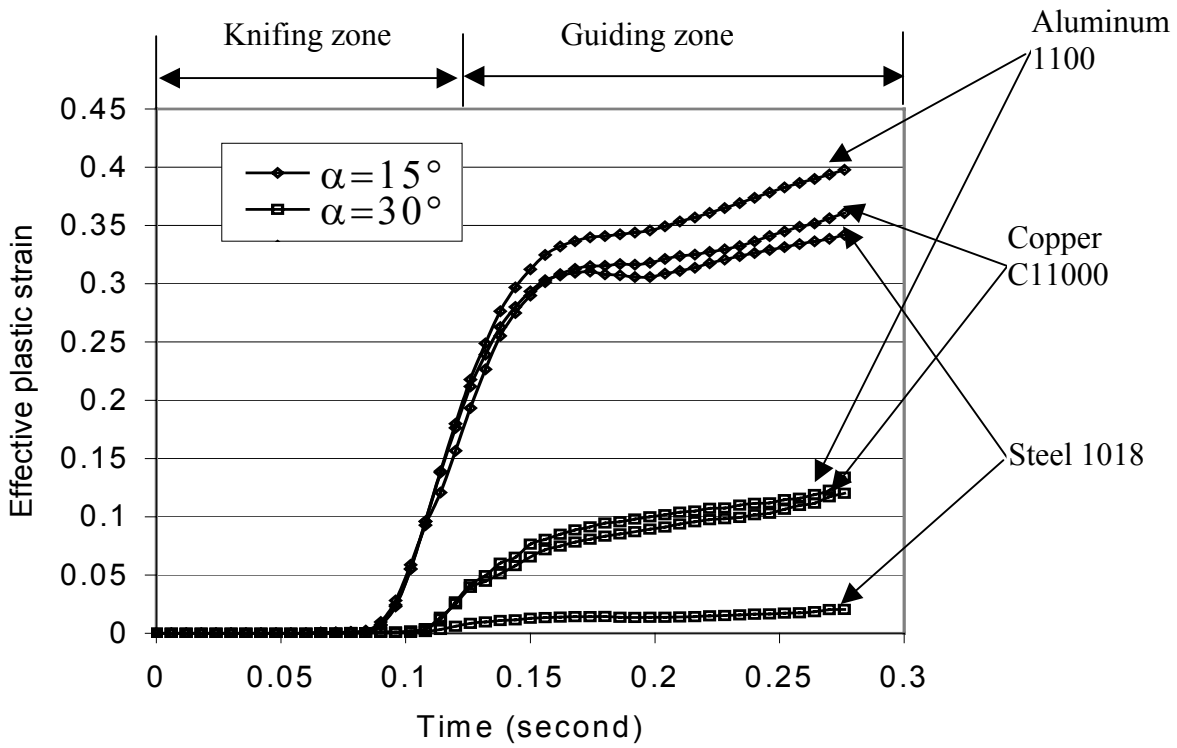

Figure 4.14 Effective plastic strain distribution of the center point

higher temperatures. Therefore, a higher temperature, the forming tools can more easily deform the workpiece. Heating the workpiece to higher temperatures increases the energy costs in the CWR process and there is a maximum benefit that can be attained by varying billet temperature. In addition, increasing the temperature of the billet also increases the likelihood of excess interfacial slip between the forming tools and workpiece. In this Chapter, the role of temperature and forming velocity will be studied utilizing the finite element method. Specifically, the influences of workpiece temperature and strain rate on the internal stress and strain in the workpiece will be determined to establish optimum operating conditions in CWR.

4.3.1 Johnson-Cook material model

In order to characterize the roles of strain rate and temperature in the CWR process, a new three-dimensional finite element model was created using the ANSYS/LS-DYNA program. The material model employed in this model is Johnson-Cook model [43], which integrates the effects of temperature and strain rate.

The Johnson-Cook material model was defined for the workpiece in the numerical analyses. The model for the von Mise tensile flow stress, σ, is expressed as follows:

$$\sigma = [A + B\varepsilon^n][1 + C\ln\dot{\varepsilon}^*][1 - T^{*m}] \qquad (4.5)$$

Where ε is the equivalent plastic strain,

$\dot{\varepsilon}^* = \dot{\varepsilon} / \dot{\varepsilon}_0$ is the dimensionless plastic strain rate for $\dot{\varepsilon}_0 = 1.0s^{-1}$,

T* is the homologus temperature, which is $T^* = \frac{T - T_{ROOM}}{T_{MELT} - T_{ROOM}}$,

A, B, n, C and m are five material constants, which are shown in Table 4.1.

The expression in the first set of brackets gives the stress as a function of strain for $\dot{\varepsilon}^* = 1.0$ and T*=0. The expressions in the second and third sets of brackets represent the effects of strain rate and temperature, respectively.

Table 4.1 Material properties of three materials in the Johnson-Cook model

	Density (Mg/m^3)	Young's Modulus (Gpa)	Possion's ratio	A (MPa)	B (MPa)	n	C	m
OFHC Copper	8.96	124	0.34	90	292	0.31	0.025	1.09
4340 Steel	7.89	121.0	0.29	792	510	0.26	0.014	1.03

4.3.2 Experimental Verification of FEM

In order to ascertain the actual internal deformation behavior of the workpiece, CWR experiments were carried out using a specially designed CWR prototype machine (see Section 3.3). As an initial step towards validating the FEM and gaining a better understanding of the internal deformation of the workpiece, CWR experiments were conducted with a forming angles of α=30°, a stretching angle of β=7° and an area reduction of Δ_A=38% and at a forming velocity of 0.1m/s. After forming, the deformed geometries of the workpiece specimens were measured using a coordinate measuring machine and averaged. Table 4.2 shows the comparison between the experimentally measured aluminum and copper workpieces and the corresponding profiles predicted by the finite element model (FEM). Examining Table 4.2, it is clear that the external configurations of the deformed workpieces derived from the FEM model match very closely with the experimentally measured values. The maximum error between the experimental and

numerical values for the copper is less than 3%. This shows that the numerical model can realistically characterize the external shape and overall deformation of the workpiece in a CWR process. This is to be expected, as CWR is a volume-preserving process and the amount of deformation is controlled by the shape of the forming tools.

4.3.3 Influence of temperature

To evaluate the role of temperature and strain rate in CWR, the numerical model will monitor the effective stress and effective plastic strain at the centroid of the workpiece. This point was specifically chosen because it is known to be the location for void and crack initiation [38].

Table 4.2 External configuration of the CWR experiment product (copper)

Locations along the axis (mm)	Profile radial length from FEM (mm)	Profile radial length from experiments (mm)
-25	12.7	12.7
-22	12.7	12.7
-18	12.7	12.69
-14	13.13	12.98
-10	11.843	11.86
-6	9.824	9.85
-2	9.824	9.83
2	9.824	9.83
6	9.824	9.85
10	11.843	11.88
14	13.13	12.9
18	12.7	12.69
22	12.7	12.7
25	12.7	12.7

Based on the previous work by the author [38], it was determined that the effective plastic strain was another important parameter for optimizing the tool design in CWR. The effective plastic strain rate and strain are defined as follows:

$$\dot{\varepsilon} = \sqrt{\frac{2}{9}\left[\left(\dot{\varepsilon}_1 - \dot{\varepsilon}_2\right)^2 + \left(\dot{\varepsilon}_2 - \dot{\varepsilon}_3\right)^2 + \left(\dot{\varepsilon}_3 - \dot{\varepsilon}_1\right)^2\right]} \tag{4.6}$$

$$\varepsilon = \sum \dot{\varepsilon} \cdot \Delta t \tag{4.7}$$

where ε_1, ε_2 and ε_3 are the principal strain rate.

In the Johnson-Cook fracture model, a parameter to measure failure is given as:

$$D = \sum \frac{\Delta \varepsilon}{\varepsilon^f} \tag{4.8}$$

where $\Delta\varepsilon$ is the increment of effective plastic which happens in one integration, and ε^f is the effective strain to fracture. Fracture occurs once D reaches 1.0.

In order to determine the role of temperature and strain rate in optimizing the CWR process, the finite element model described in Section 4.3.1 was parameterized to generate results at 18 distinct operating conditions, the conditions included varying the initial workpiece temperature (297K, 497K, 697K), strain rate (1, 100,10,000 1/sec) and workpiece material (steel and copper).

In the finite element analysis, the effective plastic strain was first monitored at the centroid for copper and steel for initial workpiece temperatures of 297K, 497K and 697K. As depicted in Figure 4.15 (a) for copper, there is a very little variation in the maximum effective plastic strain under these temperatures. This is especially true in the first two zones, where the effective plastic strain curves coincide for all three temperatures. The lack of the plastic strain with temperature can be explained by the fact that the geometry of the forming tool determines

the amount of plastic deformation in the workpiece. This geometry remains unchanged with the variation of temperature, which means the variation of workpiece temperature will primarily influence the forces required to form the billet and the effective stress in the workpiece.

Unlike the effective strain plots in Figure 4.15(a), Figure 4.15(b) shows that the distribution of the effective stress substantially changes with initial workpiece temperature. Closely examining Figure 4.15(b), it is found that the effective stress curves behave identically for the three working temperatures studied. Specifically, the effective stress sharply increases in the knifing zone and then maintains a small range of variation in the guiding zone. This can be explained by the fact that the tool initially knifes into the billet before forming a uniform V–shaped groove around its circumference where the stress will maintain a constant maximum value. In the last two zones of the tool, the effective stress increases gradually and reaches the maximum value as the workpiece material is stretched in the axial direction and forced to flow to the ends. In this figure, the effective stress values in the guiding zone are approximately 60% and 30% smaller for 697K and 497K than 297K. This is due to the fact that the yield stress for copper significantly reduces with temperature over the range investigated. The reduction of yield strength makes the workpiece significantly more compliant at high temperatures, causing them to experience lower stresses in order to attain the same final shape and deformation level. Since large tensile stress in the central portion of the workpiece have been shown to lead to internal defects, deforming the CWR process at higher temperatures will be less likely to experience failure. These results can explain that why low temperatures have been found to cause center cracks in the CWR process [44].

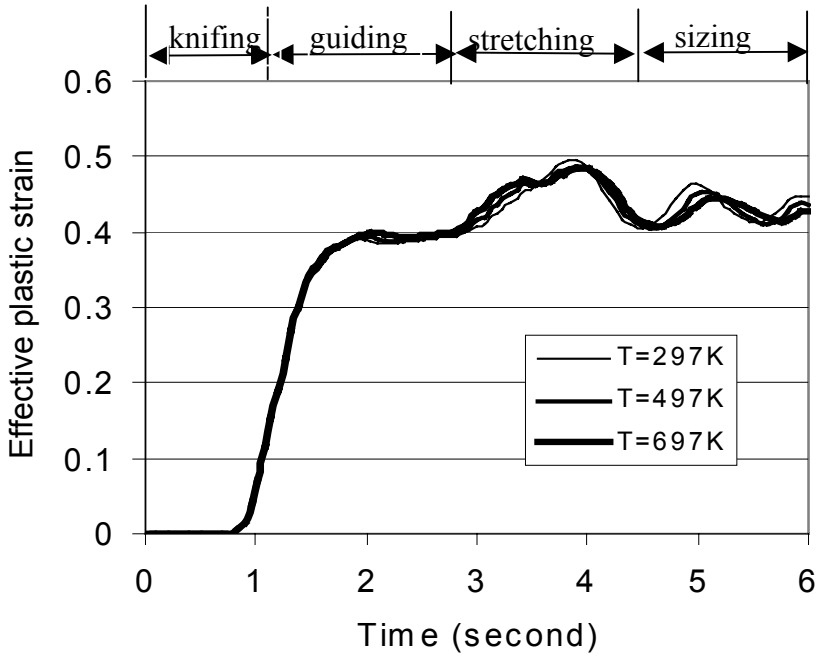

(a) Variation of effective plastic strain under different temperatures

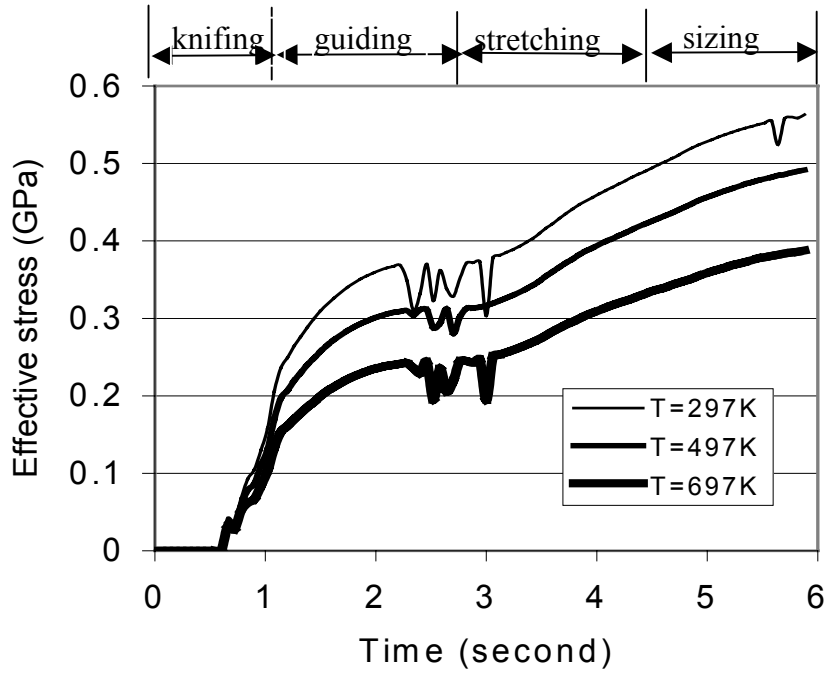

(b) Variation of effective stress under different temperatures

Figure 4.15 Effective strain and stress variation under different forming temperatures (copper)

4.3.4 Influence of strain rate

Turning our attention to the effects of strain rate, Figure 4.16(a) shows that the effective plastic strain of the centroid does not vary with strain rate. This again can be explained by the fact that the strain and deformation in the workpiece is controlled by the geometry of the forming tools. Examining the effective stress curves shown in Figure 4.16(b), it is found that the effective stress curves demonstrate identical trends for each of the three strain rates examined. At smaller strain rate, however, the effective stress is reduced. Therefore, at lower strain rates, there is less likelihood of internal void formation. It is noteworthy to mention that the variation of stress with strain rate is much less significant than with forming temperatures. As the strain rate increases from 1 to 100 1/sec, and then from 100 to 10,000 1/sec, maximum difference of the effective stress is less than 10%. Since the strain rate range studied is very large compared to the temperature range, temperature is a more critical parameter when optimizing the CWR process to eliminate internal defects.

A final point to be made about the influence of strain rate deals with increasing productivity in CWR. When the forming velocity increases, the material deforms more quickly and the strain rate correspondingly increases. Since the forming velocity in the actual manufacturing process is typically at a moderate level ($100s^{-1}$). It can be concluded that the moderately larger forming velocity can be used to increase the parts formed per minute without significantly increasing the likelihood of internal defects. It should be mentioned, however, that the forming velocity does substantially increase the chances of the excess interfacial slip failure [38].

4.3.5 Influence of Workpiece Material

In order to study the relative variation effective stress and strain with workpiece material, two common metals in the forming industry, copper and steel, were analyzed using the finite element model.

First examining the effective strain for copper and steel (under 297K and stain rate of $1s^{-1}$) in Figure 4.17(a), a significant difference in plastic strain is found by the end of the knifing zone. This difference increases gradually until the end of the CWR process. At the end of the sizing zone, the effective strain of copper is 0.45 whereas the effective strain of steel is 0.53. Though the forming conditions are the same for these two materials, the differences in Poisson's ratio, elastic moduli and yield strength can explain the differences in the effective strain. As shown in Table 4.1, since the likelihood of internal defects increases with the level of stain, copper will be less likely to experience internal defects than steel in the CWR process.

Examining the effective stress of these two materials in Figure 4.17(b), it is also found that the distribution of the effective stress is substantially different for copper and steel. In fact, in the last two zones of the tool, the effective stress of steel is dramatically larger than that of copper. Steel, for example, has an effective stress of 790 MPa at the end of this process, whereas the effective strain of copper is only 470 MPa. This again can be directly attributed to differences in material properties, and demonstrates that copper is more formable that steel in CWR.

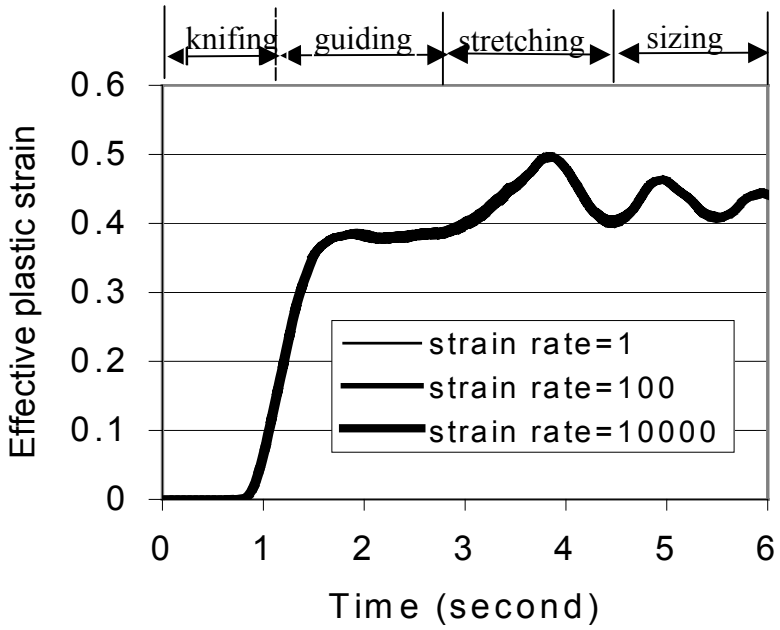

(a) Variation of effective plastic strain under different strain rates

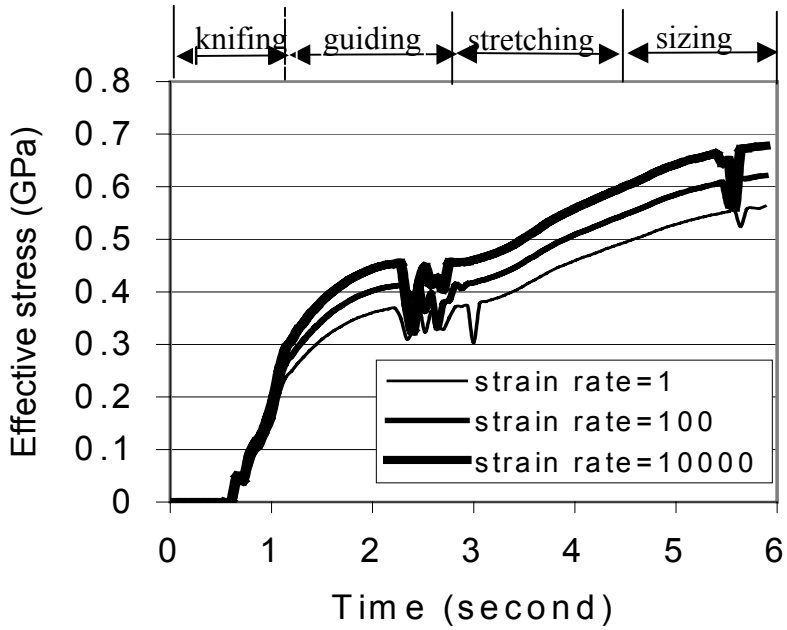

(b) Variation of effective plastic strain under different strain rates

Figure 4.16 Effective strain and stress variation under different forming strain rates (copper)

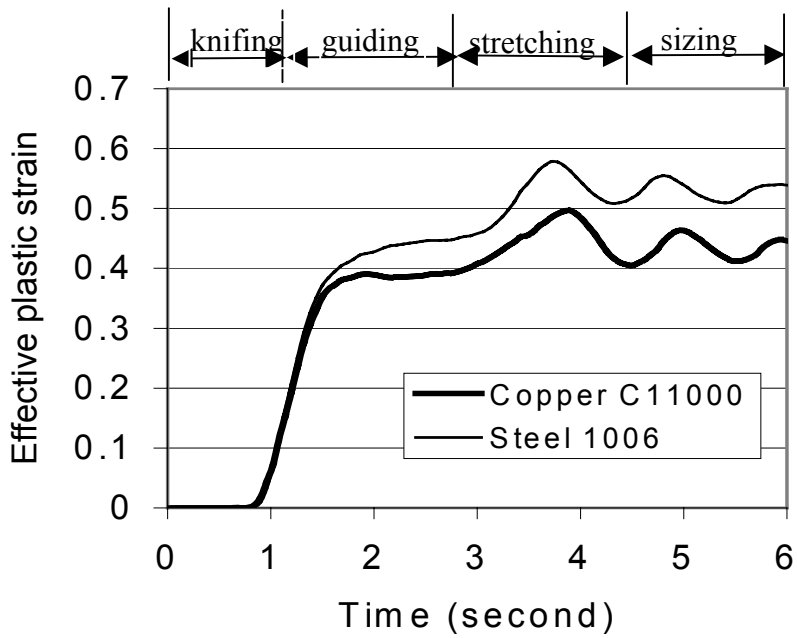

(a) Variation of effective plastic strain under different materials

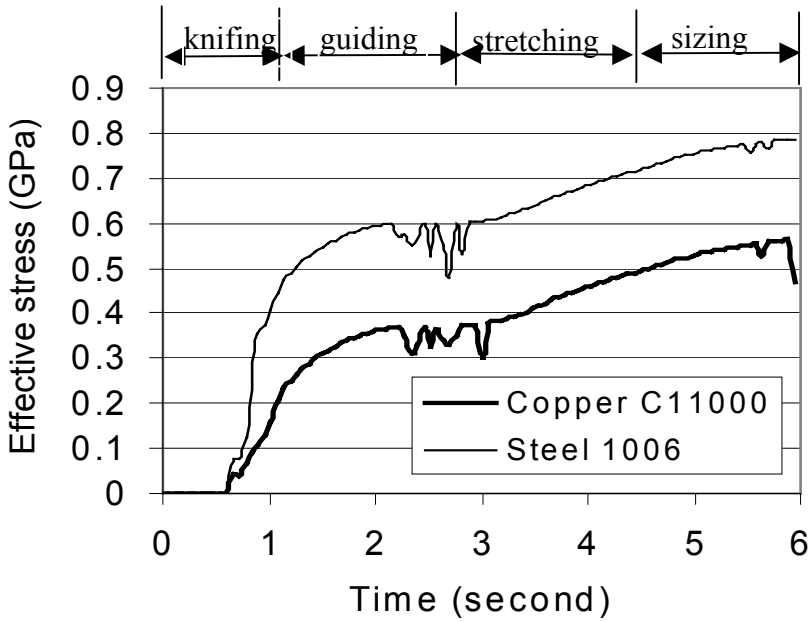

(b) Variation of effective plastic strain under different materials

Figure 4.17 Effective strain and stress variation under different materials.

4.4 Conclusion

In this chapter, an experimental study of the CWR process was performed to establish the conditions for which internal voids formed in the workpiece. Extensive experiments were conducted by varying the area reduction, forming angle, and stretching angle. For each operating condition, the workpiece specimens were cut along their longitudinal axes and examined for the presence of voids. Based on the experiments, the following conclusions can be drawn on the morphology and operating conditions that lead to void formation in the workpiece:

1) Large voids found at the completion of the CWR process develop through the coalescence and bridging of smaller voids initiated in the knifing and sizing zones; 2) When examined along a horizontal cross-section, the voids were found to have a cruciform shape that propagated along the directions of principal stress; 3) The initiation and size of voids were found to increase with decreasing forming angle, increasing stretching angle, and increasing area reduction; 4) The likelihood of void formation within the workpiece can be predicted using a non-dimensional deformation coefficient. For the material and initial geometry studied in this work, the critical deformation coefficient was found to be 0.6.

Then utilizing an finite element model, several different failure criteria were examined for predicting void initiation in the CWR process. Based on the numerical results, it was determined that the effective plastic strain was the best criterion for predicting internal failure in CWR. Such a finding was in accordance with prior work done by the author who found that void formation could be predicted by a deformation coefficient which was a measure of the plastic strain produced by the forming angle, stretching angle and area reduction.

In addition, based on an explicit dynamic finite element model, several different working parameters—the forming temperature, the strain rate and the workpiece material —were

examined for the CWR process. Based on the numerical results, the following conclusions can be drawn: 1) the effective plastic strain in a CWR process is independent of both temperature and strain rate. Rather, the strain is controlled by the geometry of the forming tools; 2) considering the maximum effective stress in the workpiece, both temperature and strain rate have an important influence. Specially, the effective stress decreases with increasing temperature and increases at higher strain rates; 3) temperature has a more dramatic effect on the effective stress within the workpiece than strain rate.

5.0 INVESTIGATION OF INTERNAL DEFECTS WITH FRACTURE MECHANICS APPROACH

Since internal defects in the cross wedge rolling process can weaken the integrity of the final product, it is imperative to investigate the mechanisms of their propagation and growth. Regardless of the physical phenomenons that cause the internal defects, it has been clearly shown that specific sets of tooling parameters lead to internal defects within the workpiece. Determining these parameters, with respect to eliminating failure in CWR, is critical to allowing the manufacturing community better to utilize the CWR process.

Over the past several decades, fracture mechanics has developed into a broadly based technology that can be applied to the strength analysis and the design to obtain improved service performance [45]. The objective of this chapter is to develop a fundamental understanding of the factors that influence the growth of internal voids from a fracture mechanics perspective. Utilizing fracture mechanics theory, a finite element model was generated to simulate the crack growth process in CWR. From the finite element results, J-integral values were evaluated under different loading conditions. The influence of varying the forming angle,α, and the initial crack length, a, on void development were subsequently ascertained and discussed.

5.1 J-integral Method

Fracture mechanics can be used to determined the likelihood of crack formation and propagation in a structure under an applied load. In fracture mechanics, analytical predictions can be made by calculating fracture parameters such as J-integrals, which are nonlinear generalizations of the elastic strain energy release rate. As discussed previously, small internal

voids in the CWR process initiate in the knifing zone, which is very early in the CWR deformation process. These voids then merge and propagate during the large plastic deformation encountered in the stretching zone. Hence, for the CWR internal defect formation, J-integrals can be applied to investigate the characteristics of the void development and parameters that influence their growth.

In a 2-D plane elastic condition, the J-integral can be defined as a path-independent line integral that measures the strength of the singular stresses and strains near a crack tip [46]. The following equation shows an expression for the J-integral. It assumes that the crack lines in the global Cartesian X-Y plane, with X parallel to the crack (see Figure 5.1).

$$J = \int_{\Gamma} W dy - \int_{\Gamma} \left(t_x \frac{\partial u_x}{\partial x} + t_y \frac{\partial u_y}{\partial y} \right) ds \qquad (5.1)$$

where

Γ is any path surrounding the crack tip,

W is the strain energy density (that is, strain energy per unit volume)

t_x is the traction vector along x axis, equal to $\sigma_x n_x + \sigma_{xy} n_y$

t_y is the traction vector along y axis, equal to $\sigma_y n_y + \sigma_{xy} n_x$

σ is the component stress

n is the unit outer normal vector to path Γ

s is the distance along the path Γ

Since the J-integral is path independent for linear or nonlinear elastic material response, the J-integral can be viewed as a parameter that characterizes the physical behavior in the region around the crack tip. From the viewpoint of energy, the J-integral is equal to the amount of

elastic- plastic strain energy per unit area of crack growth that is applied towards extending the crack in a specimen under load [45].

Due to these characteristic properties, J can be regarded as a fracture criterion. Under opening-mode loading, the criterion for crack initiation takes the form

$$J = J_{Ic} \tag{5.2}$$

where J_{Ic} is a material property for a given thickness under specified environmental conditions. The critical value J_{Ic} is the value required for the start of crack extension from a pre-existing crack. In CWR, there are several reasons for a pre-existing crack in the workpiece, such as the material impurity and stress concentration due to heat treatment. Though the above properties of the J-integral were derived under elastic material response, the J-integral can be extended to the field of ductile fracture. This is particularly true when extensive plastic deformation and stable crack growth precede fracture instability. J-integrals are used today as a fracture criterion in situations of appreciable plastic deformation. This approach makes it possible to predict the failure load of a cracked component or to measure the fracture toughness of a material, even when there is significant plastic deformation existing in the component or material sample [47],[48]. In this research, the J-integral values under different CWR working conditions will be obtained by the finite element method. From these values and prior experiment results, the crack propagation in the cross wedge rolling process will be ascertained.

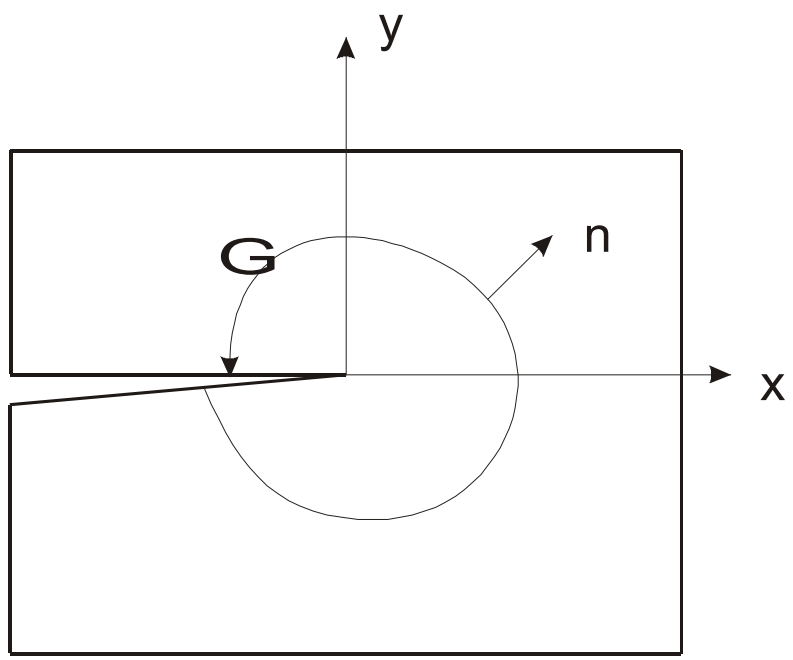

Figure 5.1 Illustration of J-integral method

5.2 Computation of J-integral with FEM

In order to numerically analyze the formation of internal defects in the CWR process using J-integrals, a finite element fracture model was created using the ANSYS program. In the CWR process, internal voids and cracks are known to initiate in the central regions of the workpiece as early as the middle of the knifing zone [38]. In the knifing zone, the central portion of the billet becomes significantly weakened when it is rotated and compressed in the diameter direction. This weakness ultimately leads to the opening of an axial void that most likely initiate from a micro-sized imperfections. The goal of the present work is to understand the void development in the central part of the workpiece after a small void has been initiated. As shown in Figure 5.2, a central portion of a workpiece sample will be modeled and analyzed. The analysis will be performed in two steps. The first step will be to use the finite element method to determine the internal loads within the workpiece section. Once the loads are obtained, the J-integrals will be computed and analyzed with respect to the magnitude of the void growth in CWR.

Utilizing the finite element model presented in the internal defect investigation of Section 4.2, the initial loads for the fracture analysis was found to be σ_1=76.3MPa and σ_2=66.2MPa under the condition of α=15°, β=7°, and Δ_A=38% with aluminum 1100. In the analysis, σ_1 and σ_2 are the effective stress in the axial and radial direction, respectively.

Based on experimental measurements at the end of the knifing zone, it was found the initial size of the crack at this stage is about 1 mm. Hence, it is reasonable to assume the geometric parameters of the finite element fracture model as shown in Table 5.1. Due to the

symmetry of the model (with respect of x axis and y axis), only ¼ of the model needs to be analyzed.

Table 5.1 Dimensions of the fracture model

Crack length a	1	mm
Length of the sample region b	10	mm
Height of the sample region h	5	mm
Thickness t	0.25	mm

As depicted in Figure 5.3 (a), the finite element model was meshed with Element SOLID 45, which is a kind of three-dimensional solid element and defined by eight nodes having three degrees of freedom at each node. At the tip of the crack, in order to capture the details and maintain the high accuracy, Element SOLID 95 was applied, which is a higher order version (20-node) of the 3-D 8-node solid element SOLID 45 and can tolerate irregular shapes. There were 110 elements and 408 nodes involved in this model. As mentioned earlier in this chapter, the properties of the J-integral were derived under elastic material response; the elastic material model was employed in the finite element model. The Young's modulus and the Possion's ratio were 6.9e+10 MPa and 0.33, correspondingly. The symmetric boundary conditions were applied at the lower and left side of the model while at the upper and right hand side σ_1 and σ_2 were loaded, respectively.

Following the definition of the J-integral, the value can be obtained by first calculating the strain energy density for each element. Then a path can be defined for integration and the strain energy density can be directly mapped onto this path. By integrating the strain energy density with respect to the global y coordinate, the first term $\int_\Gamma W dy$ is obtained. From the

definition of the specified path, the path unit normal vector can be calculated. After mapping the component stress σ_x, σ_y and σ_{xy} onto the path, together with the normal vector, the traction vector can be computed. In order to calculate the derivatives of the displacement vector, the integration path is shifted in a small distance in the positive and negative x direction. As shown in Figure 5.3(b) [22], this method brings the second term to the right hand side of the J-integral. Therefore, the overall J-integral value can be derived by adding these two terms. With the model listed in Table 7.1, the J-integral value is obtained to be 0.2478 MPa·mm.

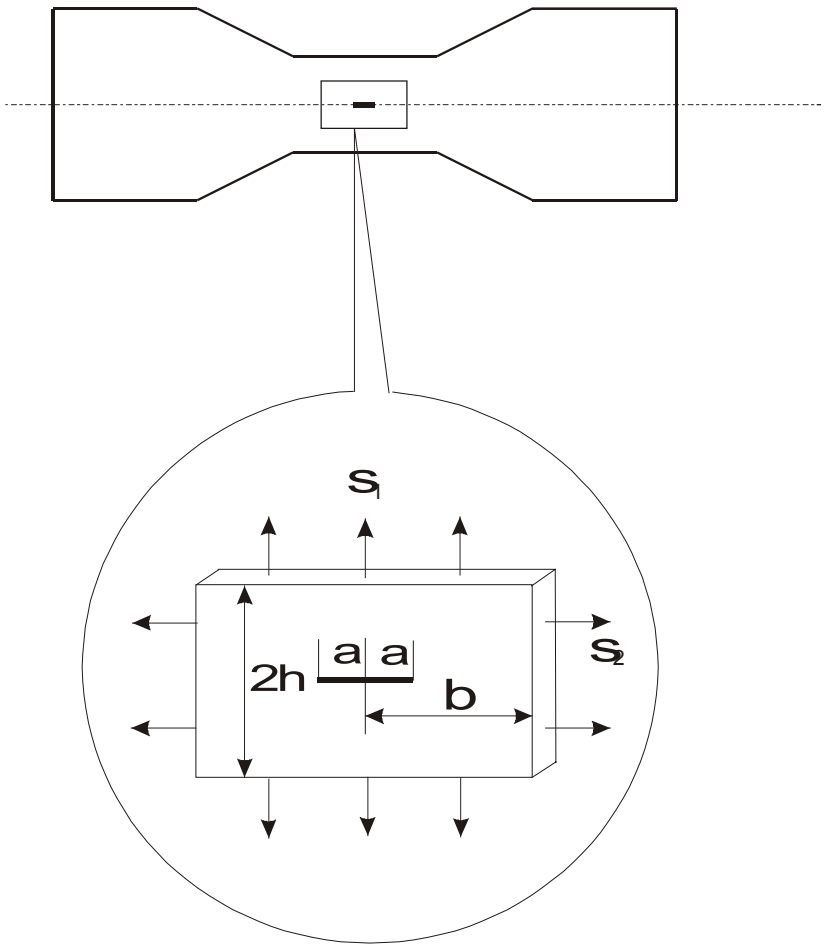

Figure 5.2 Location and shape of the analytical crack sample

5.3 Result Analysis of Fracture Model

Based on the results of the finite element model, the factors that influence void propagation can be investigated. First, the effective stress distribution around the crack was examined for forming angles of α=15° and α=30°. Recalling from Section 4.1, these analysis were specifically chosen because a forming angle of 15 degrees leads to an internal void while one of 30 degree does not. Since the forming angle α and crack length *a* have significant influence on the growth of internal defects in the cross wedge rolling process, then the relationship between the J-integral, the forming angle, and crack length will be explored.

In order to establish the effect of the forming angle on the formation of internal defects, Figure 5.5 was created for $\beta=7^o$ and Δ_A=38%. In Figure 5.5, it is found that the value of J-integral monotonically increases with decreasing the forming angle. When the forming angle is $\alpha=30^o$ and the crack length is 1mm, the J-integral is only 0.113 MPa·mm under this condition. For $\alpha=15^o$, however, the J-integral reaches 0.248 MPa·mm. Since J-integral is the rate of change of potential energy with respect to an incremental extension of the crack, the larger the J-integral, the faster the crack development and propagation. Therefore, smaller forming angles can accelerate the formation of internal void and enlarge the size as is found in experiments. In general, the range of forming angle is between 20° to 35°.

The crack length *a* is one of the key parameters of the fracture evolution, which has a strong effect on the crack development. Figure 5.5 depicts the influence of the crack length on the propagation of an internal void. In this figure, the internal void increases proportionally with the crack length. Considering the crack length of the workpiece, there is a critical value of crack length for which internal defects will develop. In general, when crack length is less than 1mm,

the J-integral must attain a moderate value to enlarge the existing crack. However, if crack length is over 2mm, the possibility of void creation increases substantially. This is expected as the effective stress and strain within the central portions of the workpiece increase and become more non-uniform with an increase in crack length. Hence, if any portion of the workpiece is in tension during the rolling process, the tensile forces will be larger at greater crack length values. Large tensile forces are known to open internal voids. In addition, from viewpoint of low cycle fatigue theory, the larger the area reduction, the more stress cycles that will be experienced by the central position of the workpiece, thus increasing the possibility of void formation.

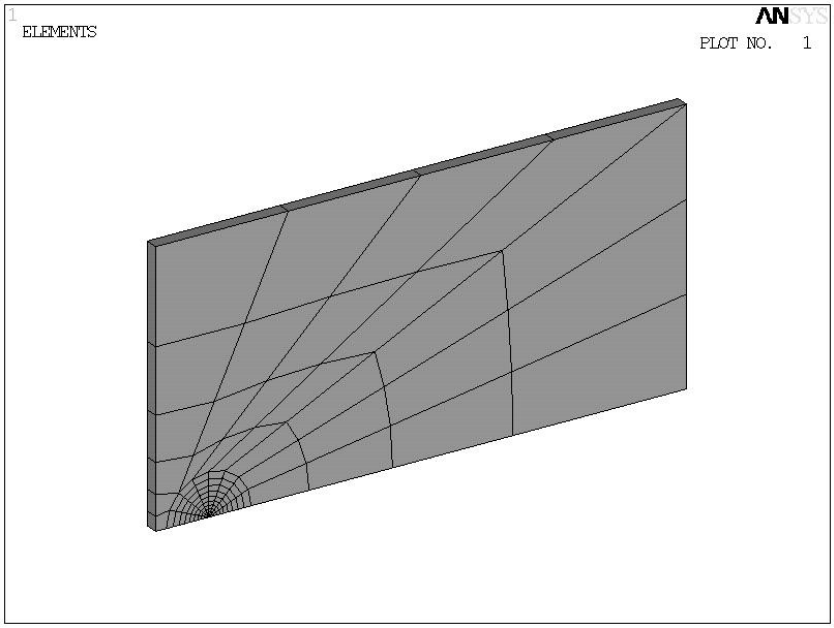

(a) The finite element fracture model

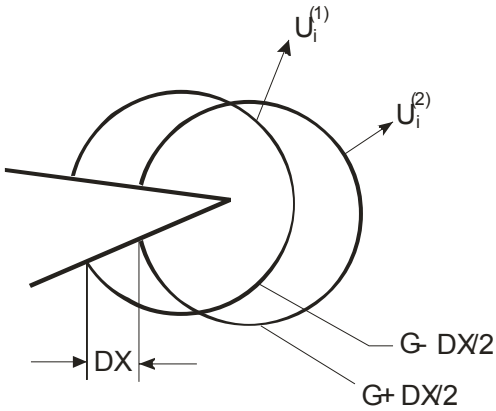

$$\frac{du_i}{dx} = \frac{u_i^{(2)} - u_i^{(1)}}{\Delta x}$$

(b) Computation of derivatives of the displacement vector

Figure 5.3 J-integral Calculation

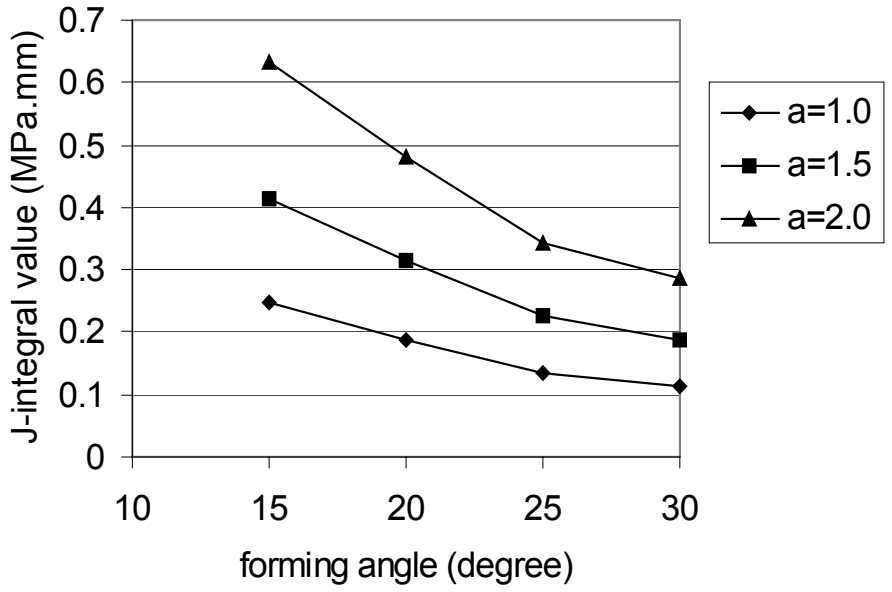

Figure 5.4 The J-integral values with different forming angles and crack length

5.4 Conclusion

The internal crack is a critical defect in the cross wedge rolling process; the crack propagation is discussed in this chapter. Based on the fracture mechanics theory, the J-integral method was introduced to investigate the crack propagation. With the finite element model, the initial loads were the finite element fracture model was employed to complete the J-integral calculation. Utilizing the finite element results, two factors that influence the crack development in CWR, the forming angle and the crack length, were investigated. It was found that the J-integral value increases with the decreasing of the forming angle. In addition, it is shown that the initial crack length has a strong effect on the likelihood of crack growth.

6.0 SUMMARY AND CONCLUSIONS

Cross Wedge Rolling (CWR) is an innovative metal forming process for manufacturing stepped rotational products, such as shafts and axles. This technique has demonstrated excellent advantages over the traditional processes. Application reported can be found in the automobile, tractor, bicycle, machinery, fastener and hand-tool manufacturing industries. Even some non-ferrous components and low ductivity materials have been successfully produced on rolling machines. Generally, in comparison with conventional forging methods, CWR offers the following economies: 20-50% lower price cost; 20-60% lower wage cost; 20-60% lower material cost; and up to 400% increased productivity. However, due to the complexity of the deformation process and the failure mechanisms involved, CWR tooling design is extremely difficult. In this work, based on extensive experimental investigation and state-of-the-art numerical simulation with explicit dynamic finite element method, the major failure mechanisms, improperly formed cross section and internal defects, were systematically studied.

The initial portion of this dissertation pertained to the improperly formed cross section failure due to excess interfacial slip. First using Bowden and Oxley's classical friction models, analytical expressions for the critical rolling condition in the CWR process were generated as a function of tool geometry (α and β) and area reduction (ΔA). As specialized experiments are currently required to predict the critical friction in CWR, the derived expressions represent an important step towards automating CWR tooling design.

A finite element model of a two-roll CWR process was then introduced for the purpose of analyzing the critical interfacial friction in a two-roll CWR process. After being validated by comparison to experiments, several process parameters were analyzed by the FEM to establish their influence on the global slip. The friction coefficient between the forming tools and the

workpiece was found to be the key parameter in controlling the interfacial slip in the two-roll CWR process. The global slip was found to increase with decreasing friction coefficient and a critical friction coefficient was found between μ=0.2 and μ=0.3. Increased forming angles resulted in larger global slip values due to the corresponding decrease in contact area with α. A substantial increase in the global slip was found between $\alpha=30^0$ and $\alpha=40^0$. The forming angle was found to have the least influence on the global slip in the guiding and sizing zones where less significant plastic deformations occur.

The latter half part of this dissertation focused on the internal defects that develop in the CWR process. Initially an experimental study of the CWR process was performed to establish the conditions for which internal voids formed in the workpiece. Extensive experiments were performed by varying the area reduction, forming angle, and stretching angle. Based on the experiments, several key points can be uncovered on the morphology and operating conditions that lead to void formation in the workpiece: 1)Large voids found at the completion of the CWR process develop through the coalescence and bridging of smaller voids initiated in the knifing and sizing zones; 2) When examined along a horizontal cross-section, the voids were found to have a cruciform shape that propagated along the directions of principal stress; 3) The initiation and size of voids were found to increase with decreasing forming angle, increasing stretching angle, and increasing area reduction; 4) The likelihood of void formation within the workpiece can be predicted using a non-dimensional deformation coefficient. For the material and initial geometry studied in this work, the critical deformation coefficient was found to be 0.6.

Utilizing an explicit dynamic finite element model, several different failure criteria were examined for predicting void initiation in the CWR process. Based on the numerical results, it was determined that the effective plastic strain was the best criterion for predicting internal

failure in CWR. Such a finding was in accordance with prior work done by the author who found that void formation could be predicted by a deformation coefficient which was a measure of the plastic strain produced by the forming angle, stretching angle and area reduction.

Based on a finite element model with the Johnson-cook material model, several different working parameters—the forming temperature, the strain rate and the workpiece material —were examined for the CWR process. The author found: 1) the effective plastic strain in a CWR process is independent of both temperature and strain rate. Rather, the strain is controlled by the geometry of the forming tools; 2) considering the maximum effective stress in the workpiece, both temperature and strain rate have an important influence. Specially, the effective stress decreases with increasing temperature and increases at higher strain rates; 3) Temperature has a more dramatic effect on the effective stress within the workpiece than strain rate. Therefore, when optimizing the productivity of a CWR process, the forming velocity and initial workpiece temperature can be increased to maximize productivity without substantially increasing the likelihood of internal defects.

Finally, since the internal void is a critical defect in the cross wedge rolling process, the crack propagation is discussed based on the experimental and numerical investigation. Utilizing fracture mechanics theory, the J-integral method is introduced to investigate the crack propagation. With finite element method, J-integrals are calculated and influential factors on crack development, such as the forming angle α and the crack length a, are investigated. It was found that the J-integral value increased with decreasing of the forming angle. In addition, the size of initial crack has a strong effect on the crack growth.

It is necessary to mention that CWR is not capable of producing high precious final product, such as pistons and aircraft shafts since the tolerance limits of CWR are approximately

±0.5mm. (Using cold CWR, greater accuracy can be obtained). However, CWR can be used as a preform process for the precision parts and subsequently machined to attain desired tolerances.

In conclusion, it is believed that this research has had profound impact on the application of the CWR process in the United States. By developing parameters for predicting critical slip and void failures, CWR has become a more viable manufacturing process. At the start of this project, there was only one company in the US utilizing CWR in production. Currently there are now four companies in the US (Impact Forge, Timken, Missouri Forge, and American Axle) that use CWR in part manufacturing. Before purchasing their CWR equipment, all of these companies have consulted the cross wedge rolling technique with the author and Professor Lovell to evaluate the benefits and drawbacks of the process.

APPENDIX

Table A.1 Internal Failure Experiment Tests in Cross Wedge Rolling (aluminum)

No.	α (°)	β (°)	$2r_{max}$ (mm)	$2r_{min}$ (mm)	Δ_{max} (%)	Δ_{min} (%)
6	15	3	22.68	21.32	29.7%	25.1%
7	15	3	22.57	21.50	28.4%	24.7%
8	15	3	23.21	22.11	31.0%	24.1%
23	15	3	21.34	20.07	37.6%	29.4%
9	15	3	21.40	19.91	38.7%	33.9%
18	15	3	20.23	18.82	45.2%	36.0%
17	15	3	20.57	18.81	45.2%	34.4%
22	15	5	22.35	20.32	34.4%	22.6%
21	15	5	21.59	19.56	40.7%	27.8%
20	15	5	22.61	19.05	43.8%	20.8%
1	15	7	23.42	21.78	26.5%	21.1%
5	15	7	23.04	20.93	32.0%	25.1%
3	15	7	23.71	19.61	40.46%	27.34%
19	15	7	21.59	19.05	43.8%	27.8%
2	15	7	20.13	18.31	49.6%	37.6%
4	15	7	21.55	17.45	52.8%	41.1%
10	15	7	19.81	16.80	56.4%	39.2%
29	15	7	23.11	20.32	36.1%	19.0%
27	15	7	23.11	19.05	43.8%	19.0%
15	20	5	------	18.81	45.2%	-------
16	20	5	23.11	21.34	29.4%	17.2%
28	20	5	21.46	19.81	39.2%	28.6%
26	20	5	21.59	19.56	40.7%	27.8%
24	20	5	21.34	18.82	45.2%	29.4%
25	20	5	21.08	18.81	45.2%	31.1%
30	20	5	20.08	19.17	43.0%	31.8%
14	30	5	22.35	21.34	29.4%	22.6%
13	30	5	20.32	19.56	40.7%	36.0%
12	30	5	19.56	18.54	46.7%	40.7%
11	30	5	17.53	17.02	55.1%	52.4%

Table A.2 Internal Failure Experiment Tests in Cross Wedge Rolling (copper)

No.	**α (°)**	**β (°)**	**$2r_{max}$(mm)**	**$2r_{min}$ (mm)**	**Δ_{max} (%)**	**Δ_{min} (%)**
C1	15	5	22.61	20.07	37.6%	21.0%
C2	15	5	22.35	20.83	32.8%	22.0%
C3	20	3	21.34	20.32	36.1%	29.4%
C4	20	3	20.32	19.56	40.7%	36.1%
C5	20	3	22.61	21.34	29.4%	20.7%
C6	20	5	21.34	19.56	40.7%	29.4%
C7	20	5	22.61	20.83	32.8%	21.0%
C8	20	5	22.61	21.34	29.4%	21.1%
C9	20	5	21.34	20.07	37.6%	29.4%
C10	20	7	21.34	19.81	39.2%	30.2%
C11	20	7	22.35	20.83	32.8%	22.1%
C12	20	7	23.37	21.84	26.1%	16.2%

BIBLIOGRAPHY

1. Dong, Y., M. Lovell, and K. Tagavi, "Analysis of Interfacial Slip in Cross Wedge Rolling: An Experimentally Verified Finite Element Model", Journal of Material Processing Technology, Vol. 80-81, (1998), pp. 273-281.

2. Hu, Z. H., Xiu, X. H. and Sha, D. Y., The Principles, Processed and Machines of Helical Rolling, and Cross Wedge Rolling, (Beijing: Metallurgy Industry Press, 1985).

3. Giffune, W., Jernberg Industries, personal communication, (1997).

4. Lovell, M. R., "Evaluation of Critical Interfacial Friction in Cross Wedge Rolling", Journal of Tribology, Vol.123, (2001), pp.424-429.

5. Johnson, W. and A. G. Mamalis, "A survey of some physical defects arising in metal working processes," Proceedings of the 17th International MTDR Conference, 1977, London, U.K., pp. 607-621

6. Fu, X. P. and T. A. Dean, "Past Developments, Current Applications and Trends in the Cross Wedge Rolling Process", International Journal of Machine Tools Manufacturing, Vol. 33, (1993), pp. 367-400.

7. Pater, Z., "A Study of Cross Wedge Rolling Process," Journal of Material Processing Technology, Vol. 80, (1998)pp. 370-375.

8. Glab, R., F. Hahn, M. Kolbe, and L.W. Meyer, "Process of Partial Bulk Metal Forming – Aspects of Technology and FEM Simulation", Journal of Material Processing Technology, Vol. 80, (1998), pp. 174-178.

9. Li, Q., M. R. Lovell and Z. Deng, "Analysis of interfacial slip in a two-roll cross wedge rolling process", Transactions of the North American Manufacturing Research Institute of SME, Vol.29, (2001), pp. 9-16.

10. Bortunov,E.M., G.N. Burkhan et al., "Surface defects in helical rolled profiles", Stal, Vol.11, (1961), pp.827-830.

11. Grechkin, N. A., A. P. Sichennio et al. , "Three hight 120 mill at Dzerzhinskiii works for rolling circular periodic sections", Stal, vol.5, (1964), pp.369-371.

12. Thompson G. and J. B. Hawkyard, "Crack formation in transverse rolling- a review", Proceedings of 1st International conference On Rotary Metalworking Processes, London,.U.K. , 1979, pp.171-184,

13. Smirnov, V.S., "The Deformation Process in Cross Rolling", stal, Vol.7, No.6, (1947), p.511.

14. Danno, A. and Tanaka, T., "Hot forming of stepped steel shafts by wedge rolling with three rolls", Journal of Material Processing Technology, No.9, (1984), pp.21-35.

15. Teterin, P.K. and Liuzin, J.F. "The mechanism of metal rupture in cross rolling", stal Vol.10, (1960), pp.930-933.

16. Tselikov, A. I., V.M. Lugovsko, and E. M. Tretiyakov, (1961), "The Theory of Cross Cold Rolling on Three-roll Machine", Vestn. Mashinostroeniya, Vol. 7, pp. 49-54.

17. Xiong, H., 2000, Experimental characteristics of CWR process under different area reduction, Master Thesis, Univ. of Kentucky.

18. Deng, Z. Lovell, M. and Tagavi, K. A., "The role of tool segments in determining failure characteristics of cross wedge rolling", Transactions of the North American Manufacturing Research Institute of SME, Vol. 27, (1999), pp. 31-36.

19. Deng, Z. Lovell, M. and Tagavi, K. A., "Influence of material properties and forming velocity on the interfacial slip characteristics of cross wedge rolling", Journal of Manufacturing Science and Engineering, Vol.123, (2001), pp.647-653.

20. Bowden, F.P.and D. Tabor, "Mechanism of metallic friction", Nature, 150, (1942), pp.197-199.

21. Challen, J., and Oxley, P., "An Explanation of the different regimes of friction and wear using asperity deformation models", Wear, Vol.53, (1979), pp. 228-243

22. Halling, J., Principle of Tribology, (London: MacMillan Press Ltd, 1975)

23. ANSYS, Theory Reference 6.0, ANSYS Inc. Canonsburg, PA, 2001.

24. ABAQUS, Technical Notes 5.8, ABAQUS Inc., Pawtucket, Rhode Island, 1998

25. NASTRAN, Reference Manual, MSC.Software Corporation, Santa Ana, CA,1999

26. LS-DYNA, Keyword Manual, Livermore Software Technology Corp, 1999

27. Cowper, G. R. and Symonds, P. S., "Strain-hardening and strain-rate effects in the impact loading of cantilever beams", Technical Report 28, Division of Applied Mathematics, Brown University, (1957).

28. Tsao, M. C. C. and Campbell, J. D., "Plastic shear properties of metals and alloys at high strain rates", Technical Report AFML-TR-73-177, Air Force Materials laboratory, Wright Patterson AF Base, Ohio, (1973).

29. Dong, Y., Tagavi, K. A. and Lovell, M. R., "Analysis of interfacial slip in cross-wedge rolling: a numerical and phenomenological investigation", Journal of Material Processing Technology, Vol. 97, (2000), pp. 44-53.

30. Yano, M., Takahashi, M. et al, "Forming of axially symmetrical shaft with complexed steps by cross rolling method", Mitsubishi Juko Giho, Vol. 8, No.5, (1971), pp.56-62.

31. Hu, Z. H., "The working conditions and stretching angle of cross wedge rolling process", Forging and Stamping Technology, Vol.5, No.5, (1980), pp.10-15.

32. Yie, Q. R., "The investigation of various forming angles and stretching angles of two-roll cross wedge rolling process", Forging and Stamping Technology, Vol. 7, No.5, (1982), pp. 9-12.

33. Pater, Zb, W. Weronski, J. Kazanecki and A. Gontarz, "Study of the Process Stability of Cross Wedge Rolling", Journal of Material Processing Technology, Vol. 92-93, (1999), pp.458-462

34. Hosford, W. F. and Caddell, R. M., Metal forming: mechanics and metallurgy, Prentice-Hall, Englewood Cliffs, N.J. USA, (1993).

35. Hancock, J.W., and A.C. Mackenzie, "On the Mechanisms of Ductile Failure in High-Strength Steels Subjected to Multi-Axial Stress-States", Journal of the Mechanics and Physics of Solids, Vol. 24, (1976), pp.147-169.

36. Mise, S., T. Okamoto, and A. Funashi, "Metal Flow in Oblique Rolling", Sumitoto Metals, Vol. 9, (1957), pp. 21-27.

37. Fu, X. P. and T. A. Dean, "A Study of Defects in Cross Wedge Rolling", Technical Report 4, School of Manufacturing and Mechanical Engineering, Univ. Birmingham, U.K. (1991).

38. Q. Li, M. R. Lovell and W. Slaughter, "Investigation of the Morphology of Internal Defects in Cross Wedge Rolling", to appear in, Journal of Materials Processing Technology, (2003).

39. Y. Huang, J. W. Hutchinson and V. Tvergaard, "Cavitation Instabilities in Elastic-Plastic Solids", Technical Report MECH-153, Harvard University Division of Applied Science, (1989).

40. G. C. Li, X. W. Ling and H. Shen, "On the mechanism of void growth and the effect of straining mode in ductile materials", International Journal of Plasticity, Vol. 16, (2000), pp.39-57.

41. T. A. Khraishi, M.A. Khaleel and H. M. Zbib, "A parametric-experimental study of void growth in superplastic deformation", International Journal of Plasticity, Vol. 17, (2001), pp.397-315.

42. J. A. Collins, Failure of materials in mechanical design: analysis, prediction, and prevention, (New York: John Wiley& Sons, 1993).

43. Johnson, G. R. and W. H. Cook, "Fracture Characteristics of Three Metals Subjected to Various Strains, Strain Rates, Temperatures and Pressures", Engineering Fracture Mechanics, Vol. 21, No. 1, (1985), pp.31-48.

44. G.V. Andreev, E. M. Makushok, V. M. Segal et al, Cross wedge rolling, Vestn. Mashinotroeniya, Vol. 8, (1974), pp.74-79.

45. Campbell J. E., William W. Gerberich and John H. Underwood, "Application of Fracture Mechanics for Selection of Metallic Structural Materials", (American Society For Metal: Metal Park, Ohio, 1982).

46. Rice J.R., "A path independent integral and the approximate analysis of strain concentration by notches and cracks", Journal of Applied Mechanics, Vol. 35, (1968), pp.379-386.

47. Shih, C.F. and German, M,D, "Requirements for a one parameter characterization of crack tip fields by the HRR singularity", International Journal of Fracture, Vol. 17, (1981), pp.27-43.

48. Hutchinson, J. W., "Fundermentals of the phenonmentnological theory of nonlinear facture mechanics", Journal of Applied Mechanics, Vol.50, (1983), pp.1042-1051.